PREPARATION AND CHARACTERIZATION OF CHEMICALLY MODIFIED AMORPHOUS CARBON ELECTRODES

Catherine Grace McKenas

A dissertation submitted to the faculty at the University of North Carolina at Chapel Hill in partial fulfillment of the requirements for the degree of Doctor of Philosophy in the Department of Chemistry in the School of Arts and Sciences.

Chapel Hill
2019

Approved by:

Matthew Lockett

Jillian Dempsey

Mark Wightman

Carrie Donley

Samuel Pazcini

ABSTRACT

Catherine Grace McKenas: PREPARATION AND CHARACTERIZATION OF CHEMICALLY MODIFIED AMORPHOUS CARBON ELECTRODES
(Under the direction of Matthew Lockett)

Chemically modified materials are an important component of dye-sensitized solar cells. Metal oxides are a common electrode material in dye-sensitized solar cells; the dye molecule that undergoes photon absorption must be attached the metal oxide nanomaterial. While dye molecule attachment can be covalent or non-covalent in nature, covalent linkages offer an advantage due to their greater stability. However, covalent modifications of metal oxide surfaces degrade upon exposure to electrochemical cycling, rendering the chemistry inefficient for use in solar cells where long-term stability is needed.

Amorphous carbon is an attractive alternative material to replace metal oxide film electrodes due to its semi-conducting nature and ability to be readily chemically modified. In this work, I developed four new strategies to modify amorphous carbon films, including approaches compatible with: thiol-ene click reactions, azide-alkyne click reactions, and direct surface attachment with an *in situ* Grignard reaction. These surface modifications were fully characterized with: x-ray and ultraviolet photoelectron spectroscopies, scanning electron and atomic force microscopies, water contact angle measurements, and cyclic voltammetry. The analysis of these covalent modifications revealed low coverages and formation of disordered monolayers. The monolayers formed by many of the covalent modification strategies for metal oxides are disordered in nature; this makes the electron transfer through these monolayers more

complex than traditionally accepted models of electron transfer for self-assembled monolayers on gold. These modified amorphous carbon films make a great test-bed to understand electron transfer through disordered films; therefore, the electron transfer through these films was analyzed. Overall, this work outlines new chemistries on amorphous carbon as well as offers a new perspective on understanding electron transfer through disordered films.

To my family: David and Laurie McKenas, and Erin McKenas Joyner.

None of this would be possible without you all. I love you each so much.

ACKNOWLEDGEMENTS

I would first like to thank my adviser, Dr. Matthew Lockett. Thank you for giving me the opportunity to work in your lab 5 years ago. I am so thankful for your support, patience, understanding, and guidance; your enthusiasm about science has always been so inspiring. Thank you for believing in me and my ability to succeed, even when I did not. I have grown so much both as a person and a scientist, and I cannot say thank you enough.

A huge thanks to Dr. Debanjan Dhar and Dr. Jillian Dempsey for making the data and findings presented in the last chapter possible. I am so excited about our collaboration and am looking forward to seeing it through. Thank you to funding sources from UNC and Eli Lilly. Thank you to Chapel Hill Analytical and Nanofabrication Laboratory (CHANL) for use of instrumentation, to Collin McKinney from UNC's CRiTCL Electrons Design Core for construction of a UV LED used in this work, to Dr. Matthew Brennaman, from the Instrumentation Facility established by the UNC EFRC: Center for Solar Fuels, an Energy Frontier Research Center, for use of an energy meter used in this work, and to the T.J. Meyer Lab for use of FTO substrates. A special thanks to each of the following people for contributions made towards this work: Dan Kurtz, Jennifer Middlebrooks, Dr. Xiaoning Zhang, Nathan Whitman, Matthew Boyce, and Dr. Dmitrij Rappoport.

Thank you to the Chemistry Department and Dr. Druscilla French for financial support during my time here. Thank you to everyone in Morehead Laboratories, including: Dr. Kathleen Nevins, Dr. Nita Eskew, and Mark Koza, for giving me countless opportunities to teach laboratories and grow as an educator.

Thank you to my other unofficial academic mentors throughout this journey: Dr. Carrie Donley and Dr. Karla McCain. You both have offered me a listening ear and much needed advice during much of my graduate school career. Thank you for being a stable source of support and encouragement. Thank you to Dr. Amar Kumbhar, Dr. Bob Geil, Dr. Jun Yan, and Dr. Wallace Ambrose at CHANL for providing advice and laughter during my time in CHANL.

Thank you to each of the undergraduates that allowed me to serve as their graduate student mentor during their time in the lab: Julia Fehr, Briana Fletcher, Benedict Liu, and Andrew Pendergast. You each helped me become a better teacher, and I learned so much from each of you. I am so excited to see where life takes each of you.

Thank you to my lab mates (past and present) for providing interesting lunch time discussions and lots of laughs. A special thanks to: Nathan Whitman whose unwavering support and friendship I am so grateful for. You are going to do great things, and I cannot wait to witness it. To Julie McIntosh, I am so grateful for your friendship; your work ethic and determination is inspiring, and I am so excited to see where your journey takes you. To Rachael Kenney, thank you for being a good friend to me, especially when things were tough.

To my other chemistry friends: Kristina Herrera, Nicole Smiddy, Kelsey Miller, and Katie Moeller. Thank you for being my friend and for doing fun things outside of the lab with me; you all are such a great support system. I cannot say thank you enough to each of you.

To my friends from around Chapel Hill: Claire and Mac Gilliland, Patty and Alan Haydon, Charlie and Owen Hyland, Kathleen Jasinskas, Laura and Jessime Kirk, Chelsey McElwee, Julia Ward, and Chris Wommack. You all have made all the difference in my life here in Chapel Hill. Thank you for so many fun memories and all of the laughs. I love you each so much, and I look forward to visiting each of you wherever you all end up.

To my friends who are far away: Anna Sliz, Liann Harris Payne, Saman Najmi, and Chris Joseph. I am so thankful to have been able to keep in touch with each of you during graduate school. Your encouragement and advice is so appreciated. I love each of you!

To the wonderful staff and people of University Presbyterian Church, specifically Rev. John Rogers and Rev. Kate Fiedler. John, I am so grateful to be able to serve with you and the campus ministry. Kate, I am so appreciative of your support and providing great opportunities for the young adults.

To my cat, Louie. You truly are the best cat, and I love you so much.

To my sister, Erin McKenas Joyner. Thank you for finding Austin College so that I could end up there, too. You are such an inspiration to me, and I am so proud of all you have overcome and accomplished in life. I love you so much.

Finally, to my parents, David and Laurie McKenas. Thank you for answering all my questions as a child and encouraging me to be curious about the world around me. Thank you for letting me explore all of my interests from ballet to science. Thank you for raising me in such a loving home. Thank you for making higher education accessible to me by funding my entire college experience. You both have shown me how important it is to work hard for your dreams and to never give up. You truly have both gone above and beyond as parents, and I love you both fiercely.

TABLE OF CONTENTS

LIST OF TABLES xiv

LIST OF FIGURES xvi

LIST OF SCHEMES xviii

LIST OF ABBREVIATIONS AND SYMBOLS xix

CHAPTER 1—AMORPHOUS CARBON THIN FILMS AS AN ALTERNATIVE MATERIAL IN DYE-SENSITIZED SOLAR CELLS 1

1. Introduction 1

1.1 Energy Crisis 1

1.2 Solar Cells 1

1.2.1 Overview 1

1.2.2 Dye-Sensitized Solar Cells 2

2. Metal Oxides 3

2.1 Overview 3

2.2 Chemical Modification of Metal Oxides 4

3. Alternative Semiconductor Materials 5

3.1 Silicon 5

3.2 Carbon-Based Materials 6

3.2.1 Diamond 7

3.2.2 Graphene 8

3.2.3 Glassy Carbon 9

3.2.4 Amorphous Carbon 9

3.2.5 Carbon-Based Nanomaterials 11

4. Characterization Methods 11

4.1 Microscopy 12

4.2 Spectroscopy 12

4.3 Cyclic Voltammetry 14

4.4 Other Methods 15

5. Overview of Work 15

5. Figures 17

REFERENCES 21

CHAPTER 2-THIOL-ENE MODIFIED AMORPHOUS CARBON SUBSTRATES: SURFACE PATTERNING AND CHEMICALLY MODIFIED ELECTRODE PREPARATION 28

1. Introduction 28

2. Experimental Section 30

2.1 Chemicals and materials. 30

2.2 Thin film preparation and modification 30

2.3 Thin film characterization. 31

2.4 Statistical tests. 32

3. Results and Discussion 33

3.1 Thiol-terminated aC film preparation and characterization. 33

3.1.1 XP spectroscopic analysis. 33

3.1.2 Surface stability. 35

3.1.3 Surface roughness measurements. 35

3.1.4 Surface wettability measurements. 36

3.2 Specificity of the thiol-ene reaction 37

3.2.1 Terminal thiols enhance the attachment of alkene-containing molecules to the aC film. 37

3.2.2 Alkene-containing molecules preferentially react with terminal thiols on the aC film. 38

3.2.3 A radical initiator is not needed to promote thiol-ene reactions on the aC films. 39

3.2.4 Non-specific attachment of alkene-containing molecules to the aC films is prevented with lower energy UV wavelengths. 39

3.3 Patterning thiol-terminated aC films. 40

3.4 Preparing thiol-ene modified aC electrodes. 40

4. Conclusion 41

5. Figures and Tables 43

REFERENCES 52

CHAPTER 3- MECHANISTIC INSIGHTS INTO UV-INITIATED THIOL-ENE REACTIONS ON AMORPHOUS CARBON FILMS 56

1. Introduction 56

2. Experimental Methods 57

2.1 Chemicals and Materials. 57

2.2 Thin Film Preparation and Modification. 58

2.3 Thin film illumination and modification. 58

2.4 Thin Film Characterization. 59

2.5 Statistical analysis. 60

3. Results and Discussion 60

3.1 Surface preparation, characterization, and stability. 60

3.2 Thiol-ene reaction selectivity on aC films depends on photon flux. 62

3.3 The attachment of 4-fluorobenzyl mercaptan molecules to the aC films is not mediated by oxygen-containing radicals. 64

3.4 Attachment of 4-fluorobenzyl mercaptan molecules is likely initiated by thiyl radical formation. 64

3.5 Methyl- or vinyl-termination does not alter the electronic properties of the amorphous carbon films. 66

3.6 Vinyl-aC films favor greater coverages and faster kinetics than thiol-aC films when performing thiol-ene click reactions. 67

3.7 Possible mechanisms responsible for non-specific attachment. 68

4. Conclusions 69

5. Figures and Tables 70

REFERENCES 75

CHAPTER 4- AZIDE-ALKYNE CLICK REACTIONS TO PREPARE CHEMICALLY MODIFIED AMORPHOUS CARBON ELECTRODES 78

1. Introduction 78

2. Materials and Methods 80

2.1 Reagents and Materials 80

2.2 Amorphous carbon film deposition and functionalization 80

2.3 Surface characterization 81

3. Results 82

3.1 Characterization of the aC Films 82

3.2 Preparation, Characterization, and Reactivity of Azide-Terminated aC Films 83

3.3 Electrochemical Characterization of Ferrocene-modified aC Films 85

4. Discussion 86

4.1 New Strategies for Generating CuAAC-compatible Surface Chemistries 86

4.2 Amorphous Carbon Films as Modified Electrodes 87

5. Conclusions 89

6. Figures and Tables 90

REFERENCES 98

CHAPTER 5- MODIFICATION OF AMORPHOUS CARBON FILMS WITH IN SITU GRIGNARD REACTIONS 102

1. Introduction 102

2. Materials and Methods 105

2.1 Chemicals and Materials 105

2.2 Amorphous carbon film preparation and functionalization 106

2.3 Surface characterization 107

3. Results and Discussion 107

4. Conclusions 111

5. Figures and Tables 113

REFERENCES 117

APPENDIX A: SUPPLEMENTAL INFORMATION FOR CHAPTER 2 122

APPENDIX B: SUPPLEMENTAL INFORMATION FOR CHAPTER 3 132

APPENDIX C: EXAMPLE CALCULATION FOR CHAPTER 3 146

APPENDIX D: SUPPLEMENTAL INFORMATION FOR CHAPTER 4 147

APPENDIX E: EXAMPLE CALCULATION FOR CHAPTER 4 157

APPENDIX F: EXAMPLE CALCULATION FOR CHAPTER 4 158

REFERENCES 159

LIST OF TABLES

Table 2.2. Summary of quantitative analyses of modified surfaces. 48

Table 2.3. Bromine-to-carbon ratios for H-aC and HS-aC surfaces. 49

Table 3.1. Quantitative characterization of vinyl-aC and methyl-aC films. 71

Table 4.1. Elemental composition of aC films after each chemical modification. 91

Table 4.2. Selected reaction conditions evaluated for azide attachment on aC films. 92

Table 4.3. Electrochemical properties of ferrocene-modified carbon electrodes. 96

Table 5.1. XPS atomic concentration values. 114

Table 5.2. Summary of quantitative results. 116

Table S2.1. Attempted thiolation reaction conditions. 122

Table S2.2. Binding energies and relative composition values of representative high-resolution C1s XP spectra. 124

Table S2.3. Elemental composition of aC films. 126

Table S2.4. Percentage of reduced and oxidized sulfur atoms. 127

Table S2.5. XPS elemental composition of aC films in Figure S4. 129

Table S2.6. Bromine-to-carbon ratios of aC films. 131

Table S3.1. ΔO/C ratios for vinyl-aC films as a function of storage condition. 135

Table S3.2. Sulfur-to-carbon (S/C) and fluorine-to-carbon (F/C) ratios for different surface chemistries exposed to 1 M of 4-fluorobenzyl mercaptan 136

Table S3.3. Summary of XPS data for vinyl-aC films modified with 4-fluorobenzyl mercaptan molecules. 140

Table S3.4. F/C and S/C ratios for H-aC and vinyl-aC films exposed to benzene containing 1 M 4-FBM and 0.01 μM butylated hydroxytoluene (BHT) 142

Table S3.5. Work function and elemental composition data obtained from UPS and XPS measurements. 143

Table S3.6. F/C and S/C ratios for vinyl-aC reacted with 4-FBM or thiol-aC films reacted with 4-FS molecules as a function of illumination time. 144

Table S4.1. Reaction conditions tested to prepare N_3-aC films. 147

Table S4.2. Cyclic voltammetry data for ferrocene-terminated aC films. 154

Table S4.3. Scan rate values 155

LIST OF FIGURES

Figure 1.1. Diagram of a dye-sensitized solar cell. 17

Figure 1.2. Ternary phase diagram of amorphous carbon. 18

Figure 1.3. Modification strategies for carbon-based materials. 19

Figure 1.4. Overview of modification schemes presented in this work. 20

Figure 2.2. Representative atomic force micrographs. 46

Figure 2.3. Representative static contact angle images. 47

Figure 2.4. SEM images of an 11-bromo-1-undecene patterned aC film. 50

Figure 2.5. Summary of electrochemical experiment using ferrocene. 51

Figure 3.1. XPS results for thiol-ene click experiments. 72

Figure 3.2. Energy diagrams for H-aC, Cl-aC, vinyl-aC, and methyl-aC films. 73

Figure 3.3. Reaction completion percentage as a function of total illumination energy. 74

Figure 4.1. Summary of characterization of aC films as electrodes. 93

Figure 4.2. XPS summary for azide-alkyne click reaction. 94

Figure 4.3. Summary of electrochemical data obtained for ferrocene-terminated aC film. 95

Figure 5.1. XPS data for Fe 2p region for an H-aC and Cl-aC films exposed to *in situ* Grignard reaction conditions. 113

Figure 5.2. Summary of electrochemical data and analysis. 115

Figure S2.1 Representative high-resolution XP spectra of the C1s electrons. 123

Figure S2.2. Representative XP survey spectra. 125

Figure S2.4. Representative XP survey spectra. 128

Figure S3.1. Representative XPS datasets for methyl-aC films. 132

Figure S3.2. Representative XPS datasets for vinyl-aC films. 133

Figure S3.3. Representative UPS datasets for H-aC, Cl-aC, methyl-aC, and vinyl-aC films. 134

Figure S3.4. S/C ratios as a function of ΔO/C for methyl-aC films. 137

Figure S3.5. S/C ratios as a function of ΔO/C for vinyl-aC films. 138

Figure S3.6. S/C ratios as a function of ΔO/C for H-aC films. 139

Figure S3.7. F/C ratios as a function of percentage of oxidized sulfur. 141

Figure S3.8. Oxidized sulfur percentages for vinyl-aC and thiol-aC films exposed to benzene containing either 1M 4-FBM or 1M 4-FS, at different powers of UV light. 145

Figure S4.1. Representative XP survey spectrum of an unmodified aC film on an FTO substrate. 148

Figure S4.2. Representative XPS data. 149

Figure S4.3. Representative XPS data. 150

Figure S4.4. Representative XPS data. 151

Figure S4.5. Representative XPS data. 152

Figure S4.6. Tauc plot of aC film on a quartz substrate. 153

Figure S4.7. Cyclic voltammogram of ferrocene-modified aC film 156

LIST OF SCHEMES

Scheme 2.1. Reaction scheme of thiol-terminated aC thin film preparation. 43

Scheme 3.1. Reactions and molecules used in this work. 70

Scheme 4.1. Modification of aC films. 90

LIST OF ABBREVIATIONS AND SYMBOLS

$/W	price/peak watt
%	percent
i_p	peak current
μA	microamps
μm	micrometers
Γ	surface coverage
ΔCl/C	change in chlorine-to-carbon
ΔE_p	peak-to-peak separation
ΔO/C	change in oxygen-to-carbon ratio
η	overpotential
π- π	pi-pi
Ω/sq	ohm per square
Ωm	ohm meters
v	scan rate
4-FBM	4-fluorobenzyl mercaptan
4-FS	4-fluorostyrene
4-FT	4-fluorotoluene
A	area of electrode
aC	amorphous carbon
ACN	acetonitrile
AFM	atomic force microscopy
Ag/AgCl	silver/silver chloride
arb. units	arbitrary units

at. %	atomic percentage
ATR	attenuated total reflectance
BDD	boron-doped diamond
BHT	butylated hydroxytoluene
Br	bromine
Br/C	bromine-to-carbon
BUD	11-bromo-1-undecene
C	carbon
Cl	chlorine
Cl-aC	chlorine-terminated amorphous carbon
cm/s	centimeters per second
cm^2	squared centimeters
CO_2	carbon dioxide
Cu	copper
CuAAC	copper-catalyzed azide-alkyne cycloaddition
CV	cyclic voltammetry
DC	direct current
DLC	diamond-like carbon
DMF	*N*,*N*-dimethyl formamide
DMPA	2,2-dimethoxy-2-phenylacetophenone
DMSO	dimethyl sulfoxide
DNA	deoxyribonucleic acid
DSSCs	dye sensitized solar cells
E	energy
e.g.	exempli gratia

E_F	energy of fermi level
E_{FWHM}	potential at full-width half-maximum
E^o	formal potential
E^o_{red}	reduction potential
et al.	and others
eV	electron volts
E_{vacuum}	energy vacuum level
F	Faraday's constant
F	fluorine
F/S	fluorine-to-sulfur ratio
Fc	ferrocene
Fc-aC	ferrocene-terminated amorphous carbon
Fe	iron
FTIR	Fourier-transform infrared spectroscopy
FTO	fluorine-doped tin oxide
GC	glassy carbon
GO	graphene oxide
h	hours
H_2O_2	hydrogen peroxide
H_2SO_4	sulfuric acid
H-aC	hydrogen-terminated amorphous carbon
HCl	hydrochloric acid
He	helium
HOMO	highest occupied molecular orbital
HS-aC	thiol-terminated amorphous carbon

I	iodine
in situ	in the original place
in vacuo	in a vacuum
IN_3	iodine azide
IPCC	Intergovernmental Panel on Climate Change
IR	infrared
IRRAS	infrared reflection absorption spectroscopy
ITO	indium tin oxide
J	joules
kHz	kilohertz
kJ/mole	kilojoules per mole
kV	kilovolts
LED	light-emitting diode
LUMO	lowest unoccupied molecular orbital
M	molar
methyl-aC	methyl-terminated amorphous carbon
meV	milli electron volts
Mg	magnesium
MHz	mega hertz
mins	minutes
mL	milliliter
ML	monolayer
mm	millimeters
mM	millimolar
mmol	millimole

molecules/cm^2	molecules per squared centimeters
mV	millivolts
mV/n	millivolts per number of electrons
mV/s	millivolts per second
mW	milliwatts
mΩ/cm	milliohms/centimeter
N	nitrogen
n	number of replicates
N/C	nitrogen-to-carbon
N/m	Newtons/meter
N_2	nitrogen gas
N_3	azide
N_3-aC	azide-terminated amorphous carbon
nA	nanoamps
NaCl	sodium chloride
NaN_3	sodium azide
NaSH	sodium hydrosulfide
Nb_2O_5	niobium oxide
NIH	National Institute of Health
nm	nanometers
NR	not reported
n-type	electron donating material
^{o}	degree
O/C	oxygen-to-carbon
^{o}C	degrees Celsius

p	probability value
PCl_5	phosphorus pentachloride
PET	polyethylene terephthalate
PG	pyrolytic graphite
PPF	pyrolyzed photoresist films
p-type	electron accepting material
PVD	physical vapor deposition
Q	charge
RF	radio-frequency
RMS	root-mean squared
RO	reverse-osmosis
S	sulfur
S/C	sulfur-to-carbon ratio
S/N	signal-to-noise
s^{-1}	per second
SAM	self-assembled monolayer
SCE	saturated calomel electrode
SEM	scanning electron microscopy
SI	supplementary information
Si(100)	silicon 100
TBAI	tetrabutyl ammonium iodide
TBAPF	tetrabutylammonium hexafluorophosphate
TEM	transmission electron microscopy
temp	temperature
THF	tetrahydrofuran

thiol-aC	thiol-terminated amorphous carbon
TiO_2	titanium dioxide
Torr	torricelli
TW	terawatts
uL	microliters
UPS	ultraviolet photoelectron spectroscopy
UV	ultra-violet
V	volts
V/sec	volts per second
v/v	volume-by-volume
VACNF	vertically-aligned carbon nanofibers
vinyl-aC	vinyl-terminated amorphous carbon
W	watts
w/w	weight by weight
XP	x-ray photoelectron
XPS	x-ray photoelectron spectroscopy
ZnO	zinc oxide

CHAPTER 1—AMORPHOUS CARBON THIN FILMS AS AN ALTERNATIVE MATERIAL IN DYE-SENSITIZED SOLAR CELLS

1. Introduction

1.1 Energy Crisis

In 2018, the Intergovernmental Panel on Climate Change (IPCC) predicted a global temperature increase of 1.5^{o}C from pre-industrial temperatures as early as 2030 if significant effort was not made to reduce anthropogenic contributions to climate change. Such an increase in global temperature will lead to unfortunate consequences; some examples include: extremities in regional climate, disappearance of different ecosystems, food insecurity, and increased poverty. While anthropogenic emissions are unlikely to be the sole cause of a global warming of 1.5^{o}C, they will still contribute to climate change. The emission of greenhouse gases from the burning of fossil fuels is one such anthropogenic contribution.[1] Therefore, there has been a push towards finding alternative energy sources that do not generate greenhouse gases.

1.2 Solar Cells

1.2.1 Overview

In order to meet the increasing demand for alternative energy sources, harnessing solar energy through solar cells is an ever-growing field. The amount of energy from the sun is equivalent to 120,000 TW which is 6000-times more than the world-energy consumption;[2] therefore, if a solar cell is able to harness just around 20% of the sun's energy, that would be enough to meet our energy demands. While there are a number of solar cells that have been

developed, there are also certain criteria that the ideal solar cell needs to meet. These criteria include: 1) efficiency, as measured by a percentage, which describes the fraction of energy from the sun that was converted into electricity; 2) stability, which describes how well the device retains its structure and efficiency over time and upon exposure to different environments; and 3) cost, which describes the amount of money required in price/peak Watt ($/W) to make the cell.

Solar cells can be loosely categorized into the following: silicon-based, group III-IV, thin film chalcogenide, dye-sensitized, organic, perovskite, and multi-junction cells. While there are a number of reports in the literature of efficiencies of different solar cells, only those efficiencies that were confirmed by a designated test center[3] were considered in this discussion. Currently, multi-junction cells comprised of group III-V elements have obtained the highest efficiencies, around 45%, closely followed by perovskites and crystalline silicon.[3] Unfortunately, group III-V elements are expensive making it difficult to generate a cost-effective solar cell.[4] Perovskite-based solar cells have yet to meet short-term and long-term stability requirements, and an alternative approach to mitigate the use of toxic elements (such as lead) in perovskites is still being investigated.[5] While dye-sensitized solar cells (DSSCs) have only achieved efficiencies around 12%,[3] there is still quite a push to investigate DSSCs as they offer a non-toxic, low-cost, and stable approach towards developing ideal solar cells.[2]

1.2.2 Dye-Sensitized Solar Cells

Introduced in 1991, DSSCs consist of mesoporous, semiconducting oxide materials, usually TiO_2 nanoparticles, that are functionalized with dye molecules (**Figure 1**).[6] Upon photoexcitation of the dye, an electron is injected into the conduction band of the semiconductor. The resulting oxidized dye is regenerated upon reduction by an electrolyte—typically an

iodide/triiodide redox couple. There are a number of electron transfer processes in DSSCs that are not energetically favorable and require large overpotentials. The injection of an electron from the dye complex into the conduction band of the oxide is one such electron transfer reaction. The required overpotential for this electron transfer reaction is one of the main reasons solar cells have not achieved their maximum theoretical efficiency of ~32%.[7] Previous studies have indicated that the kinetics of the electron injection is dictated by the molecular orientation of the dye relative to the metal oxide surface as well as the alignment of their respective energy levels.[8,9] The kinetics of electron injection can be tuned by changing the linkage length or type of attachment chemistry used to anchor the dye to the TiO_2 nanoparticle. Current methods used to anchor dyes onto TiO_2 nanoparticles include adsorption methods via the interaction of terminal acidic groups with the terminal hydroxyl groups on TiO_2; however, this attachment method has shown to lead to detachment and degradation of the dye complex upon electrochemical cycling.[10]

2. Metal Oxides

2.1 Overview

When considering the metal oxide material for a DSSC, there are a couple of characteristics that the material needs to have: thermal stability, chemically inert, non-toxic, and cheap. Additionally, the semiconductor should have high band-gap energy to limit unwanted electron recombination, and a nano-structured mesoscopic morphology to maximize surface area for dye attachment.[4]

Traditionally, anatase TiO_2 has been used as the metal oxide nanoparticle material in dye-sensitized solar cells because it is is inexpensive and non-toxic. Unfortunately, the density of trap states in TiO_2 is problematic as it slows down the electron transfer process. ZnO offers a lower

density of trap states and longer carrier lifetime as compared to TiO_2; however, ZnO is not stable under the acidic conditions often encountered in dye-sensitized solar cells. Nb_2O_5 offers a larger bandgap energy than anatase TiO_2 and better chemical stability than ZnO. However, there exist few studies that explore the electron transfer process when Nb_2O_5 is used.[11]

Nanoparticles are the traditional form of nanomaterial used in dye-sensitized solar cells; however, the diffusion length for an electron through a nanoparticle film is around 15-20 μm due to morphology and porosity of the film,[12] making unwanted electron recombination reactions more favorable. To decrease this diffusion length while maintaining a high surface area, there has also been exploration into other types of nanomaterials that are one-dimensional, such as: nanorods, nanofibers, and nanowires. These materials have shown great promise as alternative nanomaterials for dye-sensitized solar cells;[11] however, further studies are needed to fully understand the properties of these materials before extensive use in DSSCs.

2.2 Chemical Modification of Metal Oxides

There are about six different categories of functional groups that will react with oxide materials: silanes, phosphonates, carboxylates, catechols, alkenes/alkynes, and amines.[13] Of these chemistries, only silanes and alkenes/alkynes form covalent attachments on metal oxides; the other functional groups attach through electrostatic interactions. While there have been numerous studies characterizing these attachment chemistries on different metal oxide materials, there are still significant downfalls. Silane and phosphonate linkages are prone to hydrolysis upon exposure to reaction conditions commonly encountered in dye-sensitized solar cells. Catechol and alkene/alkyne attachment chemistries form multilayers, which is undesirable as monolayer formation is required for dye-sensitized solar cells. Finally, depending on the metal

oxide material and modification chemistry used, some combinations form more well-ordered monolayers than others. For example, silanes form extremely well-ordered and well-packed monolayers on glass, but not nearly as well on TiO_2. Therefore, depending on the material, careful consideration must be taken when choosing the modification chemistry to attach organic molecules to the surface.

3. Alternative Semiconductor Materials

3.1 Silicon

Semiconductors are not only important materials in dye-sensitized solar cells, but the microelectronics industry as well.[14] For example, the ability to modify semiconductors with molecules is not only applicable to attaching dye molecules to these materials for solar cell applications, but also to prevent formation of self-terminating insulating oxide layers within the microelectronics industry. Therefore, the microelectronics industry spurred interest in other semiconductor materials such as gallium arsenide, germanium, and silicon. Silicon is a common semiconductor material that is used in other types of solar cells as it is inexpensive, lends itself to large-scale production, and is non-toxic. Therefore, there has been much interested in understanding the reactivity and stability of the surface of silicon.[15]

One of the important features that a semiconductor needs to have for solar cell applications is the ability to tune its work-function; this value directly impacts the interfacial energy level alignment between monolayers and the silicon substrate itself.[14] This energy level alignment is important as it dictates the charge transfer process within the solar cell. Due to its crystalline structure, silicon can be doped with n-type (donors) or p-type (acceptor) atoms to fine-tune the

interfacial energy level alignment. Silicon can also be chemically modified in a directional and stable manner; in particular, a Si-C bond is exceptionally strong and can withstand oxidation.

Silicon can be chemically modified in vacuo and under ambient conditions using wet chemical approaches. Under vacuum, silicon, commonly the (001) crystal face, undergoes surface rearrangement. This surface rearrangement favors the formation of dimers; therefore, cycloaddition reactions have developed as one approach to functionalize silicon with organic monolayers.[16] Another in vacuo approach involves the cleavage of X-H bonds in thiol, amino, or hydroxyl groups (X = S, N, or O) for surface attachment.[17–20]

Ambient chemical modification strategies offer more experimental control over monolayer formation. This approach requires an etching step to remove the native oxide layer of silicon followed by a passivation step to prevent unwanted oxidation.[16] A wet chemical hydrogen-termination is the most common passivation step; however the hydrogens are still labile and subject to oxidation over time. Chlorine-termination results in a more reactive surface and silane self-assembled monolayers allow for well-ordered films. There have been a number of studies that utilize molecules with a terminal alkene functionality which requires initiation via a chemical,[21] thermal,[22] or photochemical[23] method; these monolayers are often disordered. Silicon can also react with thiols, aldehydes, and alcohols under ambient conditions; however, these reactions also form disordered monolayers.

3.2 Carbon-Based Materials

Recently, there has been interest in exploring carbon-based materials due to their intrinsic stability and ability to modify their surfaces using common organic reactions. Furthermore, carbon-based materials have tunable semiconductor-like properties via the sp^2/sp^3 ratio, allowing

them to be used as an alternative material in solar cells.[24] A generic way to classify a carbon-based material is by the relative amount of sp, sp^2, or sp^3 character (**Figure 2**).[25] Four different allotropes of carbon will be discussed: diamond, graphite, glassy carbon, and amorphous carbon. A brief overview of carbon-based nanomaterials will tie up the end of this section.

3.2.1 Diamond

Diamond is a material that is made up of sp^3 hybridized carbons in a tetrahedral configuration forming a crystalline lattice. Diamond is a commercially expensive material; deposition processes to grow diamond films usually involve a plasma-initiated vapor deposition from a methane source. In order to enhance conductivity, diamond can also be doped with boron or nitrogen, via incorporation of such a source during deposition. Boron-doped diamond (BDD) films are an attractive electrode material.[26] Due to its optical transparency, BDD films have found application as a photo-catalyst platform for nitrogen reduction.[27] One of the first examples of chemical modification of diamond involved the photochemical attachment of alkenes to form DNA arrays.[28] Unfortunately, not all molecules are compatible with 254 nm UV light required to utilize this attachment strategy; biomolecules readily degrade under this part of the UV spectrum. Furthermore, this photochemical approach is a radical-mediated attachment mechanism; therefore, this type of attachment strategy can be prone to multilayer formation. Another common approach for the functionalization of diamond is through the electrochemical reduction[29] or chemical grafting[30] of aryl diazonium molecules. The electrochemical approach results in multilayer formation; whereas the chemical approach results in homogenous monolayers.

3.2.2 Graphene

Graphite is a material where 100% of the carbon atoms are in the sp^2 configuration. Graphene is a material that can be derived from graphite where the carbon atoms are arranged in a two-dimensional honeycomb crystal lattice structure.[31] Graphene has outstanding electrical and thermal conductivity making it a popular material in the microelectronics industry. There are two different planes present in graphite-based materials: the edge and basal planes.[32] Therefore, uniform chemical modification of these materials is difficult, as different chemistries will preferentially react with the edge or basal plane. This effect leads to non-homogenous coverage of graphite-based materials.

In order to chemically functionalize graphene, many approaches start with graphene oxide (GO).[33] The presence of the hydrophilic oxide groups allows for solubility in various solvents, and the labile oxygen functionalities at the edge planes of this material allow for ease of further chemical modification. Generally speaking, there are two routes to chemical modification: covalent and non-covalent attachment.

Covalent modification strategies can be broadly categorized into the following four groups: nucleophilic substitution, electrophilic addition, condensation, and addition.[31] Most nucleophilic substitution reactions take advantage of the epoxy groups present at the GO surface and utilize amine-terminated molecules for chemical attachment to GO. Electrophilic additions displace a hydrogen atom with an electrophile; a common example of this is the spontaneous grafting of aryl diazonium salts.[34] An example of a condensation reaction is the condensation of isocyanate compounds with GO.[35] Finally, an example of an addition reaction is the cycloaddition of azomethine ylide.[36] Non-covalent modifications strategies utilize Van der Waals, hydrophobic, or electrostatic interactions. While non-covalent modifications have been

widely used on graphene,[31] the main downfall is that long-term use of modified materials require covalent modifications as this approach favors more stable linkages.

3.2.3 Glassy Carbon

Glassy carbon materials are characterized as "ribbon-like" structures of sp^2 carbon atoms. This material is well known in the electrochemistry world as it is a common electrode material. As this material is made via the controlled pyrolysis of polymers, it is easy to add dopants to this material by simply introducing dopants during the heating process.

Many of the chemical modifications that have already been discussed have also been applied to glassy carbon materials, such as the aryl diazonium salt reduction approach.[37] Another approach involves the electrochemical hydrogenation and chlorination of glassy carbon films in order to attach thiol-terminated molecules.[38] This chlorination approach was first described by Bansal et al. via the halogenation and subsequent alkylation via a Grignard reaction of silicon surfaces.[39] This wet, chemical approach introduced by Bansal offers a facile method for halogenation of materials. Similar to the photochemical attachment of alkenes to diamond previously discussed, glassy carbon can also photochemically react with alkenes and alkynes.[40]

3.2.4 Amorphous Carbon

Amorphous carbon (aC) films are a mixture of sp^2 and sp^3 hybridized carbons; this ratio is dependent on the deposition parameters used. Given the presence of sp^3 hybridized carbons, this material is often referred to as diamond-like carbon (DLC).[25] Therefore, this material has many of the advantages that diamond does, such as: mechanical hardness, chemical inertness, and a wide band-gap. As the roughness of this material is dependent on the sp^2/sp^3 ratio, the deposition

parameters dictate the root-means squared roughness. One study investigated the following deposition approaches: RF glow discharge, DC magnetron sputtering, and carbon ion beam. They found that the overall roughness of these films was less than 0.4 nm when using an RF glow discharge deposition, less than 1.5 nm when using DC magnetron sputtering at room temperature, and less than 0.3 nm using a carbon ion-beam.[41] The resistivity of the film is dependent on its thickness, but is generally around 50 mΩ/cm for films thicker than 50 nm; this characteristic has caused interest in developing aC films as electrode materials.[42]

The chemical modification approaches previously discussed, as applied to amorphous carbon substrates, are summarized in **Figure 3**. A typical pre-treatment of aC films involves hydrogenation in a plasma chamber. This pre-treatment ensures that dangling bonds at the surface have a hydrogen atom.[24] A wet, chemical approach to chlorinate aC films has been used to install alkyl thiols and alkyl groups via Grignard reactions.[43,44] Reactions of aryl diazonium salts have also been applied to amorphous carbon films via a spontaneous covalent attachment mechanism.[45] Photochemical attachment of alkenes using 254 nm light has also been explored on aC films, but the downfalls of this approach previously described for diamond also apply to aC films.[46,47] While each of these strategies offers a unique approach to install molecules on aC films, there are inherent downfalls for each approach. The Grignard reactions are limited by the ability to form a Grignard reagent out of the desired functionality; these reactions involve carbanions which are strong nucleophiles, making them difficult to couple to certain reagents such as biomolecules.[24] The aryl diazonium salt reduction reactions are known to form multilayers, making it difficult to obtain monolayer coverage.[32] Finally, the photochemical approach requires initiation with 254 nm photons, which limits the types of functional groups that can be used due to the possibility of unwanted radical side reactions.

3.2.5 Carbon-Based Nanomaterials

Other types of carbon-based materials include nanomaterials such as carbon nanotubes and graphite particles. These materials have excellent electrical, thermal, and mechanical properties, but increase the available surface-area for dye-attachment due to the high surface-to-volume aspect ratios. There have been efforts to use carbon-based nanomaterials to replace many components of a DSSC, including the transparent electrode, counter electrode, semiconducting material, and electrolyte.[48] However, when carbon nanomaterials were used as an active-layer in solar cells, the highest efficiency recorded was only 1.3% possibly due to the impurity of the material which resulted in unwanted electron recombination.[49] Therefore, further investigation of carbon nanomaterials towards applications of DSSCs is needed to fully understand the potential of this approach.

4. Characterization Methods

The surface characterization of modified materials requires a multi-instrumentation approach, as no single technique can simultaneously answer questions about its structure, topography, chemical composition, electronic and physical properties. A recent study revealed that out of 13 different research groups who had performed studies on the surface modification of silicon using alkenes, half of the papers used three or fewer techniques.[50] This analytical problem is not only applicable to modified planar materials, but to nanomaterials as well.[51] Reasons for incomplete characterization range from the high cost associated with certain instrumentation to the expertise needed to maintain, use, and analyze the data from certain instrumentation. In order to form a more-complete picture of the modified materials in this work, microscopy, spectroscopy,

electrochemistry, and other surface-centric methods were used. The rationale and importance of each technique will be discussed below.

4.1 Microscopy

When trying to understand the morphology or topology of a material, microscopy methods become important to include in analysis. For a DSSC, the surface area of the material needs to be maximized in order to attach a large number of dye molecules to the material; while certain materials, such as silicon, are atomically flat, many materials are not. Atomic force microscopy (AFM) is a technique that allows one to probe the roughness of the film by utilizing a mechanical probe. First introduced in 1986, this technique has atomic resolution making it an ideal method to image modified materials to understand how chemical functionalization influences surface roughness.[52,53]

Scanning electron microscopy (SEM) is a technique that rasters an electron beam across the surface of a material to image the topography and composition. Depending on the detector used, this technique can be sensitive to different signals arising from the interaction of the electron beam with the material. Two such signals are secondary and back-scattered electrons. Secondary electrons give information about surface topography.[54] Back-scattered electrons are sensitive to elemental changes in the sample as the signal from back-scattered electrons is dependent on atomic number.[55] Therefore, detection of back-scattered electrons is frequently used as a way to image patterns generated via photo-initiated reactions.[56,57]

4.2 Spectroscopy

Spectroscopic techniques are of importance when determining the elements, molecular structure, or types of bonds present at a modified surface. X-ray photoelectron spectroscopy

(XPS) is an elemental analysis technique that probes only the top 10 nm of the surface.[58] As X-rays interact with the material, core electrons are emitted and sorted by binding (or kinetic) energy. The core electrons of each element have unique energies. The bonding environment can slightly alter these energies by a few eV, providing information about the bonding patterns at the surface. For example, XPS can not only deduce a semi-quantitative atomic concentration of carbon in a sample, but also reveal the type of binding environment the carbon was in (i.e.: C-O, C=O, etc.). For metals, XPS can distinguish the number of oxidation states present at the surface of a material. Therefore, when trying to confirm successful modification of a material, XPS is powerful technique.

Ultraviolet photoelectron spectroscopy (UPS) is a technique that bombards the material with ultraviolet (UV) photons and measures the emitted photoelectrons.[59] This technique reveals information regarding the electronic structure of the material. One such energy called the work function of the material is a measure of the amount of energy needed to eject an electron from the material into vacuum. This value becomes very important when considering generating functional, modified materials for DSSCs; as the surface is chemically modified, the work function can be monitored to understand how the modification changed the energetics of photoelectron ejection.

Fourier-transform infrared (FTIR) spectroscopy is a technique that measures the amount of IR light absorbed by a sample.[60] Molecules will undergo different types of vibrational modes depending on their electronic structure. IR spectroscopy is sensitive to molecules with dipole moments. For example, CO_2 has two stretching modes, symmetric or asymmetric, but only the asymmetric stretching mode is IR active because that mode has a change in dipole associated with it whereas the symmetric stretch does not. Therefore, this technique is useful when

determining functional groups present in material. When coupled with an attenuated total reflectance (ATR) accessory, this technique can be used to measure surface modifications of thin films.[61] Infra-red reflection-absorption spectroscopy (IRRAS) is a technique that is sensitive to the orientation of molecules at a modified surface.[62] However, both ATR and IRRAS are not very sensitive to sub-monolayer coverage making it only ideal for materials modified with a full monolayer.

4.3 Cyclic Voltammetry

As electron transfer processes are what define the efficiency for a DSSC, it is important to use a characterization technique that can assess the electron kinetics of the modified material when employed as an electrode. Cyclic voltammetry measures the current response of a redox active analyte when a triangular potential wave is applied with respect to time.[63] Conventional cyclic voltammograms of diffusion-limited electron transfer are characterized by their "duck-like" shape and have a peak-to-peak separation of 57 mV/*n*, where *n* is the number of electrons being transferred during the reduction (or oxidation) process. However, a surface-bound electron transfer process should ideally have a peak-to-peak separation of 0 mV, as there are no diffusion-limiting processes occurring.[64] Interestingly, this 0 mV is rarely observed experimentally as there are non-idealities in surface-bound electron transfer.[40,56,73–76,65–72] CV data of a modified surface allows for quantification of surface coverage, via the integration of the current resulting in charge. By obtaining data at multiple scan rates, a rate constant can be determined through analysis of a "trumpet" plot.[77] Therefore, CV is an excellent technique when assessing the electron transfer kinetics between a surface-bound species and electrodes making it an ideal method to characterize materials for DSSCs.

4.4 Other Methods

An additional surface-centric method called goniometry measures the contact angle of a water droplet on a modified material to assess the relative degree of hydrophobicity.[78,79] This technique is a simple and rapid way to assess changes in the chemical composition of modified surface, but it is important to couple AFM measurements with this analysis as it is also sensitive to changes in roughness. This technique also gives a macroscopic analysis of the surface; therefore, this technique cannot detect if the coverage is homogenous or heterogeneous given the averaging effect of the analysis.

5. Overview of Work

The goal of this work was to identify and characterize new chemical modification approaches for aC films (**Figure 4**), providing alternative strategies for linking chromophores to a surface via a monolayer. The first three chapters of this work focus on click chemistries, specifically the thiol-ene and azide-alkyne click reaction. The fourth chapter utilizes an *in-situ* Grignard reaction for chemical modification. Within these chapters, the surface modifications were robustly characterized with water contact, AFM, XPS, UPS, SEM, and electrochemistry. When feasible, these modified materials were examined as electrode materials to evaluate electron transfer reactions for molecules bound to a surface. To determine the robustness of each surface modification, they were each evaluated using the following four criteria when experimentally possible: selectivity, surface coverage, stability, and electron transfer kinetics. These four themes dictated the direction of the work after the completion of each chapter. For example, chapter two introduced a chemical approach involving the modification of aC films with thiol groups to perform thiol-ene click reactions. While this modification was successful, it did not rank highly

in any of the four criteria. Chapter three introduces the modification of aC films with vinyl groups to perform thiol-ene click reactions. This approach improved on stability and surface coverage, but not in the other two criteria. Chapter four illustrates the surface modification of aC films with azide groups to perform azide-alkyne click chemistry. This approach improved on selectivity, but was not as robust in the other three criteria. Finally, chapter five introduces an approach to modify aC films via an *in-situ* Grignard; this reaction greatly improved on each of the four criteria.

Overall, this work offers promising new chemistries for the selective modification of aC films to form stable attachment between dye molecules and the semiconductor surface. The hope is that these aC films could be a promising alternative to metal oxide materials in dye-sensitized solar cells, as they offer more robust surface chemistries with greater stability.

5. Figures

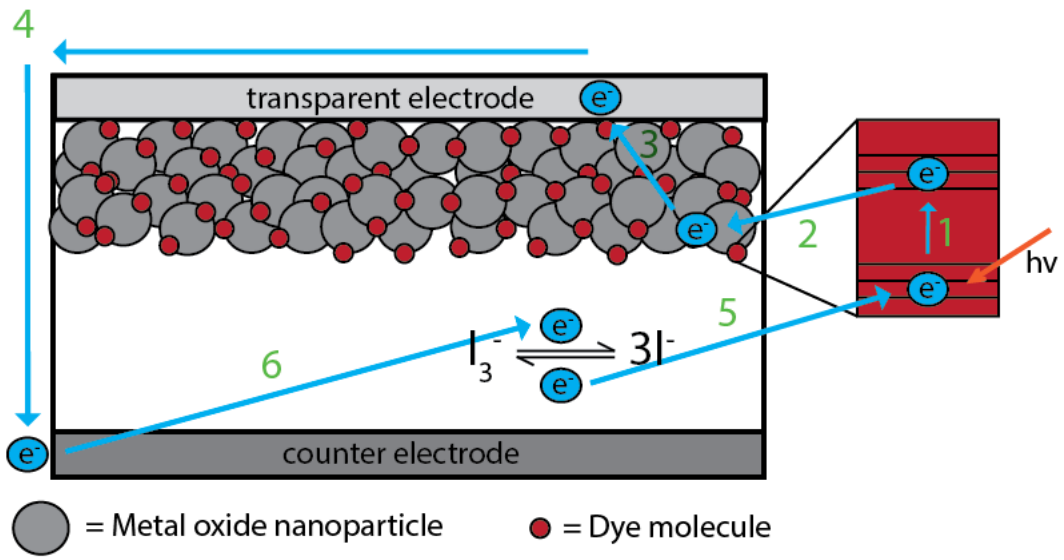

Figure 1.1. Diagram of a dye-sensitized solar cell showing the different electron transfer processes: (1) upon photo-excitation, an electron in a dye molecule is excited from its highest occupied molecular orbital (HOMO) to its lowest unoccupied molecular orbital (LUMO); (2) this electron is injected into the conduction band of the metal oxide nanoparticle; (3) the electron travels through the metal oxide material and the transparent electrode; (4) the electron travels through external circuitry where work is done; (5) the redox couple reduces the oxidized dye; and (6) then the couple is regenerated at the counter electrode.

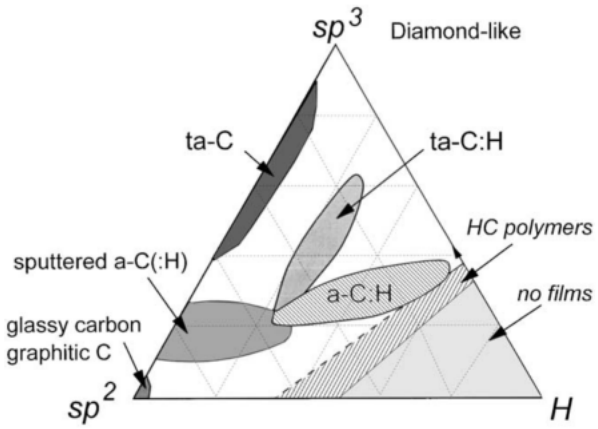

Figure 1.2. Ternary phase diagram of amorphous carbon. Reprinted from[25] with permission.

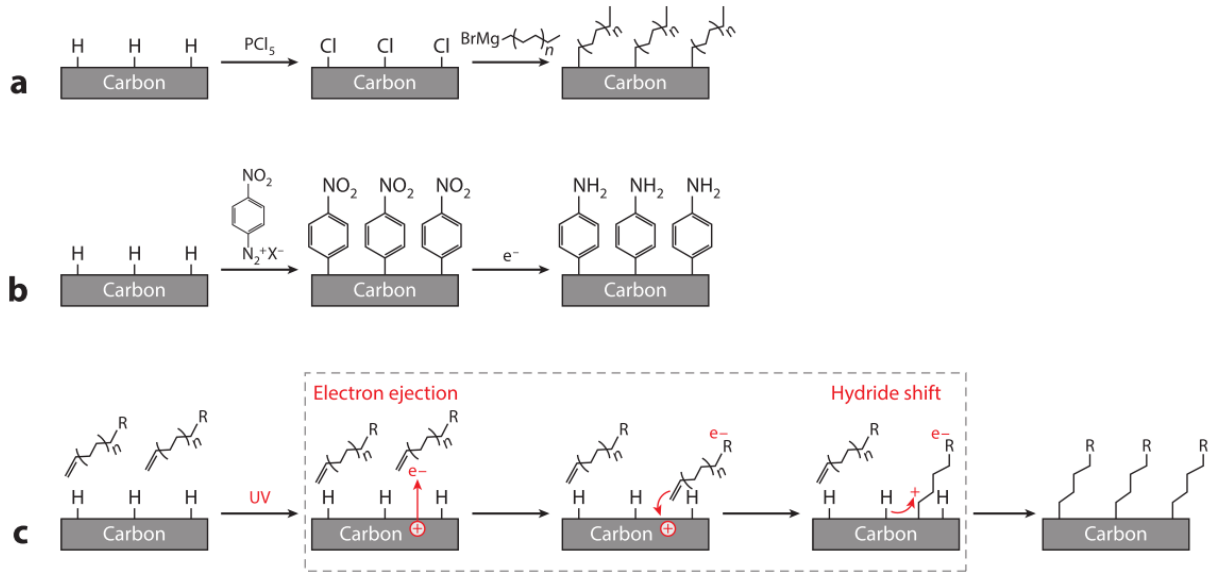

Figure 1.3. Modification strategies for carbon-based materials: (a) Grignard reactions via a halogenation step; (b) aryl diazonium salt reductions; and (c) photochemical attachment of alkenes. Reprinted from[24] with permission.

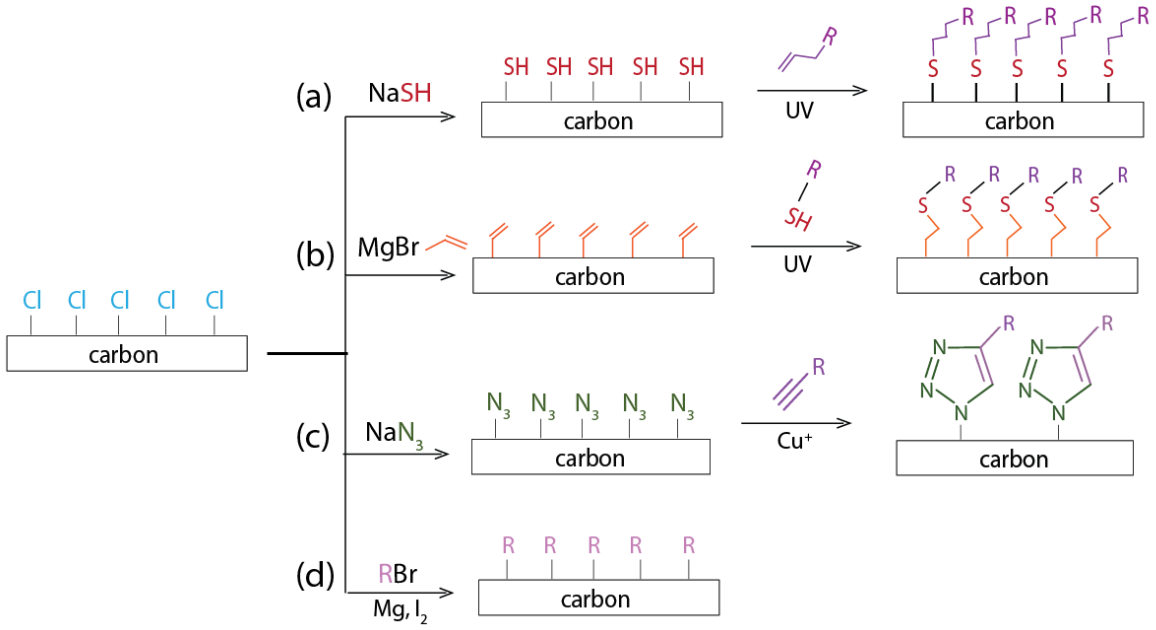

Figure 1.4. Overview of modification schemes presented in this work: (a) thiol-ene click modification via a thiol termination; (b) thiol-ene click modification via a vinyl termination; (c) azide-alkyne click modification via an azide-termination; and (d) in-situ Grignard modification.

REFERENCES

1. [Masson-Delmotte, V., P. Zhai, H.-O. Pörtner, D. Roberts, J. Skea, P.R. Shukla, A. P.; W. Moufouma-Okia, C. Péan, R. Pidcock, S. Connors, J.B.R. Matthews, Y. Chen, X. Zhou, M.I. Gomis, E. L.; T. Maycock, M. Tignor, and T. W. (eds. . *IPCC, 2018: Summary for Policymakers. In: Global Warming of 1.5°C. An IPCC Special Report on the Impacts of Global Warming of 1.5°C above Pre-Industrial Levels and Related Global Greenhouse Gas Emission Pathways, in the Context of Strengthening the Global*; Geneva, Switzerland, 2018.

2. Grätzel, M. Recent Advances in Sensitized Mesoscopic Solar Cells. *Acc. Chem. Res.* **2009**, *42* (11), 1788–1798.

3. Green, M. A.; Hishikawa, Y.; Dunlop, E. D.; Levi, D. H.; Hohl-Ebinger, J.; Yoshita, M.; Ho-Baillie, A. W. Y. Solar Cell Efficiency Tables (Version 53). *Prog. Photovoltaics Res. Appl.* **2019**, *27* (1), 3–12.

4. Goncalves, L. M.; De Zea Bermudez, V.; Ribeiro, H. A.; Mendes, A. M. Dye-Sensitized Solar Cells: A Safe Bet for the Future. *Energy Environ. Sci.* **2008**, *1* (6), 655–667.

5. Yang, S.; Fu, W.; Zhang, Z.; Chen, H.; Li, C. Z. Recent Advances in Perovskite Solar Cells: Efficiency, Stability and Lead-Free Perovskite. *J. Mater. Chem. A* **2017**, *5* (23), 11462–11482.

6. O'Regan, B.; Gratzel, M. A Low-Cost, High-Efficiency Solar-Cell Based on Dye-Sensitized Colloidal TiO_2 Films. *Nature* **1991**, *353* (6346), 737–740.

7. Hardin, B. E.; Snaith, H. J.; McGehee, M. D. The Renaissance of Dye-Sensitized Solar Cells. *Nat. Photonics* **2012**, *6* (3), 162–169.

8. Nikiforov, M. P.; Zerweck, U.; Milde, P.; Loppacher, C.; Park, T. H.; Uyeda, H. T.; Therien, M. J.; Eng, L.; Bonnell, D. The Effect of Molecular Orientation on the Potential of Porphyrin-Metal Contacts. *Nano Lett.* **2008**, *8* (1), 110–113.

9. Johansson, P. G.; Kopecky, A.; Galoppini, E.; Meyer, G. J. Distance Dependent Electron Transfer at TiO2interfaces Sensitized with Phenylene Ethynylene Bridged RuII-Isothiocyanate Compounds. *J. Am. Chem. Soc.* **2013**, *135* (22), 8331–8341.

10. Hyde, J. T.; Hanson, K.; Vannucci, A. K.; Lapides, A. M.; Alibabaei, L.; Norris, M. R.; Meyer, T. J.; Harrison, D. P. Electrochemical Instability of Phosphonate-Derivatized, Ruthenium(III) Polypyridyl Complexes on Metal Oxide Surfaces. *ACS Appl. Mater. Interfaces* **2015**, *7* (18), 9554–9562.

11. Jose, R.; Thavasi, V.; Ramakrishna, S. Metal Oxides for Dye-Sensitized Solar Cells. *J. Am. Ceram. Soc.* **2009**, *92* (2), 289–301.

12. Benkstein, K. D.; Kopidakis, N.; van de Lagemaat, J.; Frank, A. J. Influence of the Percolation Network Geometry on Electron Transport in Dye-Sensitized Titanium

Dioxide Solar Cells. *J. Phys. Chem. B* **2003**, *107* (31), 7759–7767.

13. Pujari, S. P.; Scheres, L.; Marcelis, A. T. M.; Zuilhof, H. Covalent Surface Modification of Oxide Surfaces Angewandte. *Angew. Chemie Int. Ed.* **2014**, *53*, 6322–6356.

14. Vilan, B. A.; Yaffe, O.; Biller, A.; Salomon, A.; Kahn, A.; Cahen, D. Molecules on Si : Electronics with Chemistry. *Adv. Mater.* **2010**, *22*, 140–159.

15. Bent, S. F. Organic Functionalization of Group IV Semiconductor Surfaces: Principles, Examples, Applications, and Prospects. *Surf. Sci.* **2002**, *500* (1–3), 879–903.

16. Hamers, R. J. Formation and Characterization of Organic Monolayers on Semiconductor Surfaces. *Annu. Rev. Anal. Chem.* **2008**, *1*, 707–736.

17. Cao, X.; Coulter, S. K.; Ellison, M. D.; Liu, H.; Liu, J.; Hamers, R. J. Bonding of Nitrogen-Containing Organic Molecules to the Silicon(001) Surface: The Role of Aromaticity. *J. Phys. Chem. B* **2001**, *105* (18), 3759–3768.

18. Coulter, S. K.; Schwartz, M. P.; Hamers, R. J. Sulfur Atoms as Tethers for Selective Attachment of Aromatic Molecules to Silicon(001) Surfaces. *J. Phys. Chem. B* **2002**, *105* (15), 3079–3087.

19. Casaletto, M. P.; Carbone, M.; Piancastelli, M. N.; Horn, K.; Weiss, K.; Zanoni, R. A High Resolution Photoemission Study of Phenol Adsorption on Si(1 0 0)2 × 1. *Surf. Sci.* **2005**, *582* (1–3), 42–48.

20. Rummel, R. M.; Ziegler, C. Room Temperature Adsorption of Aniline (C6H5NH2) on Si(100)(2 × 1) Observed with Scanning Tunneling Microscopy. *Surf. Sci.* **1998**, *418* (1), 303–313.

21. Linford, M. R.; Chidsey, C. E. D. Alkyl Monolayers Covalently Bonded to Silicon Surfaces. *J. Am. Chem. Soc.* **1993**, *115* (26), 12631–12632.

22. Sieval, A. B.; Demirel, A. L.; Nissink, J. W. M.; Linford, M. R.; van der Maas, J. H.; de Jeu, W. H.; Zuilhof, H.; Sudhölter, E. J. R. Highly Stable Si−C Linked Functionalized Monolayers on the Silicon (100) Surface. *Langmuir* **1998**, *14* (7), 1759–1768.

23. Effenberger, F.; Götz, G.; Bidlingmaier, B.; Wezstein, M. Photoactivated Preparation and Patterning of Self-Assembled Monolayers with 1-Alkenes and Aldehydes on Silicon Hydride Surfaces. *Agnew. Chem. Int. Ed.* **1998**, *37* (18), 2462–2464.

24. Lockett, M. R.; Smith, L. M. Carbon Substrates: A Stable Foundation for Biomolecular Arrays. *Annu. Rev. Anal. Chem.* **2015**, *8* (1), 263–285.

25. Robertson, J. Diamond-like Amorphous Carbon. *Mater. Sci. Eng.* **2002**, *37*, 129–281.

26. Wächter, N.; Munson, C.; Jarošová, R.; Berkun, I.; Hogan, T.; Rocha-Filho, R. C.; Swain, G. M. Structure, Electronic Properties, and Electrochemical Behavior of a Boron-

Doped Diamond/Quartz Optically Transparent Electrode. *ACS Appl. Mater. Interfaces* **2016**, *8*, 28325–28337.

27. Zhu, D.; Zhang, L.; Ruther, R. E.; Hamers, R. J. Photo-Illuminated Diamond as a Solid-State Source of Solvated Electrons in Water for Nitrogen Reduction. *Nat. Mater.* **2013**, *12* (9), 836–841.

28. Yang, W.; Auciello, O.; Butler, J. E.; Cai, W.; Carlisle, J. A.; Gerbi, J. E.; Gruen, D. M.; Knickerbocker, T.; Lasseter, T. L.; Russell, J. N.; et al. DNA-Modified Nanocrystalline Diamond Thinfilms as Stable, Biologically Active Substrates. *Nat. Mater.* **2002**, *1*, 253–257.

29. Wang, J.; Firestone, M. A.; Auciello, O.; Carlisle, J. A. Surface Functionalization of Ultrananocrystalline Diamond Films by Electrochemical Reduction of Aryldiazonium Salts. *Langmuir* **2004**, *20* (26), 11450–11456.

30. Lud, S. Q.; Steenackers, M.; Jordan, R.; Bruno, P.; Gruen, D. M.; Feulner, P.; Garrido, J. a.; Stutzmann, M. Chemical Grafting of Biphenyl Self-Assembled Monolayers on Ultrananocrystalline Diamond. *J. Am. Chem. Soc.* **2006**, *128* (51), 16884–16891.

31. Kuila, T.; Bose, S.; Kumar, A.; Khanra, P.; Kim, N. H.; Lee, J. H. Chemical Functionalization of Graphene and Its Applications. *Prog. Mater. Sci.* **2012**, *57* (7), 1061–1105.

32. Mccreery, R. L. Advanced Carbon Electrode Materials for Molecular Electrochemistry Advanced Carbon Electrode Materials for Molecular Electrochemistry. *Chem. Rev.* **2008**, *108*, 2646–2687.

33. Kuila, T. Bose, S. Mishra, A. K. Khanra, P. Kim, N. H. Lee, J. H. Chemical Functionalization of Graphene and Its Applications. *Prog. Mater. Sci.* **2012**, *57* (7), 1061–1105.

34. Bekyarova, E.; Itkis, M. E.; Ramesh, P.; Berger, C.; Sprinkle, M.; Heer, W. A. De; Haddon, R. C. Chemical Modification of Epitaxial Graphene : Spontaneous Grafting of Aryl Groups. *J. Am. Chem. Soc.* **2009**, *131*, 1336–1337.

35. Stankovich, S.; Dikin, D. A.; Dommett, G. H. B.; Kohlhaas, K. M.; Zimney, E. J.; Stach, E. A.; Piner, R. D.; Nguyen, S. T.; Ruoff, R. S. Graphene-Based Composite Materials. *Nature* **2006**, *442* (July).

36. Georgakilas, V. Bourlinos, A. B. Zboril, R. Steriotis, T. A. Dallas, P. Stubos, A. K. Trapalis, C. Organic Functionalisation of Graphenes. *Chem. Commun.* **2010**, *46*, 1766–1768.

37. Saby, C.; Ortiz, B.; Champagne, G. Y.; Be, D. Electrochemical Modification of Glassy Carbon Electrode Using Aromatic Diazonium Salts . 1 . Blocking Effect of 4-Nitrophenyl and 4-Carboxyphenyl Groups. *Langmuir* **1997**, *13*, 6805–6813.

38. Debela, A. M.; Ortiz, M.; Beni, V.; O'Sullivan, C. K. Facile Electrochemical Hydrogenation and Chlorination of Glassy Carbon to Produce Highly Reactive and Uniform Surfaces for Stable Anchoring of Thiolated Molecules. *Chem. - A Eur. J.* **2014**, *20* (25), 7646–7654.

39. Bansal, A.; Li, X.; Lauermann, I.; Lewis, N. S. Alkylation of Si Surfaces Using a Two-Step Halogenation / Grignard Route. *J. Am. Chem. Soc.* **1996**, *118* (11), 7225–7226.

40. Yu, S. S. C.; Downard, A. J. Photochemical Grafting and Activation of Organic Layers on Glassy Carbon and Pyrolyzed Photoresist Films. *Langmuir* **2007**, *23*, 4662–4668.

41. Peng, X. .; Barber, Z. .; Clyne, T. . Surface Roughness of Diamond-like Carbon Films Prepared Using Various Techniques. *Surf. Coatings Technol.* **2001**, *138* (1), 23–32.

42. Schlesinger, R.; Bruns, M.; Ache, H. Development of Thin Film Electrodes Based on Sputtered Amorphous Carbon. *J. Electrochem. Soc.* **1997**, *144* (1), 6.

43. Lockett, M. R.; Smith, L. M. Attaching Molecules to Chlorinated and Brominated Amorphous Carbon Substrates via Grignard Reactions. *Langmuir* **2009**, *25* (6), 3340–3343.

44. Lockett, M. R.; Smith, L. M. Formation and Stability of Alkylthiol Monolayers on Carbon Substrates. *J. Phys. Chem. C* **2010**, *114* (29), 12635–12641.

45. Murphy, D. M.; Cullen, R. J.; Jayasundara, D. R.; Scanlan, E. M.; Colavita, P. E. Study of the Spontaneous Attachment of Polycyclic Aryldiazonium Salts onto Amorphous Carbon Substrates. *RSC Adv.* **2012**, *2* (16), 6527.

46. Colavita, P. E.; Sun, B.; Tse, K. Y.; Hamers, R. J. Photochemical Grafting of N-Alkenes onto Carbon Surfaces: The Role of Photoelectron Ejection. *J. Am. Chem. Soc.* **2007**, *129* (44), 13554–13565.

47. Colavita, P. E.; Sun, B.; Wang, X.; Hamers, R. J. Influence of Surface Termination and Electronic Structure on the Photochemical Grafting of Alkenes to Carbon Surfaces. *J. Phys. Chem. C* **2009**, *113* (4), 1526–1535.

48. Brennan, L. J.; Byrne, M. T.; Bari, M.; Gun'ko, Y. K. Carbon Nanomaterials for Dye-Sensitized Solar Cell Applications: A Bright Future. *Adv. Energy Mater.* **2011**, *1* (4), 472–485.

49. Bernardi, M.; Lohrman, J.; Kumar, P. V.; Kirkeminde, A.; Ferralis, N.; Grossman, J. C.; Ren, S. Nanocarbon-Based Photovoltaics. *ACS Nano* **2012**, *6* (10), 8896–8903.

50. Jensen, D. S.; Kanyal, S. S.; Madaan, N.; Hancock, J. M.; Dadson, A. E.; Vail, M. A.; Vanfleet, R.; Shutthanandan, V.; Zhu, Z.; Engelhard, M. H.; et al. Multi-Instrument Characterization of the Surfaces and Materials in Microfabricated, Carbon Nanotube-Templated Thin Layer Chromatography Plates. An Analogy to "The Blind Men and the Elephant." *Surf. Interface Anal.* **2013**, *45* (8), 1273–1282.

51. Thevuthasan, S.; Kuchibhatla, S. V. N. T.; Karakoti, A.; Baer, D. R.; Wang, H.; Elder, A.; Mueller, K.; Lai, J.; Baisch, B. L.; Moon, D.; et al. Surface Characterization of Nanomaterials and Nanoparticles: Important Needs and Challenging Opportunities. *J. Vac. Sci. Technol. A Vacuum, Surfaces, Film.* **2013**, *31* (5), 050820.

52. Binnig, G.; Quate, C. F.; Gerber, C. Atomi Force Microscope. *Phys. Rev. Lett.* **1986**, *56* (9).

53. Giessibl, F. J. Advances in Atomic Force Microscopy. *Rev. Mod. Phys.* **2003**, *75*, 949–983.

54. Suganuma, T. Measurement of Surface Topography Using SEM with Two Secondary Electron Detectors Tadao. *J. Electron Microsc. (Tokyo).* **1985**, *34* (4), 328–337.

55. Goldstein, J. I. Newbury, D. E. Michael, J. R. Ritchie, N. W. M. Scott, J. H. J. Joy, D. C. *Scanning Electron Microscopy and X-Ray Microanalysis*, 4th ed.; Springer Science+Business Media LLC: Newy York City, 2017.

56. Fabre, B.; Pujari, S. P.; Scheres, L.; Zuilhof, H. Micropatterned Ferrocenyl Monolayers Covalently Bound to Hydrogen-Terminated Silicon Surfaces: Effects of Pattern Size on the Cyclic Voltammetry and Capacitance Characteristics. *Langmuir* **2014**, *30* (24), 7235–7243.

57. Maat, J. ter; Yang, M.; Scheres, L.; Kuypers, S.; Zuilhof, H. Light-Enhanced Microcontact Printing of 1-Alkynes onto Hydrogen-Terminated Silicon. *Chem. Commun. (Camb).* **2010**, *46* (42), 8005–8007.

58. Moulder, J. F.; Stickle, W. F.; Sobol, P. E.; Bomben, K. D. *Handbook of X-Ray Photoelectron Spectroscopy*; 1995.

59. Ishii, B. H.; Sugiyama, K.; Ito, E.; Seki, K. Energy Level Alignment and Interfacial Electronic Structures at Organic / Metal and Organic / Organic Interfaces **. *Adv. Mater.* **1999**, *11*, 605–625.

60. Skoog, D. A. Holler, F. J. Crouch, S. R. *Principles of Instrumental Analysis*; Cengage learning, 2017.

61. Harrick, N. J.; Beckmann, K. H. *Internal Reflection Spectroscopy*; Kane, P. F. ., Larrabee, G. B., Eds.; Springer: Boston, MA, 1974.

62. Greenler, R. G. Infrared Study of Adsorbed Molecules on Metal Surfaces by Reflection Tehniques. *J. Chem. Phys.* **1966**, *44* (1), 310–315.

63. Elgirshi, N.; Rountree, K. J.; Mccarthy, B. D.; Rountree, E. S.; Eisenhart, T. T.; Dempsey, J. L. A Practical Beginner ’ s Guide to Cyclic Voltammetry. *J. Chem. Educ.* **2018**, *95*, 197–206.

64. Finklea, H. O. Hanshew, D. D. Electron-Transfer Kinetics in Organized Thiol Monolayer

with Attached Pentaamine(Pyridine)Ruthenium Redox Centers. *J. Am. Chem. Soc.* **1992**, *114* (4), 3173–3181.

65. Hanna, C. M.; Sanborn, C. D.; Ardo, S.; Yang, J. Y. Interfacial Electron Transfer of Ferrocene Immobilized onto Indium Tin Oxide through Covalent and Noncovalent Interactions. *ACS Appl. Mater. Interfaces* **2018**, *10* (15), 13211–13217.

66. Li, C.; Ren, B.; Zhang, Y.; Cheng, Z.; Liu, X.; Tong, Z. A Novel Ferroceneylazobenzene Self-Assembled Monolayer on an ITO Electrode : Photochemical and Electrochemical Behaviors. *Langmuir* **2008**, *24*, 12911–12918.

67. Wu, L.; Eberhart, M.; Shan, B.; Nayak, A.; Brennaman, M. K.; Miller, A. J. M.; Shao, J.; Meyer, T. J. Stable Molecular Surface Modification of Nanostructured, Mesoporous Metal Oxide Photoanodes by Silane and Click Chemistry. *ACS Appl. Mater. Interfaces* **2019**, *11* (4), 4560–4567.

68. Ruther, R. E.; Cui, Q.; Hamers, R. J. Conformational Disorder Enhances Electron Transfer through Alkyl Monolayers: Ferrocene on Conductive Diamond. *J. Am. Chem. Soc.* **2013**, *135* (15), 5751–5761.

69. Meziane, D.; Barras, A.; Kromka, A.; Houdkova, J.; Boukherroub, R.; Szunerits, S. Thiol-Yne Reaction on Boron-Doped Diamond Electrodes: Application for the Electrochemical Detection of DNA-DNA Hybridization Events. *Anal. Chem.* **2012**, *84* (1), 194–200.

70. Das, M. R.; Wang, M.; Szunerits, S.; Gengembre, L.; Boukherroub, R. Clicking Ferrocene Groups to Boron-Doped Diamond Electrodes. *Chem. Commun. (Camb).* **2009**, No. 19, 2753–2755.

71. Evrard, D.; Lambert, F.; Policar, C.; Balland, V.; Limoges, B. Electrochemical Functionalization of Carbon Surfaces by Aromatic Azide or Alkyne Molecules: A Versatile Platform for Click Chemistry. *Chem. - A Eur. J.* **2008**, *14* (30), 9286–9291.

72. McKenas, C. G.; Fehr, J. M.; Donley, C. L.; Lockett, M. R. Thiol-Ene Modified Amorphous Carbon Substrates: Surface Patterning and Chemically Modified Electrode Preparation. *Langmuir* **2016**, *32* (41), 10529–10536.

73. Fehr, J. M.; McKenas, C. G.; Liu, B.; Lockett, M. R. Azide-Alkyne Click Reactions to Prepare Chemically Modified Amorphous Carbon Electrodes. *Appl. Surf. Sci.* https://doi.org/10.1016/j.apsusc.2019.02.151.

74. Landis, E. C.; Harriers, R. J. Covalent Grafting of Redox-Active Molecules to Vertically Aligned Carbon Nanofiber Arrays via “Click” Chemistry. *Chem. Mater.* **2009**, *21* (4), 724–730.

75. Li, F.; Basile, V. M.; Pekarek, R. T.; Rose, M. J. Steric Spacing of Molecular Linkers on Passivated Si(111) Photoelectrodes. *ACS Appl. Mater. Interfaces* **2014**, *6* (22), 20557–20568.

76. Kang, O. S.; Bruce, J. P.; Herbert, D. E.; Freund, M. S. Covalent Attachment of Ferrocene to Silicon Microwire Arrays. *ACS Appl. Mater. Interfaces* **2015**, *7* (48), 26959–26967.

77. Nicholson, R. S. Theory and Application of Cyclic Voltammetry for Measurement of Electrode Reaction Kinetics. *Anal. Chem.* **1965**, *37* (11), 1351–1355.

78. Cassie, A. B. D. Baxter, S. Wettability of Porous Surfaces. *Trans. Faraday Soc.* **1944**, *40*, 546–551.

79. Wenzel, R. N. Resistance of Solid Surfaces to Wetting by Water. *Ind. Eng. Chem.* **1936**, *28* (8), 988–994.

CHAPTER 2-THIOL-ENE MODIFIED AMORPHOUS CARBON SUBSTRATES: SURFACE PATTERNING AND CHEMICALLY MODIFIED ELECTRODE PREPARATION[1]

1. Introduction

The reliance of the microelectronics industry on silicon has prompted a number of chemical strategies to passivate its surface.[1–3] While many of these surface chemistries reduce the rate of silicon oxide formation, they cannot prevent it from occurring. Carbon-based materials are an attractive alternative to silicon because their electronic properties are tunable, they are relatively chemically inert, and they do not readily oxidize under ambient conditions or when interfaced with aqueous solutions.[4–6] Thin films of amorphous carbon (aC) have been applied to a number of materials, imparting the chemical stability of carbon while preserving the chemical and physical properties of the underlying substrate.

The electronic, optical, and chemical properties of can be experimentally controlled through the introduction of particular functional groups.[5,7,8] Photo-catalyzed reactions are an attractive means of selectively patterning surfaces with different functional groups or molecules of interest. Alkene-containing molecules have been directly attached to the surface of diamond and amorphous carbon substrates with an ultraviolet (UV) light-catalyzed reaction. The conditions needed to promote this reaction (λ=254 nm, greater than 12 hours) limit the types of functional groups that can be introduced to the surface. There is a need for alternative chemistries capable of modifying the surfaces of carbon-based materials, in a photo-addressable manner.

[1] This article previously appeared as an article in Langmuir. The original citation is as follows: McKenas, C. G.; Fehr, J. M.; Donley, C. L.; Lockett, M. R. Thiol-Ene Modified Amorphous Carbon Substrates: Surface Patterning and Chemically Modified Electrode Preparation. *Langmuir* **2016**, *32* (41), 10529–10536

Due to their selective reactivity, thiol-click chemistries[9,10] are an attractive means of modifying the surface of aC films. The thiol-ene reaction involves the addition of a thiol radical across an alkene. This particular reaction is appealing for surface modification because it is rapid, largely independent of solvent, and compatible with photo-patterning as the reaction is initiated with near-UV light.[11] We present here a chemical strategy for modifying the surface of aC films with thiol-ene chemistries by first installing terminal thiol groups with a two-step wet chemical process. Similar two-step strategies have been used to modify the surfaces of carbon, silicon, and germanium substrates with Grignard reagents or alkanethiols.[12–17] Unlike previously described methods of preparing thiol-modified carbon nanotubes or nanodiamond substrates,[18–20] our strategy does not expose the surface or its underlying substrate to prolonged exposure of harsh chemical conditions.

Variations of thiol-ene reactions have been used to append organic and biological molecules to the surfaces of silicon, glass, diamond, and polymeric materials such as polyethylene terephthalate (PET).[21–32] Our strategy also differs significantly from these previously reported examples because: i) We install terminal thiols on the surface, instead of alkene groups. The thiol groups expand the possible attachment chemistries that can be utilized because the surface is not only compatible with thiol-ene reactions, but also Michael additions and the formation of disulfide bonds. ii) We install the terminal thiols directly onto the surface, eliminating the need for chemical spacers present in other examples. Several studies have shown that the length of the chemical spacer separating the surface and the molecule of interest can greatly affect its reactivity and its charge transport properties.[33]

Here, we thoroughly characterize aC films during the thiolation process, optimize the reaction conditions needed to modify them with thiol-ene reactions, and demonstrate the utility

of these thiol-terminated surfaces with examples of photo-patterning and the preparation of chemically modified electrodes.

2. Experimental Section

2.1 Chemicals and materials.

All reagents were used as received, unless otherwise noted. Acetonitrile, dimethyl sulfoxide (DMSO), ethanol (200 proof), hydrogen peroxide (30%), sodium chloride, sodium hydrosulfide flakes, and conc. sulfuric acid were purchased from Fisher Scientific. Anhydrous benzene, benzoyl peroxide, 1-bromoundecane, 11-bromo-1-undecene (BUD), 2,2-dimethoxy-2-phenylacetophenone (DMPA), anhydrous *N*,*N*-dimethyl formamide (DMF), phosphorus pentachloride, tetrabutyl ammonium iodide (TBAI), tetrabutyl ammonium perchlorate, and vinylferrocene were purchased from Sigma-Aldrich.

2.2 Thin film preparation and modification.

Thin films of 25 nm amorphous carbon were deposited onto silicon (100) substrates, by DC magnetron sputtering (Kurt Lesker PVD 75) a graphite target (Plasmaterials). The chamber was kept under argon at a base pressure of $5x10^{-5}$ Torr and a deposition pressure of $3x10^{-3}$ Torr. Prior to usage, all silicon and quartz substrates were cleaned in piranha solution (3:1, 96.3% H_2SO_4: 30% H_2O_2) at 160°C for 20 minutes. **Caution: piranha solutions react violently with many organic materials and should be handled with extreme care.**

Amorphous carbon films were hydrogen terminated in a 13.56 MHz inductively coupled hydrogen plasma (Diener Electronic) for 10 minutes prior to usage. The films were chlorine-terminated in a nitrogen-purged reaction vessel containing a 5:1 volume ratio of 100 mM PCl_5

and 40 mM benzoyl peroxide in anhydrous benzene (80°C, 1 hour). Films were rinsed in ethanol and dried under a stream of nitrogen before being placed in a nitrogen-purged reaction vessel containing 10 mM TBAI and 500 mM sodium hydrosulfide in anhydrous DMF. Thiolation reaction conditions were 50°C for 8 hours, unless otherwise noted. The surfaces were rinsed with water and ethanol and dried under a stream of nitrogen prior to characterization or further chemical modification.

To attach alkene-containing molecules to the thiol-terminated surfaces, each surface was spotted with 4-6 µL of a neat alkene liquid. In some reactions the alkene liquid contained 1% (w/w) of a radical initiator, DMPA. A quartz coverslip (0.50 mm thickness, Ted Pella) was placed on the films to ensure homogeneous coverage of organic liquid across the surface, and illuminated with a mercury arc lamp (Newport, 275 W) equipped with a 300 ± 100 nm dichroic filter. A 360 ± 15 nm bandpass filter (Newport) was used in some experiments, as noted. Surfaces were sonicated in ethanol to remove non-specifically adsorbed organic molecules, rinsed with ethanol, and dried under a stream of nitrogen prior to analysis. TEM grids (SPI Supplies) were utilized in surface photo-patterning experiments.

2.3 Thin film characterization.

Static water contact angles were measured from 1 µL droplets of RO water using a Ramé Hart goniometer equipped with DropImageCA software. Reported values are the average of at least three droplets, placed in different regions of the surface. Scanning electron microscopy (SEM) images were acquired with a Hitachi S-4700 Cold Cathode Field Emission SEM at an accelerating voltage of 2.0 kV.

X-ray photoelectron (XP) spectroscopic characterization was carried out in an ultrahigh vacuum system (Kratos Axis Ultra DLD) with a base pressure of $5x10^{-9}$ Torr, a monochromatic Al Kα source, and a hemispherical analyzer. Survey (1.0 eV resolution) and high-resolution (0.1 eV resolution) spectra were collected at a 0° takeoff angle from surface normal and analyzed with Kratos Vision 2.0 software. Each high-resolution spectrum was referenced to the C1s peak (284.6 eV) and fit with Voigt functions (70% Gaussian, 30% Lorentzian) after a Shirley background correction.

Atomic force microscopy (AFM) images were obtained on an Asylum Research MFP3D AFM. Tapping mode measurements were acquired with an aluminum reflex-coated silicon cantilever (force constant of 40 N/m) at a resonant frequency of 300 kHz. Reported roughness values are the average and standard deviation of three separate 5x5 µm regions on the same surface.

Electrochemical measurements were performed using a three-electrode Teflon cell attached to a WaveNano potentiostat (Pine). Copper tape was used to make an ohmic connection with the aC working electrode (0.13 cm^2 working area). The auxiliary electrode was a platinum coil and the reference was Ag/AgCl (3 M NaCl). Tetrabutyl ammonium perchlorate (0.1 M) in anhydrous acetonitrile was used as the supporting electrolyte. Data was analyzed using AfterMath (Pine).

2.4 Statistical tests.

To examine statistical significance, a two-tailed t-test was used to compare each set of reaction conditions, unless otherwise noted. Reported values are the average and standard deviation of n = 3 surfaces, unless otherwise noted. Statistically significant values are defined as $p < 0.05$.

3. Results and Discussion

3.1 Thiol-terminated aC film preparation and characterization.

We prepared amorphous carbon thin films by magnetron sputtering a graphite target under an argon atmosphere onto freshly cleaned Si(100) substrates. Each film underwent a series of chemical modifications to yield a thiol-terminated surface compatible with thiol-ene reactions (**Scheme 1**). To ensure substrates prepared at different times had a similar chemical composition, we placed each film in an RF-generated hydrogen plasma. Next, the aC films were chlorinated in a PCl_5-containing solution. Lastly, the surface-bound chlorine atoms were replaced with thiols by incubating the aC films in a solution containing NaSH and TBAI.

We utilized a number of surface techniques to characterize the aC films after each chemical modification: hydrogen termination (H-aC), chlorination (Cl-aC), and thiolation (HS-aC). XP spectroscopy confirmed the attachment of the chlorine atoms or thiol groups to the surface and was used to estimate monolayer coverage with a previously described overlayer model.[34] AFM and static water contact angle measurements determined the root mean square (RMS) roughness of the films and their wettability, respectively.

3.1.1 XP spectroscopic analysis.

Incubating the H-aC films in the presence of phosphorous pentachloride and benzoyl peroxide yielded 0.52 ± 0.10 monolayers of chlorine atoms (**Table 1**). The binding energy of the Cl2p electrons (200.0 eV) is consistent with the formation of chlorine-carbon bonds. Confirming the presence of carbon-chlorine bonds from the high-resolution spectrum of C1s electrons is somewhat difficult as carbon-chlorine and carbon-oxygen species have similar binding energies

(~286.0 eV). Survey XP spectra reveal the carbon-to-oxygen and carbon-to-nitrogen ratios on the aC films did not significantly change after chlorination, allowing us to attribute changes in the C1s spectrum to the formation of C-Cl bonds (Figure S2 and Table S2).

We tried a number of reaction conditions to replace terminal chlorine atoms on the aC surface (Table S1) with hydrogen sulfide ions, thioacetate ions, or thiourea groups. Incubating the Cl-aC films in a DMF solution containing 500 mM NaSH and 10 mM TBAI at 50°C for 8 hours consistently yielded 0.20 ± 0.06 thiol monolayers. This monolayer coverage did not increase significantly when the reaction time was increased to 24 hours, suggesting the complete replacement of surface-bound chlorines and the formation of a theoretical monolayer is limited by steric hindrance and not an incomplete reaction. **Figure 1A** contains a representative high-resolution XP spectrum of the S2p electrons for a Cl-aC film after thiolation with NaSH. The doublet at 164.0 eV is consistent with the formation of a carbon-sulfur bond. The doublet at 168.0 eV is due to oxidized sulfur species (e.g., thiolsulfinates and thiolsulfonates).[35] Approximately 88% of the surface-bound sulfurs are in their reduced form. To illustrate the importance of the terminal chlorine atoms, we incubated a H-aC film under the exact same reaction conditions. This surface contained less than 0.03 of a thiol monolayer (**Fig. 1B**), and approximately 50% of the sulfurs were oxidized.

XP analysis of the aC films before and after each reaction step revealed the oxygen-to-carbon and nitrogen-to-carbon ratios did not change significantly until the surface is thiolated (**Table 2**). We attribute this increased oxygen-to-carbon ratio of the HS-aC surface to oxidized sulfur atoms and not the carbon atoms. Representative survey and high-resolution C1s XP spectra for each chemical modification of the aC films, as well as a table listing the binding energies and percent compositions of the fit peaks can be found in the Supporting Information.

3.1.2 Surface stability.

While aC films are chemically inert over a wide variety of reaction conditions,[6] thiol-terminated materials oxidize readily under ambient conditions.[36,37] To determine the optimal storage conditions for the HS-aC films, we measured the ratio of reduced and oxidized sulfurs over a 28-day period when stored under: ambient conditions, in dry conditions, or a mild vacuum. These experiments showed that HS-aC films should be used immediately after preparation as greater than 10% of the sulfurs were oxidized after three days, regardless of storage condition (Table S4). Similar oxidation rates of terminal thiols were observed on thiol-terminated layer-by-layer assemblies of polyallylamine hydrochloride and polyacrylic acid.[36] These studies found a substantial number of thiol groups were removed from the film when stored for 48h at ambient conditions, greater than 50% of the remaining thiols were oxidized.

3.1.3 Surface roughness measurements.

The solution-based chlorination reaction used in this work was previously shown to significantly roughen the surface of glassy carbon electrodes.[38] Increases in surface roughness can greatly alter its electrochemical properties, limiting the material's utility after chemical modification. To ensure neither step of the thiolation process was substantially roughening its surface, we used AFM to measure the root mean squared (RMS) roughness values of the aC films after: hydrogenation, chlorination, and thiolation. Although there is a slight observable increase in surface roughness after each modification (**Fig. 2**), this increase was not statistically significant (**Table 2**).

We attribute the differences observed on our aC films and the glassy carbon substrates to both the composition and smoothness of our films. Our films have an RMS value of 1.41 ± 0.36

nm as deposited, a value comparable to previously reported sputtered aC films.[39] The presence of sp^3 hybridized carbons and lack of edge planes, which are common in the graphitic ribbons that compose glassy carbon, in the aC film also likely lessen surface roughening during chlorination.

3.1.4 Surface wettability measurements.

Surface wettability measurements support XP measurements and confirm the introduction of particular functional groups or overall changes in the chemical composition of the surface. We were able to reliably use static contact angle measurements to track changes in surface chemistry (**Fig. 3**) because the roughness of the aC films did not significantly change after modification. We report the average and standard deviation of contact angles measured for the films where the average consists of three different spots on the same surface measured three times (**Table 2**). The measured contact angles for different regions on the same film were reproducible and indicate that the surface chemistry across a single film is homogeneous on the millimeter length scale.

We note that the H-aC, Cl-aC, and HS-aC films had significantly different wetting properties. The untreated aC films were the most hydrophilic (**Fig. 3A**). The hydrophobicity of the surface increased after hydrogenation and chlorination, with the Cl-aC films being the most hydrophobic (**Fig. 3C**). A similar trend of increased contact angle post-chlorination has also been reported for hydrogen-terminated nanocrystalline diamond films.[40] We attribute the decreased contact angle of the thiol-terminated films, in part, to the increased oxidation of the surface as indicated by XP spectra.

3.2 Specificity of the thiol-ene reaction.

To illustrate the selective reactivity of the HS-aC films, we determined the optimal reaction conditions to attach alkene-containing molecules to the surface. These studies compared the attachment of 11-bromo-1-undecene (BUD) molecules to H-aC and HS-aC surfaces. We chose BUD molecules because the bromine atom served as an elemental tag, allowing us to compare the relative numbers of molecules attached to the surface with bromine-to-carbon ratios obtained from high-resolution XP spectra. Successful attachment of BUD molecules to the surface also highlighted the mild reaction conditions needed for thiol-ene reactions, as the 254 nm light needed to directly attach alkene-containing molecules to H-aC films promotes unwanted radical side reactions (e.g., the formation of elemental bromine) that render the films unusable.

In these studies, we specifically determined that: i) a thiol group on the surface is needed for specific alkene attachment; ii) an alkene functional group on the organic molecule is needed for surface attachment; iii) illumination of the surface is necessary for the reaction to proceed, and that wavelengths shorter than 365 nm promote the non-specific attachment of BUD molecules to H-aC films; and iv) a radical initiator, which is commonly used in solution-based thiol-ene reactions, is not required for aC films.

3.2.1 Terminal thiols enhance the attachment of alkene-containing molecules to the aC film.

We illuminated H-aC and HS-aC films in the presence of BUD molecules and 1% (w/w) DMPA to determine if their photo-catalyzed attachment was specific to the thiol-terminated films. A 10-minute illumination time resulted in a significant amount of BUD molecules attaching to both surfaces, with 3.2-fold more molecules attached to the HS-aC films. Increasing

the illumination time to 60 minutes, increased the number of BUD molecules attached to both surfaces (**Table 3**): 1.1-fold more molecules attached to the HS-aC films.

While these results show the presence of the thiol promoted BUD attachment, the significant bromine-to-carbon (Br/C) ratio on the H-aC films suggested the molecules were either directly attaching to the surface or adhering through strong non-covalent interactions. Through a series of washing experiments, we confirmed the molecules were not adsorbed on the surface, but rather attaching through an unwanted side reaction. Specifically, we incubated H-aC and HS-aC films in the presence of BUD and DMPA molecules but in the absence of illumination before thoroughly rinsing and sonicating the films in ethanol. A signal from bromine electrons was not detectable by XPS.

3.2.2 Alkene-containing molecules preferentially react with terminal thiols on the aC film.

We also illuminated H-aC and HS-aC surfaces in the presence of neat 1-bromoundecane, the alkane-containing analog of BUD. These experiments allowed us to compare differences in attachment of BUD molecules when the alkene functional group is removed. When an HS-aC surface was spotted with neat 1-bromoundecane and illuminated for 1 hour, the Br/C ratio is half that of the analogous experiment with the alkene (**Table 3**). When 1-bromoundecane was spotted on an H-aC film and illuminated for 1 hour, we were unable to detect bromine. These results support the notion that an alkene groups is necessary for surface attachment–a non-specific attachment in the case of the H-aC films.

3.2.3 A radical initiator is not needed to promote thiol-ene reactions on the aC films.

While there is experimental evidence that radical initiators are needed for large conversion rates in solution-phase thiol-ene reactions,[41] a recent study showed thiol-ene reactions occur in less than five minutes on the surface of porous polymer materials in the absence of these initiators.[32] Removal of the DMPA did not increase the selectivity of BUD attachment to the HS-aC surfaces. Illuminating a HS-aC surface in the presence of DMPA-containing DMF, however, removed the majority of sulfur from the surface. The remaining 0.07 monolayers of thiols on the surface were completely oxidized.[42] These results suggest that DMPA could be causing undesirable side reactions, which could lead to surface oxidation or the removal of surface-bound thiols.

3.2.4 Non-specific attachment of alkene-containing molecules to the aC films is prevented with lower energy UV wavelengths.

While we are uncertain of the exact mechanism by which the BUD molecules attach to H-aC films, we attribute some of these unwanted reactions to the unfiltered mercury light source ~~we~~ used in the majority of our experiments. Previous work focused on the direct attachment of alkenes to diamond and aC surfaces showed that high energy UV photons ($\lambda < 290$ nm) were needed to drive this reaction.[43,44]

By placing a 360 nm bandpass filter between the light source and the surfaces, we were able to selectively attach BUD molecules to only the HS-aC film (Table S6). To correct for the reduced number of photons reaching the surface in this setup and make comparisons to our previously run experiments (1 hour, 728 J), we increased the illumination time to 6-hour (691 J). Under these conditions the HS-aC film contained comparable Br/C ratios to the surfaces we prepared without the bandpass filter. The Br/C ratio of the H-aC film decreased by 3.5-fold,

indicating the majority of the attachment we observed was arising from non-specific and possibly radical-catalyzed surface reactions.[45] This data also supports a thiol-ene reaction mechanism is occurring on the HS-aC films.

3.3 Patterning thiol-terminated aC films.

To demonstrate the utility of the HS-aC films, we patterned the surface with BUD molecules using 100-mesh (250 µm boxes, **Fig. 4A**) and a 400-mesh (62 µm boxes, Fig. 4C) TEM grids. Using ImageJ software (NIH), we confirmed the average feature size and signal-to-noise (S/N) ratio for each pattern. The features of the 100-mesh pattern are easily distinguished from background and have a S/N ratio of 59 (**Fig. 4B**), but are slightly smaller than the grid itself (227 ± 4 µm).[46] The average feature size of the 400-mesh pattern (41 ± 5 µm, **Fig. 4C**) is also smaller than the grid itself. We attribute these differences in size to the patterning setup, as the grids were not in direct contact with the surface but separated by a quartz coverslip. We were unable to determine the signal-to-noise ratio for smaller of features (**Fig. 4D**), illustrating a potential limit of this photo-patterning approach.

A plausible reason for this limitation in feature resolution is the thiol-ene reaction itself. The photo-generated radical species could be diffusing into neighboring regions that are not illuminated and attaching to the surface.

3.4 Preparing thiol-ene modified aC electrodes.

Thin aC films are an attractive electrode material because they can be deposited onto a number of substrates, including optically transparent substrates that allow for spectroelectrochemical measurements. To prepare a chemically modified electrode using thiol-

ene chemistry, we illuminated a HS-aC film in the presence of 0.1 M vinyl ferrocene (with no DMPA) in DMF for 30 minutes under an argon atmosphere. XP survey spectrum confirmed the presence of iron species on the surface. The high-resolution XP spectrum of the Fe2p electrons revealed both Fe^{+2} and Fe^{+3} species were present on the surface (**Fig. 5A**), suggesting the aC film can act as a potentially tunable redox mediator. This mixed iron valency has also been observed on ferrocene-modified silicon surfaces.[47]

We used cyclic voltammetry to determine if the ferrocene groups were covalently attached to the aC film (**Fig. 5B**). We observed a linear trend between peak current (i_p) and scan rate (v) indicative of electron transfer to surface-bound species (**Fig. 5C**). A linear relationship between i_p and $v^{1/2}$, indicative of diffusion-limited species in solution, was not observed.[48] This plot also reveals that peak currents are no longer at unity when a scan rate of 10 mV/s is exceeded. While we are still investigating the underlying mechanism of this trend, similar results have been reported for boron-doped diamond electrodes.[49] The low conductivity of diamond limits the scan rate to less than 100 mV/s.

4. Conclusion

In this work we prepared thiol-terminated aC films, using a two-step reaction scheme that installs thiol groups directly onto the surface. Through careful characterization, we show that the thiol groups are covalently attached to the surface, primarily in the reduced state, and capable of reacting selectively with alkene-containing molecules. We show that the reaction conditions can be tuned to ensure molecules are attached only to HS-aC films through a thiol-ene reaction. We also determined that including a radical initiator does not enhance the selectivity, yield, or kinetics of this reaction, but rather promotes the increased oxidation of the surface-bound thiols.

A drawback with the current chemistry is the need to use the HS-aC surfaces immediately after they are prepared. Alternative methods such as re-examination of introducing thioacetate groups or other protected thiol-species could improve the shelf-life of these films.

The ability to rapidly pattern the surface of aC films offers a new means of preparing chemical or biomolecule arrays, biosensors, and modified electrodes. The near-UV illumination conditions favor the direct attachment of biomolecules such as oligonucleotides or proteins, both of which are known to undergo unwanted side reactions when exposed to UV light for prolonged periods. While the illumination times for the thiol-ene reactions are much shorter than for the direct attachment of alkene-containing molecules to H-aC surfaces, we believe that further reaction optimization (e.g., a higher power light source, capable of emitting only 360 nm light) could result in even shorter reaction times. Due to the promising performance of the ferrocene-modified aC electrodes, we also envision this chemistry having applications in generating electroactive surfaces for biosensing applications.

5. Figures and Tables

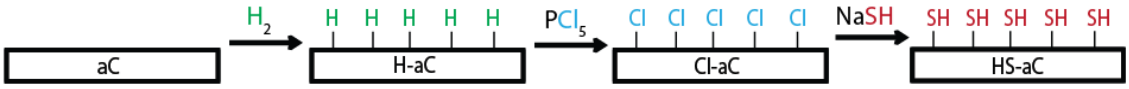

Scheme 2.1. Reaction scheme of thiol-terminated aC thin film preparation.

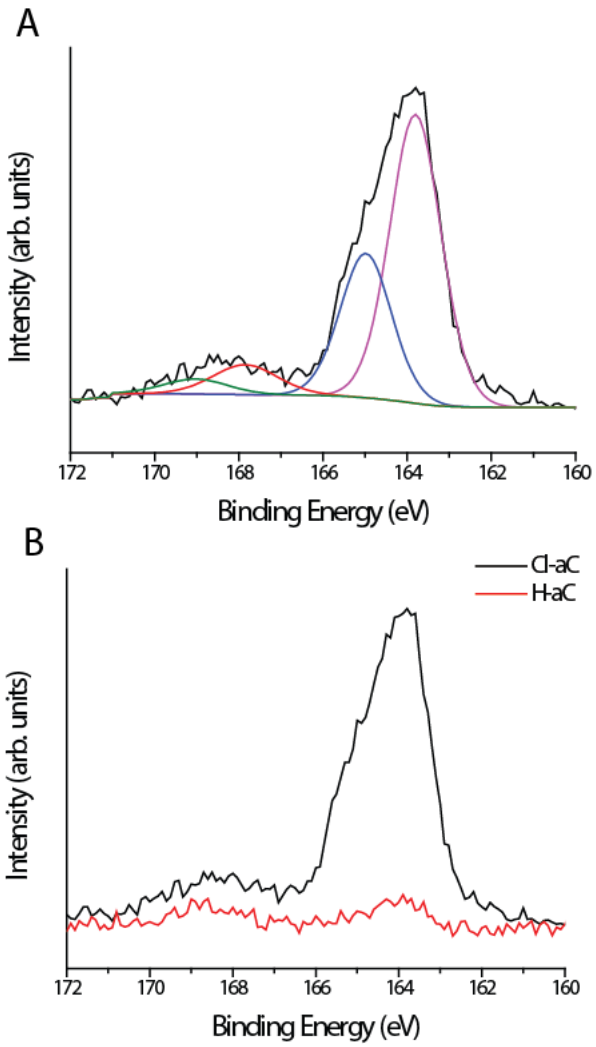

Figure 2.1. XPS data for thiol modified films. (A) High-resolution XP spectrum of S2p electrons for a representative HS-aC surface. Raw data is represented with a solid black line, and individual Voigt-fit components are represented with solid colored lines. (B) Raw data from high-resolution XP spectra of Cl-aC (black, solid line) and H-aC (red, solid line) films exposed to identical thiolation conditions.

Table 2.1. Calculated chlorine and thiol monolayer coverages for Cl-aC and HS-aC surfaces. [a]

	Cl ML [b]	**SH ML** [c]
Cl-aC	0.52 ± 0.10	--
HS-aC	0.07 ± 0.03	0.20 ± 0.06

[a] Monolayer coverage calculations are based on the overlayer model described in reference 34. This calculation assumes the films are atomically smooth.

[b] Values are the average and standard deviation of n = 5 replicates, obtained from separate surfaces prepared and analyzed on separate days.

[c] Values are the average and standard deviation of n = 7 replicates, obtained from separate surfaces prepared and analyzed on separate days.

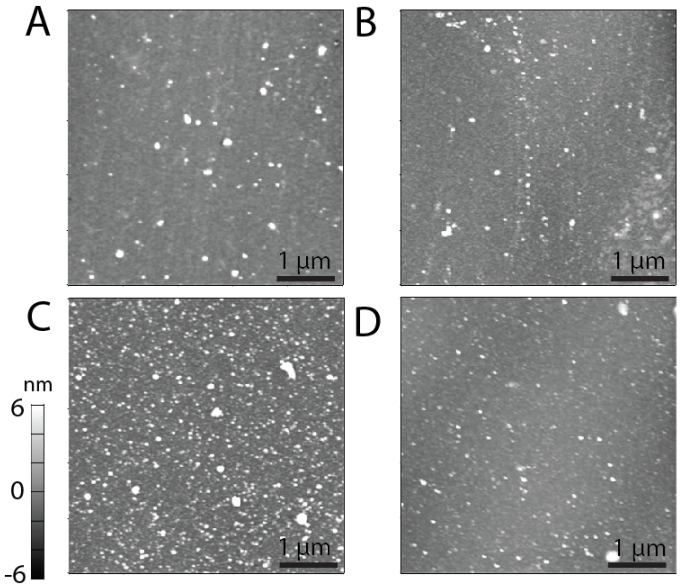

Figure 2.2. Representative atomic force micrographs of an (A) aC film, (B) H-aC film, (C) Cl-aC film, and (D) HS-aC film. Each micrograph represents a 5x5 µm area obtained under tapping-mode conditions with a cantilever oscillation frequency of 300 kHz.

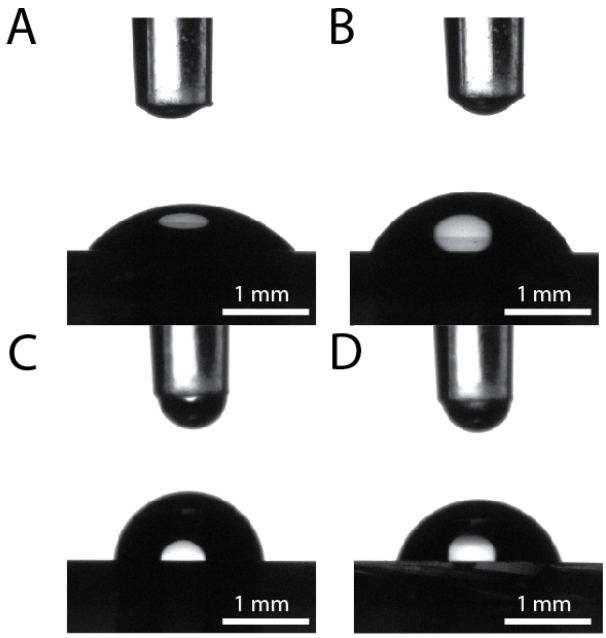

Figure 2.3. Representative static contact angle images of one μL drops of RO water resting on an (A) aC film, (B) H-aC film, (C) Cl-aC film, and (D) HS-aC film.

Table 2.2. Summary of quantitative analyses of modified surfaces.

	O:C ratio [a]	**RMS roughness (nm)** [b]	**Contact angle (°)** [c]
aC	0.14 ± 0.02	1.41 ± 0.36	50 ± 2*
H-aC	0.11 ± 0.01	1.95 ± 1.13	64 ± 1
Cl-aC	0.11 ± 0.01	2.70 ± 0.45	86 ± 2*
HS-aC	0.14 ± 0.02*	2.41 ± 1.24	73 ± 5*

*indicates statistical significance from the H-aC surface.

[a] n=3 for aC, n=4 for H-aC, n=5 for Cl-aC, and n=7 for HS-aC.

[b] n=3 where each replicate is a different spot on the same surface.

[c] n=3 where each replicate is a different spot on the same surface measured three times.

Table 2.3. Bromine-to-carbon ratios for H-aC and HS-aC surfaces reacted with 11-bromo-1-undecene (alkene) or 1-bromoundecane (alkane) under different reaction conditions.

Reaction conditions [a]	**Br/C ratio**			
	H-aC, 10 mins	**H-aC, 60 mins**	**HS-aC, 10 mins**	**HS-aC, 60 mins**
Alkene + light	0.0015 ± 0.0008	0.0073 ± 0.0013	0.0041 ± 0.0004^	0.0113 ± 0.0027*
Alkene + DMPA + light	0.0011 ± 0.0010	0.0113 ± 0.0072 [b]	0.0036 ± 0.0006ǂ	0.0125 ± 0.0041
Alkene	--	0 ± 0	--	0 ± 0
Alkene + DMPA	--	0.0001 ± 0.0001	--	0.0004 ± 0.0005
Alkane + light [c]	--	0	--	0.0062

[a] The 300 ± 100 nm mercury arc lamp was used for all trials where "light" is listed. Values are the average and standard deviation of n = 3 replicates, unless otherwise specified, obtained from separate surfaces prepared and analyzed on separate days, unless otherwise specified.
[b] Values are n=5.
[c] Values are n=1.
* $p<0.05$ compared to HS-aC, 60 mins, alkene.
^ $p<0.05$ compared to H-aC, 10 mins, alkene + light.
ǂ $p<0.05$ compared to H-aC, 10 mins, alkene + DMPA + light.

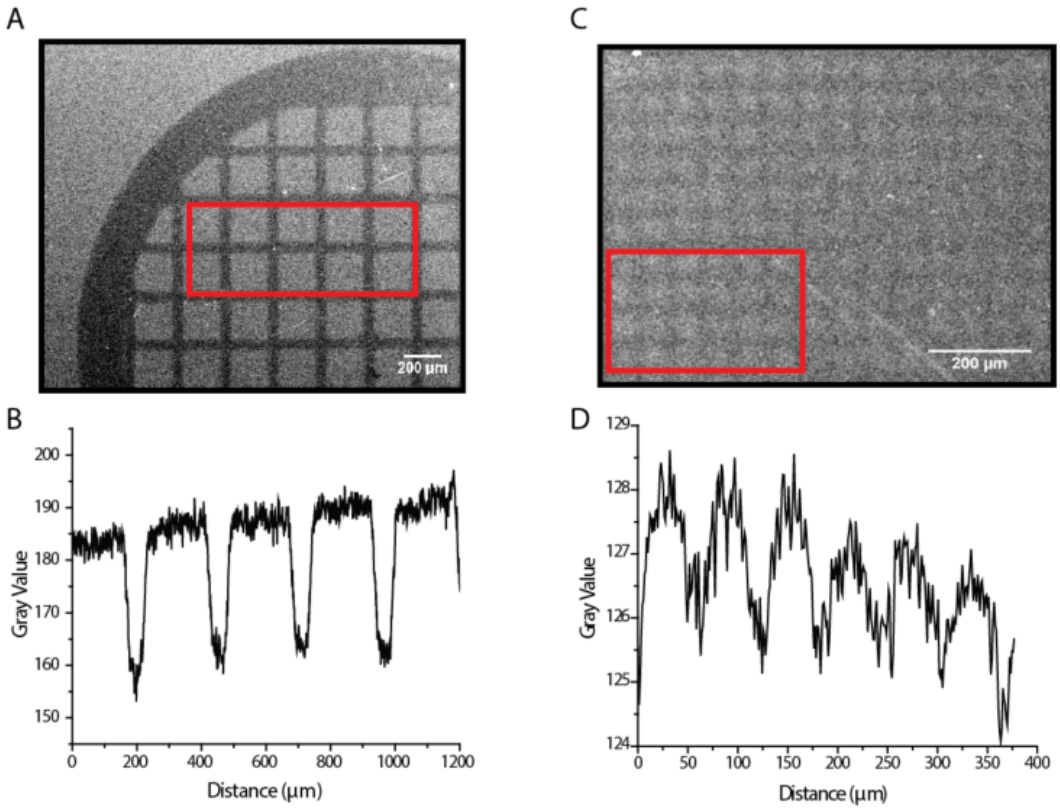

Figure 2.4. SEM images of an 11-bromo-1-undecene patterned aC film with (A) a 100-mesh and (C) a 400-mesh TEM grid. Plot profiles of the area encased by the red rectangle in (B) image A and (D) image C. Images were acquired at 2.0 kV accelerating voltage.

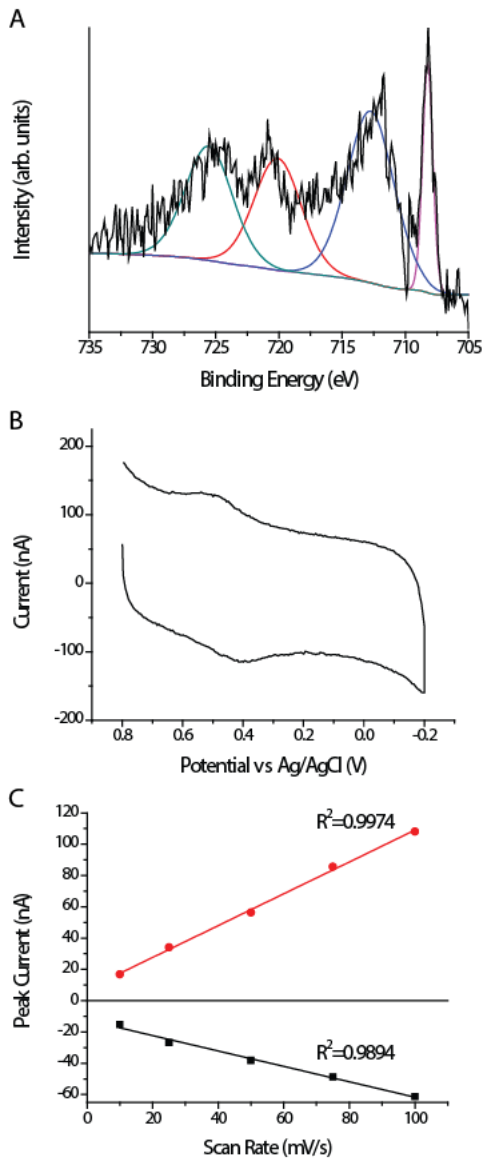

Figure 2.5. Summary of electrochemical experiment using ferrocene. (A) XP high-resolution spectrum of Fe2p electrons of a HS-aC surface to which vinyl ferrocene molecules were attached. Raw data (black, solid line) as well as individual Voigt-fit components (colored, solid lines) shown. (B) CV of surface in 0.1 M tetrabutyl ammonium perchlorate in acetonitrile; scan rate=0.25 mV/s, electrode area=0.13 cm^2. (C) Scan rate vs. peak current analysis.

REFERENCES

1. Peng, W.; Rupich, S. M.; Sha, N.; Gartstein, Y. N.; Malko, A. V; Chabal, Y. J. Silicon Surface Modification and Characterization for Emergent Photovoltaic Applications Based on Energy Transfer. *Chem. Rev.* **2015**, *115*, 12764–12796.

2. Vilan, B. A.; Yaffe, O.; Biller, A.; Salomon, A.; Kahn, A.; Cahen, D. Molecules on Si : Electronics with Chemistry. *Adv. Mater.* **2010**, *22*, 140–159.

3. Buriak, J. M. Illuminating Silicon Surface Hydrosilylation: An Unexpected Plurality of Mechanisms. *Chem. Mater.* **2014**, *26* (1), 763–772.

4. Hamers, R. J. Formation and Characterization of Organic Monolayers on Semiconductor Surfaces. *Annu. Rev. Anal. Chem.* **2008**, *1*, 707–736.

5. Lockett, M. R.; Smith, L. M. Carbon Substrates: A Stable Foundation for Biomolecular Arrays. *Annu. Rev. Anal. Chem.* **2015**, *8* (1), 263–285.

6. Robertson, J. Diamond-like Amorphous Carbon. *Mater. Sci. Eng.* **2002**, *37*, 129–281.

7. Mochalin, V. N.; Shenderova, O.; Ho, D.; Gogotsi, Y. The Properties and Applications of Nanodiamonds. *Nat. Nanotechnol.* **2011**, *7*, 11–23.

8. Barrière, F.; Downard, A. J. Covalent Modification of Graphitic Carbon Substrates by Non-Electrochemical Methods. *J. Solid State Electrochem.* **2008**, *12*, 1231–1244.

9. Hoyle, C. E.; Lowe, A. B.; Bowman, C. N. Thiol-Click Chemistry: A Multifaceted Toolbox for Small Molecule and Polymer Synthesis. *Chem. Soc. Rev.* **2010**, *39* (4), 1355–1387.

10. Escorihuela, J.; Marcelis, A. T. M.; Zuilhof, H. Metal-Free Click Chemistry Reactions on Surfaces. *Adv. Mater. Interfaces* **2015**, *2* (13), 1–42.

11. Hoyle, C. E.; Bowman, C. N. Polymer Chemistry Thiol – Ene Click Chemistry. *Angew. Chemie* **2010**, *49*, 1540–1573.

12. Lockett, M. R.; Smith, L. M. Attaching Molecules to Chlorinated and Brominated Amorphous Carbon Substrates via Grignard Reactions. *Langmuir* **2009**, *25* (6), 3340–3343.

13. Ardalan, P.; Sun, Y.; Pianetta, P.; Musgrave, C. B.; Bent, S. F. Reaction Mechanism , Bonding , and Thermal Stability of 1-Alkanethiols Self-Assembled on Halogenated Ge Surfaces. *Langmuir* **2010**, *26* (9), 8419–8429.

14. Ardalan, P.; Musgrave, C. B.; Bent, S. F. Formation of Alkanethiolate Self-Assembled Monolayers at Halide-Terminated Ge Surfaces. *Langmuir* **2009**, *25* (4), 2013–2025.

15. Bansal, A.; Li, X.; Lauermann, I.; Lewis, N. S. Alkylation of Si Surfaces Using a Two-

Step Halogenation / Grignard Route. *J. Am. Chem. Soc.* **1996**, *118* (11), 7225–7226.

16. Knapp, D.; Brunschwig, B. S.; Lewis, N. S. Chemical, Electronic, and Electrical Properties of Alkylated Ge(111) Surfaces. *J. Phys. Chem. C* **2010**, *114* (28), 12300–12307.

17. Lockett, M. R.; Smith, L. M. Formation and Stability of Alkylthiol Monolayers on Carbon Substrates. *J. Phys. Chem. C* **2010**, *114* (29), 12635–12641.

18. Hsu, M.; Chuang, H.; Cheng, F.; Huang, Y.; Han, C. Directly Thiolated Modification onto the Surface of Detonation Nanodiamonds. *ACS Appl. Mater. Interfaces* **2014**, *6*, 7198–7203.

19. Curran, S. a.; Cech, J.; Zhang, D.; Dewald, J. L.; Avadhanula, A.; Kandadai, M.; Roth, S. Thiolation of Carbon Nanotubes and Sidewall Functionalization. *J. Mater. Res.* **2006**, *21* (04), 1012–1018.

20. Hsu, M.-H.; Chuang, H.; Cheng, F.-Y.; Huang, Y.-P.; Han, C.-C.; Pao, K.-C.; Chou, S.-C.; Shieh, F.-K.; Tsai, F.-Y.; Lin, C.-C.; et al. Simple and Highly Efficient Direct Thiolation of the Surface of Carbon Nanotubes. *RSC Adv.* **2014**, *4* (28), 14777–14780.

21. Sun, Z.; Han, C.; Song, M.; Wen, L.; Tian, D.; Li, H.; Jiang, L. Fabrication of Cysteine-Responsive Biomimetic Single Nanochannels by a Thiol-Yne Reaction Strategy and Their Application for Sensing in Urine Samples. *Adv. Mater.* **2014**, *26* (3), 455–460.

22. Meziane, D.; Barras, A.; Kromka, A.; Houdkova, J.; Boukherroub, R.; Szunerits, S. Thiol-Yne Reaction on Boron-Doped Diamond Electrodes: Application for the Electrochemical Detection of DNA-DNA Hybridization Events. *Anal. Chem.* **2012**, *84* (1), 194–200.

23. Bertin, A.; Schlaad, H. Mild and Versatile (Bio-)Functionalization of Glass Surfaces via Thiol-Ene Photochemistry. *Chem. Mater.* **2009**, *21* (24), 5698–5700.

24. Weinrich, D.; Lin, P. C.; Jonkheijm, P.; Nguyen, U. T. T.; Schröder, H.; Niemeyer, C. M.; Alexandrov, K.; Goody, R.; Waldmann, H. Oriented Immobilization of Farnesylated Proteins by the Thiol-Ene Reaction. *Angew. Chemie* **2010**, *49* (7), 1252–1257.

25. Lin, P. C.; Weinrich, D.; Waldmann, H. Protein Biochips: Oriented Surface Immobilization of Proteins. *Macromol. Chem. Phys.* **2010**, *211* (2), 136–144.

26. Escorihuela, J.; Bañuls, M.-J.; Puchades, R.; Maquieira, Á. Site-Specific Immobilization of DNA on Silicon Surfaces by Using the Thiol–yne Reaction. *J. Mater. Chem. B* **2014**, *2* (48), 8510–8517.

27. Wendeln, C.; Rinnen, S.; Schulz, C.; Arlinghaus, H. F.; Ravoo, B. J. Photochemical Microcontact Printing by Thiol-Ene and Thiol-Yne Click Chemistry. *Langmuir* **2010**, *26* (20), 15966–15971.

28. Wendeln, C.; Ravoo, B. J. Surface Patterning by Microcontact Chemistry. *Langmuir* **2012**, *28* (13), 5527–5538.

29. Buhl, M.; Vonhören, B.; Ravoo, B. J. Immobilization of Enzymes via Microcontact Printing and Thiol–Ene Click Chemistry. *Bioconjug. Chem.* **2015**, 1017–1020.

30. Campos, M. a C.; Paulusse, J. M. J.; Zuilhof, H. Functional Monolayers on Oxide-Free Silicon Surfaces via Thiol-Ene Click Chemistry. *Chem. Commun.* **2010**, *46* (30), 5512–5514.

31. Oberleitner, B.; Dellinger, A.; Déforet, M.; Galtayries, A.; Castanet, A.-S.; Semetey, V. A Facile and Versatile Approach to Design Self-Assembled Monolayers on Glass Using Thiol-Ene Chemistry. *Chem. Commun. (Camb).* **2013**, *49* (16), 1615–1617.

32. Feng, W.; Li, L.; Ueda, E.; Li, J.; Heißler, S.; Welle, A.; Trapp, O.; Levkin, P. A. Surface Patterning via Thiol-Yne Click Chemistry: An Extremely Fast and Versatile Approach to Superhydrophilic-Superhydrophobic Micropatterns. *Adv. Mater. Interfaces* **2014**, *1*, 1400269.

33. Baghbanzadeh, M.; Simeone, F. C.; Bowers, C. M.; Liao, K.; Thuo, M.; Baghbanzadeh, M.; Miller, M. S.; Carmichael, T. B.; Whitesides, G. M. Odd − Even Effects in Charge Transport across N -Alkanethiolate- Based SAMs. *J. Am. Chem. Soc.* **2014**, *136*, 16919–16925.

34. Bansal, A.; Li, X.; Yi, S. I.; Weinberg, W. H.; Lewis, N. S. Spectroscopic Studies of the Modification of Crystalline Si (111) Surfaces with Covalently-Attached Alkyl Chains Using a Chlorination / Alkylation Method. *J. Phys. Chem. B* **2001**, *105*, 10266–10277.

35. Pavlovic, E.; Quist, A. P.; Gelius, U.; Nyholm, L.; Oscarsson, S. Generation of Thiolsulfinates / Thiolsulfonates by Electrooxidation of Thiols on Silicon Surfaces for Reversible Immobilization of Molecules. *Langmuir* ***2003***, 19, 4217–4221.

36. Madaan, N.; Romriell, N.; Tuscano, J.; Schlaad, H.; Linford, M. R. Introduction of Thiol Moieties, Including Their Thiol-Ene Reactions and Air Oxidation, onto Polyelectrolyte Multilayer Substrates. *J. Colloid Interface Sci.* **2015**, *459*, 199–205.

37. Vericat, C.; Benitez, G. a; Grumelli, D. E.; Vela, M. E.; Salvarezza, R. C. Thiol-Capped Gold: From Planar to Irregular Surfaces. *J. Phys. Condens. Matter* **2008**, *20* (18), 184004.

38. Debela, A. M.; Ortiz, M.; Beni, V.; O'Sullivan, C. K. Facile Electrochemical Hydrogenation and Chlorination of Glassy Carbon to Produce Highly Reactive and Uniform Surfaces for Stable Anchoring of Thiolated Molecules. *Chem. A Eur. J.* **2014**, *20* (25), 7646–7654.

39. Peng, X. .; Barber, Z. .; Clyne, T. . Surface Roughness of Diamond-like Carbon Films Prepared Using Various Techniques. *Surf. Coatings Technol.* **2001**, *138* (1), 23–32.

40. Miller, J. B. Amines and Thiols on Diamond Surfaces. *Surf. Sci.* **1999**, *439* (1-3), 21–33.

41. Uygun, M.; Tasdelen, M. A.; Yagci, Y. Influence of Type of Initiation on Thiol-ene "click" Chemistry. *Macromol. Chem. Phys.* **2010**, *211* (1), 103–110.

42. Data not shown.

43. Wang, X.; Colavita, P. E.; Streifer, J. A.; Butler, J. E.; Hamers, R. J. Photochemical Grafting of Alkenes onto Carbon Surfaces: Identifying the Roles of Electrons and Holes. *J. Phys. Chem. C* **2010**.

44. Colavita, P. E.; Sun, B.; Wang, X.; Hamers, R. J. Influence of Surface Termination and Electronic Structure on the Photochemical Grafting of Alkenes to Carbon Surfaces. *J. Phys. Chem. C* **2009**, *113* (4), 1526–1535.

45. Colavita, P. E.; Sun, B.; Tse, K. Y.; Hamers, R. J. Photochemical Grafting of N-Alkenes onto Carbon Surfaces: The Role of Photoelectron Ejection. *J. Am. Chem. Soc.* **2007**, *129* (44), 13554–13565.

46. Values are representative of patterned images shown in Figure 5.

47. Li, F.; Basile, V. M.; Pekarek, R. T.; Rose, M. J. Steric Spacing of Molecular Linkers on Passivated Si(111) Photoelectrodes. *ACS Appl. Mater. Interfaces* **2014**, *6* (22), 20557–20568.

48. Bard, A. J.; Faulkner, L. R. *Electrochemical Methods: Fundamentals and Applications*, 2nd ed.; John Wiley & Sons, 2001.

49. Wächter, N.; Munson, C.; Jarošová, R.; Berkun, I.; Hogan, T.; Rocha-Filho, R. C.; Swain, G. M. Structure, Electronic Properties, and Electrochemical Behavior of a Boron-Doped Diamond/Quartz Optically Transparent Electrode. *ACS Appl. Mater. Interfaces* **2016**, *8*, 28325-28337.

CHAPTER 3- MECHANISTIC INSIGHTS INTO UV-INITIATED THIOL-ENE REACTIONS ON AMORPHOUS CARBON FILMS[2]

1. Introduction

Click chemistries provide a straightforward means of imparting a desired physical property, reactivity, or function to a material through the covalent attachment of molecules to its surface. These chemistries are becoming commonplace in materials science applications[1-3] because of their near unity reaction yields and compatibility with both organic and aqueous reaction conditions. Thiol-ene click chemistries take advantage of the reactive nature of thiols and the ability of thiyl radicals to add across alkenes in a regio- and enantio-selective manner.[4-6] While a number of studies have successfully attached thiol-containing molecules to vinyl-terminated surfaces, [7-13] the selectivity of this light-catalyzed reaction has not been well characterized.

In previous work, we uniformly modified and selectively patterned thiol-aC films with alkene-containing molecules.[14] The utility of these surfaces was hindered by the ready oxidation of the surface-bound thiol groups in ambient conditions. In this work, we installed vinyl groups onto the aC films. To probe selectivity of the thiol-ene reaction on these surfaces, we focused on two reaction variables: surface chemistry and the power of the light source. To evaluate the effects of surface chemistry, we prepared films with terminal hydrogen, methyl, or vinyl groups. The vinyl-aC films should readily and selectively react with our model compound, 4-fluorobenzyl mercaptan (4-FBM). The H-aC and methyl-aC films served as controls. The H-aC films underwent no chemical manipulation. The methyl-aC films ensured chemical modification

[2] This article previously appeared as an article in Journal of Physical Chemistry C. The original citation is as follows: McKenas, C. G.; Fehr, J. M.; Liu, B.; Donley, C. L.; Lockett, M. R. Mechanistic Insights into UV-Initiated Thiol-Ene Reactions on Amorphous Carbon Films. *J. Phys. Chem. C* **2018**, *122* (38), 21854–21860.

did not inadvertently make the surface more reactive toward thiol-containing molecules. To evaluate the lamp power, we constructed a 365 nm LED source whose power output could be adjusted.

This work yielded three significant results, highlighting the importance of detailed characterization when developing new surface modification strategies. First, the 4-FBM molecules covalently attached to each of the aC films, regardless of their surface chemistry. Similar selectivity issues may also be occurring on other materials, but would be overlooked by comparing attachment (or patterning) to a single surface chemistry in the presence and absence of illumination. Second, the power of the light source affects both the reaction rate and the selectivity of the thiol-ene reaction on aC films. Decreasing the photon flux by 10-fold reduced the number of 4-FBM molecule attached to the vinyl-aC films by 2.0-fold and the methyl-aC films by 5.5-fold; increased the selectivity of the reaction by 3.3-fold when comparing the attachment between vinyl-aC and methyl-aC films. Third, thiol-ene reactions performed on vinyl-aC films had a higher coverage and a faster rate of attachment than thiol-aC films exposed to the similar reaction conditions.

2. Experimental Methods

2.1 Chemicals and Materials.

All reagents were used as received unless otherwise noted. Ethanol, hydrogen peroxide (30%), isopropanol, sodium hydrosulfide flakes, sulfuric acid, nitric acid, and tetrahydrofuran were from Fisher Scientific. Acetonitrile, anhydrous benzene, benzoyl peroxide, cysteamine hydrochloride, dimethylformamide (DMF), 4-fluorobenzyl mercaptan (4-FBM), 4-fluorotoluene (4-FT), 4-fluorostyrene (4-FS), methylmagnesium bromide (1.4 M in 1:3 THF:toluene),

phosphorus pentachloride, tetrabutylammonium iodide, and vinyl magnesium bromide (1.0 M in THF) were from Sigma Aldrich. Tetrabutylammonium perchlorate was from Fluka. Reverse osmosis purified water (RO water, 18 Ωm) was used in all experiments.

2.2 Thin Film Preparation and Modification.

Thin films of aC were prepared as detailed previously,[14] by DC magnetron sputtering a graphite source in a 3 x 10^{-5} Torr argon atmosphere onto freshly cleaned silicon (100) substrates. The silicon substrates were cleaned in piranha solution (3:1, conc. H_2SO_4:30% H_2O_2) at 160 ^{o}C for 20 minutes, immediately before usage. **Caution: piranha solution reacts violently with many organic materials and should be handled with extreme care!**

Each aC film was hydrogen terminated in a 13.56 MHz inductively coupled hydrogen plasma (Diener Electronic) for 10 min. The films were chlorine-terminated in a nitrogen-purged reaction vessel containing anhydrous benzene, 80 mM phosphorus pentachloride, and 7 mM benzoyl peroxide (80 °C, 15 mins). Thiol-terminated films were prepared as described previously.[14] Vinyl- and methyl-terminated films were prepared by incubating the chlorine-terminated films in a nitrogen-purged reaction flask containing 7-9 mL of Grignard reagent at 80°C for 7–8 hours. All films were rinsed with isopropanol, dried under a stream of nitrogen, and stored in a desiccator under mild vacuum until needed.

2.3 Thin film illumination and modification.

Films were illuminated with a custom-built light source, modeled after a previously described setup.[15] The 365 nm UV LED source (Gen 2 emitter, Mouser Electronics) was mounted onto a single-channel metal core printed circuit board and cooled using a heatsink/fan

combination. The power of the UV LED was controlled with a DC power supply (E3616A, Hewlett Packard). Lamp output was measured with a FieldMaxII-TOP energy meter equipped with a PowerMax PM10 probe (Coherent). Each surface was placed in a quartz cuvette filled with a 1 M solution of the desired molecule and placed 20 mm below the LED. A ground glass diffuser (600 grit, ThorLabs) was placed between the source and the films to ensure a uniform field of illumination. After the thiol-ene reaction, films were sonicated (5 minutes in ethanol, 5 minutes in benzene, 5 minutes in ethanol) and dried under a stream of nitrogen.

2.4 Thin Film Characterization.

Static water contact angles were measured from 1 μL droplets of RO water using a Ramé Hart goniometer equipped with DropImageCA software. Reported values are the average of at least three droplets, each of which was measured three times, placed in different regions of the same surface. X-ray photoelectron spectroscopy (XPS) was carried out in an ultrahigh-vacuum system (Kratos Axis Ultra DLD) with a base pressure of 5×10^{-9} Torr, a monochromatic Al Kα source, and a hemispherical analyzer. Survey (1.0 eV resolution) and high-resolution (0.1 eV resolution) spectra were collected at a 0° takeoff angle from surface normal. Each high-resolution spectrum was Shirley background corrected and referenced to the C 1s peak (284.6 eV). The C1s peaks were fit with Voigt functions (70% Gaussian, 30% Lorentzian). When calculating oxidized sulfur percentages, the S 2p peaks were also fit with Voigt functions. All XP spectra were analyzed with Kratos Vision 2.0 software. Elemental ratios were determined with the following relative sensitivity factors: 0.278 for C 1 s, 0.780 for O 1s, 0.477 for N 1s, 0.891 for Cl 2p, 0.668 for S 2p, and1.000 for F 1s. Figures S1 and S2 contain representative XP spectra of a methyl-aC and a vinyl-aC films.

Ultraviolet photoelectron spectroscopy (UPS) was carried out in the Kratos Axis Ultra DLD instrument with a He I (21.2 eV) source. Survey (25 meV) and high-resolution (10 meV) spectra were collected at a 0° takeoff angle from surface normal with a –10 V applied bias. Work functions and valence band onsets were determined with the Origin software package (OriginLab Corporation). Figure S3 contains representative UP spectra of the H-aC, Cl-aC, methyl-aC, and vinyl-aC films.

2.5 Statistical analysis.

All reported values are the average and standard deviation of at least three surfaces, unless otherwise noted. A two-tailed *t*-test was used to compare datasets. Datasets were considered significant for p-values < 0.05. An F-test was used to assess the variance between datasets, which were assumed unequal for p-values < 0.05.

3. Results and Discussion

3.1 Surface preparation, characterization, and stability.

Methyl- and vinyl-terminated aC films were prepared with the two-step process outlined in **Scheme 1A**. Each film was chlorinated to promote the attachment of a nucleophilic carbanion, a strategy employed to modify the surface of other group IV semiconductors.[16-20] Sulfur-centered nucleophiles displace these surface-bound chlorine atoms in an S_N2-like fashion.[21] XPS measurements were used to track reactions on the aC films as well as quantify their atomic composition. Changes in surface chemistry were confirmed with static contact angle measurements.

Directly quantifying the attachment of vinyl or methyl groups to the aC films is challenging with XPS as neither functional group provides a unique signature in the survey or the C1s high-resolution spectra. To estimate reaction progress, we compared the chlorine coverage before and after exposure to the Grignard reagent (**Table 1**). We utilized a monolayer calculation previously described.[22] The aC films contained 0.44 ± 0.1 monolayers of chlorine atoms prior to reaction with the Grignard. Vinyl groups were able to replace 40 ± 4% of the surface-bound chlorine atoms; methyl groups were able to replace 35 ± 5%. These values account for non-specific chlorine loss (39.5%), which was determined by incubating Cl-aC films under similar reaction conditions but in the absence of the Grignard reagent (i.e., 8 h, 80 ^{o}C, anhydrous THF). Previous work by Lewis and colleagues found that silicon (111) surfaces could support a full monolayer of methyl groups.[18] The incomplete formation of a chlorine monolayer, and limited replacement of the surface-bound chlorine atoms with methyl or vinyl groups can be attributed to steric limitations arising from a surface structure or topography that is less uniform than freshly etched silicon.

There were slight changes in the oxygen-to-carbon (ΔO/C) ratios of the aC films after the Grignard reactions (**Table 1**). Our previous results showed chlorination and nucleophilic substitution reactions did not increase surface roughness,[14] allowing us to attribute changes in static contact angle to changes in surface chemistry. The aC films became more hydrophilic after alkylation. The static contact angle of the chlorinated films (86 ± 2°) decreased to 67 ± 2° upon methyl termination and to 75 ± 4° upon vinyl termination.

Once prepared, the vinyl-aC films were chemically stable and did not undergo oxidation (ΔO/C = ±0.01, Table S1) in the following conditions: 72 h storage under an inert atmosphere, 24 h in an aqueous solution of 100 mM HNO_3, 24 h in an acetonitrile solution of 100 mM

tetrabutylammonium perchlorate, or submerged in benzene and illuminated with 365 nm photons for 2h. We chose these conditions as they are commonly encountered during functionalization or usage.

3.2 Thiol-ene reaction selectivity on aC films depends on photon flux.

To determine the selectivity of the thiol-ene reaction (**Scheme 1B**) we illuminated aC films with different surface chemistries with 365 nm photons for 1 h in the presence of a 1M 4-FBM benzene solution (**Scheme 1C**). Reaction progress was tracked with XPS measurements, and the S/C ratio used to compare the number of 4-FBM molecules attached to each surface. The benzene solution did not contain a radical initiator, as we and others have shown it is not necessary for surface-based thiol-ene reactions.[14, 23]

Initial experiments were promising, with 4-FBM molecules attaching to the vinyl-aC films when illuminated at 200 mW. The selectivity of the reaction (1.20) was limited, as a significant number of 4-FBM molecules also attached to the methyl-aC and H-aC films. We defined selectivity as:

$$selectivity = \frac{\left(\text{number of 4-FBM molecules}\right)_{\text{vinyl}}}{\left(\text{number of 4-FBM molecules}\right)_{\text{methyl}}}.$$

Directly comparing our results to previous reports of thiol-ene modified surfaces is difficult for the following reasons. First, experimental conditions that could affect the rate of reaction (e.g., solvent, the structure and concentration of the thiol-containing molecule in solution, the distance of the vinyl group from the surface) vary widely. Second, many studies do not specify the photon energy or flux used. Two studies noted a lamp output that was above and below that used in our study, 6W and 5.2 mW.[7, 9] Third, selectivity comparisons are not possible as many studies fail to

incorporate surface chemistry controls such as unmodified surfaces or those containing terminal functional groups that are not a vinyl.

To determine if lamp power was responsible for the unwanted attachment of 4-FBM molecules to the control aC films, we repeated the above experiment but reduced the lamp output to 20 mW. The 10-fold decrease in photon flux significantly decreased the number of molecules that attached to both the methyl- and vinyl-aC films. It also improved the reaction selectivity to 3.30. Figure 1A summarizes the attachment results for both lamp outputs.

Similar numbers of 4-FBM molecules attached to the H-aC films at both lamp powers (Table S2), suggesting they were non-specifically adsorbing to the surface. We performed two experiments, which confirmed the 4-FBM molecules were covalently attached to the aC films. First, we established that UV illumination was necessary for attachment as there was no detectable S 2p or F 1s signal in XPS survey or high-resolution spectra when H-aC and vinyl-aC films were exposed to a 1M 4-FBM solution for 1 hour in the dark. These results also confirmed that the procedures used to rinse the surfaces were stringent enough to remove any non-specifically adsorbed molecules. Second, we established that the thiol functional group was necessary for attachment as neither H-aC nor vinyl-aC films contained a detectable F 1s signal in XPS survey or high-resolution spectra when illuminated in the presence of a 1M 4-FT (**Scheme 1C**) solution.

To better understand our results, we investigated the following variables that could promote or mediate the unwanted attachment of 4-FBM molecules to the H-aC and methyl-aC films: 1) oxygen-containing radicals, 2) the presence of other radical species, and 3) the electronics of the modified films.

3.3 The attachment of 4-fluorobenzyl mercaptan molecules to the aC films is not mediated by oxygen-containing radicals.

Thiol-ene reactions carried out in solution are relatively insensitive to the presence of oxygen or water. A combination of results confirm that the surface-based thiol-ene reactions also do not require specialized conditions, are not promoted or hindered by the presence of water or oxygen, and are not being mediated by the formation of oxygen-centered radicals. First, a comparison of the S/C ratio and the ΔO/C ratio (Figures S4–S6) showed no obvious correlation between 4-FBM molecule attachment and surface oxidation on either the methyl-aC or the vinyl-aC films. Second, cysteamine molecules in an aqueous solution to readily attach to the vinyl-aC films without an increase in surface oxidation ($\Delta O/C = 0.00 \pm 0.01$ for $n = 3$ replicates). Third, thiol-ene reaction yields on H-aC and vinyl-aC films performed at both 20 mW and 200 mW are not affected by the addition of butylated hydroxytoluene (BHT), a known radical scavenger (Table S3).

3.4 Attachment of 4-fluorobenzyl mercaptan molecules is likely initiated by thiyl radical formation.

The average F/S ratio of aC films modified with 4-FBM molecules was less than 1.0, with the exception of the methyl-aC films at 20 mW (Table S2). The F/S ratio of a SAM of 4-FBM molecules on a gold substrate was 1.4, suggesting the UV light was causing the molecules to decompose on the aC films. We chose thiophenol SAMs as a point of comparison because they are well studied in the literature,[24-26] could account for any signal attenuation arising from molecular orientation on the surface, and are prepared without illumination.

To explain these reduced F/S ratios, we considered the homolysis of the fluorine-carbon$_{phenyl}$ bond upon irradiation. This mechanism is unlikely, as the bond dissociation energy (485 kJ/mole) is much higher than the energy of photons used to promote the thiol-ene reaction. Two

alternative and much more plausible mechanisms of fluorine loss are 1) the reductive dehalogenation of the fluorobenzene or 2) the oxidation of surface-bound thioether linkages. Both of these mechanisms suggest the formation of a thiyl radical precedes surface attachment and are supported by the attachment of cysteamine to vinyl-aC films. When illuminated for 1 h at 20 mW, the S/C ratios of vinyl-aC films modified with either 4-FBM or cysteamine molecules are statistically indistinguishable: 0.0032 ± 0.001 and 0.0028 ± 0.001, respectively. A comparison of the X/C ratios, where X = F or N, also support the on-surface degradation of the 4-FBM molecules, with a F/C ratio of 0.0023 ± 0.001, and an N/C ratio of 0.0068 ± 0.0003. These data are summarized in **Figure 1B**.

The reductive dehalogenation of fluorobenzene, which results in the loss of a fluoride ion through a nucleophilic substitution, has been achieved chemically and with electroreduction.[27-28] Under electroreductive conditions, fluorine loss occurs at –2.7 V vs. SCE.[27] While it is experimentally difficult to determine if reductive dehalogenation of the fluorobenzene was occurring, we were able to track the time-dependent oxidation of sulfur atoms on 4-FBM modified aC films. The average F/S ratios reported for the vinyl-aC films (**Fig. 1**, Table S2) represent films that were not stored under inert conditions prior to analysis. To determine if oxidation under ambient conditions was causing fluorine loss, we compared the same vinyl-aC films after surface modification and then again after 48h of storage. After 4-FBM attachment, 100% of the sulfur atoms were in the reduced form, and the F/S ratio (1.42) matched the ratio obtained on gold SAMs. After a 48 h exposure to ambient conditions, 55% of the sulfur atoms were oxidized, and the F/C ratio decreased by 17% (Table S3). While it is difficult to conclude the exact mechanism of 4-FBM degradation on the aC films, the loss of fluorine under ambient conditions does support an oxidation-induced mechanism. Figure S7 further supports this

mechanism of degradation, as an increased percentage of oxidized sulfur on H-aC and methyl-aC films correlates with decreased F/C ratios.

We also considered the potential of alternative sources of thiyl radical formation that could lead to the non-selective attachment to the methyl-aC and H-aC films. One possible source is the residual surface-bound chlorine atoms. Previous studies have shown that C–Cl bonds prefer a radical-based cleavage upon exposure to UV light.[29-30] We hypothesized these chlorine radicals would abstract a hydrogen from the 4-FBM molecules to form a thiyl radical, promoting their attachment to the surface. A plot comparing 4-FBM attachment (S/C ratio) and the loss of chlorine during illumination show there is no correlation between these two variables (Figures S4 – S5). These results indicate that chlorine radicals are not the predominant reaction pathway.

3.5 Methyl- or vinyl-termination does not alter the electronic properties of the amorphous carbon films.

Modifying the surface chemistry of carbon materials can alter their electronic structure, promoting unwanted reactions through photo-ejected electrons. Such strategies have been utilized previously to promote the attachment of alkene-containing molecules directly onto the surface of carbon nanofibers, diamond, and aC substrates.[31-34] To determine if installing different functional groups on the surface of the aC films altered its electronic structure, we measured the valence band onset and work function of H-, Cl-, methyl-, and vinyl-aC films (**Figure 2**). The valence onset of each film was 0.6 eV below the Fermi level and was unaffected by surface chemistry. Previous studies have reported similar onset values for H- and O-terminated aC films.[32] Chlorination increased the work function by 0.4 eV, and can be attributed to an interfacial dipole pointed away from the surface.[35-36] The work function of the methyl- and vinyl-aC films is indistinguishable from the H-aC film, and likely is due to the lack of dipole moment

resulting from carbon-carbon bond formation. The similarity between the work functions of H-, methyl-, and vinyl-aC films suggests that the surfaces were not catalyzing unwanted reactions with photo-ejected electrons, as photons with energies greater than 4.4 eV (< 282 nm) are required.

3.6 Vinyl-aC films favor greater coverages and faster kinetics than thiol-aC films when performing thiol-ene click reactions.

Using identical reaction conditions we compared the rate of attachment of 4-FBM molecules to vinyl-terminated films and 4-FS molecules to thiol-terminated films. To more easily compare these reactions, we plotted the percentage of total surface-bound functional groups that underwent a thiol-ene reaction as a function of total energy emitted by the lamp (**Figure 3**). The details of the reaction completion calculation are presented in Appendix C.

Figure 3A shows that the number of molecules attached to the surface increases with increasing illumination energy for both thiol-ene reactions, although the maximal coverage was highly dependent on surface chemistry. The energy needed to achieve these coverages was also surface chemistry dependent with the thiol-aC films requiring ~4.6-fold more photons (324 J) than the vinyl-aC films (70 J). Attachment of the 4-FS molecules to the thiol-aC films was also dependent on lamp intensity, as an intensity of 20 mW was below the threshold needed for the reaction. The importance of photon flux is further illustrated by the absence of 4-FS molecules on the thiol-aC films after 150 J of 20 mW light but a significant number of 4-FS molecules after 100 J of 90 mW light (**Figure 3B**). These results suggest that the thiol-ene reaction is relatively inefficient due to the presence of relatively fast and deactivating side reactions, which become apparent at low concentrations of thiyl radicals.

For both surface chemistries, prolonged illumination decreased surface coverage (**Figure 3A**) and increased the percentage of oxidized sulfurs on the surface (Figure S8). These findings further support the notion that the molecules are degrading upon prolonged exposure to UV light. Our results suggest that the most efficient means of introducing a large number of molecules onto the surface with the thiol-ene click reaction is to prepare films with a terminal vinyl group. They also suggest that the resulting thioether linkage is prone to oxidation and must be stored under an inert atmosphere or used immediately upon modification.

3.7 Possible mechanisms responsible for non-specific attachment.

Given that none of the variables we investigated (oxygen-containing radicals, carbon-halogen photocleavage, and electronics of the films) were responsible for the unwanted attachment of the 4-FBM molecules to the aC films, we considered two surface-centric mechanisms of attachment. Both of these mechanisms require the formation of thiyl radicals, which our results support. First, a concerted reaction between two thiyl radicals in which one abstracts an electron (or possibly a hydrogen) from the surface, generating a surface-bound radical that in turn reacts with the second thiyl radical in solution. Second, and perhaps more likely mechanism, is the direct addition of the thiyl radical across unsaturated carbon-carbon bonds at the film's surface. Ternary diagrams of carbon materials show that magnetron sputtered films contain a high percentage of sp^2-hybridized carbons.[37-38] Future investigations of surface composition are needed to determine if the non-specific attachment is limited to materials rich in sp^2-hybridized carbons, or if our observations are a more universal problem with reactions that rely on the generation of thiyl-centered radicals.

4. Conclusions

This work demonstrates that surface chemistry can impart significantly different properties and reaction outcomes on the same material. By replacing surface-bound chlorines with vinyl groups, we were able to generate a thiol-ene compatible surface that is chemically inert under a variety of reaction conditions. This stability is much improved over our previous approach of installing terminal thiol groups onto the surface. The thiol-ene reactions on vinyl-aC films also proceeded more quickly and had greater overall coverage than their thiol-aC counterparts.

Our work also highlights the importance of including proper controls when developing and characterizing new strategies for modifying materials. By comparing thiol-ene reactions on aC films with different terminal functional groups, we found that illuminating solutions of thiol-containing molecules led to their non-selective attachment to both H-aC and methyl-aC films. Interestingly, this selectivity could be tuned by changing the power output of the UV LED source. Increased selectivity of the thiol-ene reaction on aC films comes with a significant trade-off, a decreased rate of attachment. The non-selective addition we observed may not be endemic to all thiol-ene reactions on surfaces, but rather an unfortunate effect of using a material with a high percent of sp^2–hybridized carbons. Further studies on carbon and non-carbon surfaces are needed to fully characterize reaction selectivity, and it should be noted that such studies are only possible with an UV source that has a tunable power output.

5. Figures and Tables

Scheme 3.1. Reactions and molecules used in this work. (A) Reaction to prepare the vinyl-aC and methyl-aC films. (B) The UV-initiated thiol-ene click reaction. (C) Molecules used in this work.

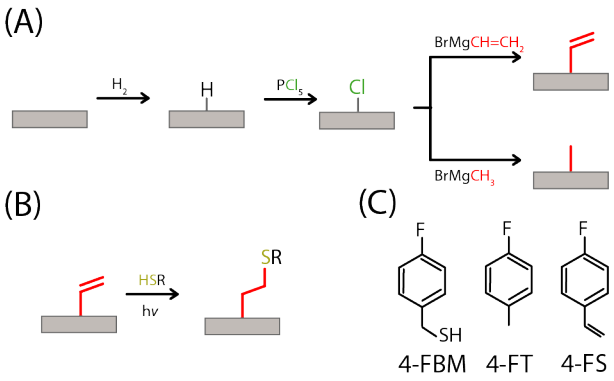

Table 3.1. Quantitative characterization of vinyl-aC and methyl-aC films.

	ΔO/C[a]	O/C ratio	% Cl monolayers[b] replaced	Static contact angle[c]
vinyl-aC	0.02 ± 0.02	0.10 ± 0.01[d]	40 ± 4[d]	75 ± 4
methyl-aC	0.01 ± 0.02	0.10± 0.02[e]	35 ± 5[e]	67 ± 2

[a] ΔO/C ratio were calculated from the corresponding Cl-aC film.

[b] Monolayer calculations have been previously detailed.[14]

[c] Value is the average of three different spots on three different films. Each droplet was measured three times.

[d] Value is the average of 29 different films.

[e] Value is the average of 10 different films.

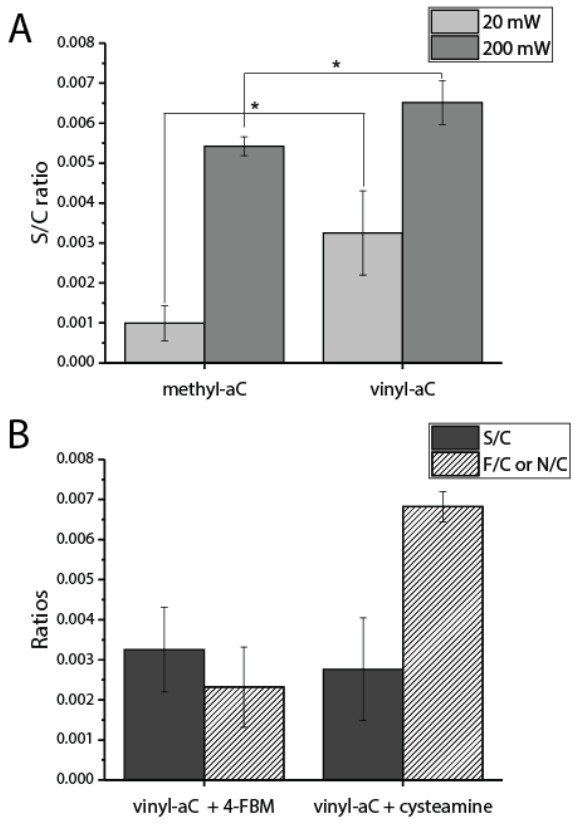

Figure 3.1. XPS results for thiol-ene click experiments. (A) Sulfur-to-carbon (S/C) ratios for methyl-aC and vinyl-aC films illuminated with 365 nm photons in the presence of a 1 M 4-FBM benzene solution for 1 hour at either 20 or 200 mW. (B) S/C ratios, fluorine-to-carbon (F/C), or nitrogen-to-carbon (N/C) ratios for vinyl-aC films illuminated for 1 h with 20 mW in the presence of either a 1 M 4-FBM benzene solution or a 1 M cysteamine hydrochloride aqueous solution. Each bar represents the average and standard deviation of at least n = 3 surfaces. *$p<0.05$

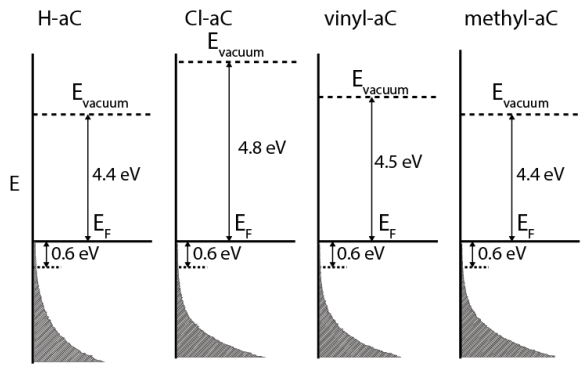

Figure 3.2. Energy diagrams for H-aC, Cl-aC, vinyl-aC, and methyl-aC films. The corresponding UPS spectra for each surface can be found in Figure S3.

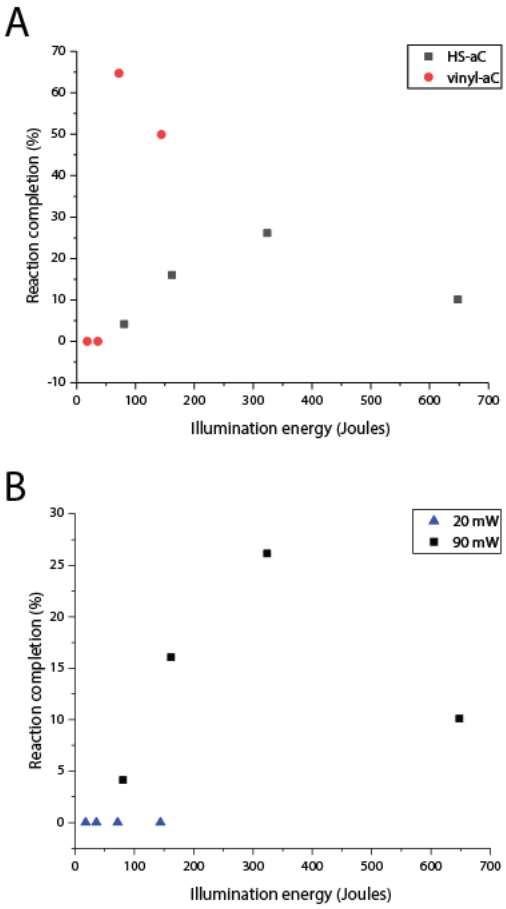

Figure 3.3. Reaction completion percentage as a function of total illumination energy for (A) vinyl-aC films reacted with a 1M 4-FBM solution at 20 mW (red circles) and thiol-aC films reacted with a 1M 4-FS solution at 90 mW (black squares), and (B) thiol-aC films reacted with a 1M 4-FS solution molecules at a lamp power of either 20 mW (blue triangles) or 90 mW (black squares). Table S6 contains the F/C and S/C ratios of each surface as a function of illumination time.

REFERENCES

1. Nandivada, H.; Jiang, X. W.; Lahann, J., Click Chemistry: Versatility and Control in the Hands of Materials Scientists. *Adv. Mater.* **2007**, *19*, 2197-2208.

2. Xi, W. X.; Scott, T. F.; Kloxin, C. J.; Bowman, C. N., Click Chemistry in Materials Science. *Adv. Funct. Mater.* **2014**, *24*, 2572-2590.

3. Lowe, A. B., Thiol-Ene "Click" Reactions and Recent Applications in Polymer and Materials Synthesis: A First Update. *Polym. Chem.* **2014**, *5*, 4820-4870.

4. Hoyle, C. E.; Bowman, C. N., Thiol-Ene Click Chemistry. *Angew. Chem. Int. Ed.* **2010**, *49*, 1540-1573.

5. Hoyle, C. E.; Lowe, A. B.; Bowman, C. N., Thiol-Click Chemistry: A Multifaceted Toolbox for Small Molecule and Polymer Synthesis. *Chem. Soc. Rev.* **2010**, *39*, 1355-1387.

6. Lowe, A. B., Thiol-Ene "Click" Reactions and Recent Applications in Polymer and Materials Synthesis. *Polym. Chem.* **2010**, *1*, 17-36.

7. van den Berg, S. A.; Tu, J.; Sliedregt, K. M.; Kros, A.; Wennekes, T.; Zuilhof, H., Clickable Mesoporous Silica Via Functionalization with 1 ,Omega-Alkenes. *Adv. Mater. Interfaces* **2014**, *1*, 1300061.

8. Campos, M. A. C.; Paulusse, J. M. J.; Zuilhof, H., Functional Monolayers on Oxide-Free Silicon Surfaces Via Thiol-Ene Click Chemistry. *Chem. Commun.* **2010**, *46*, 5512-5514.

9. Wendeln, C.; Rinnen, S.; Schulz, C.; Arlinghaus, H. F.; Ravoo, B. J., Photochemical Microcontact Printing by Thiol-Ene and Thiol-Yne Click Chemistry. *Langmuir* **2010**, *26*, 15966-15971.

10. Escorihuela, J.; Banuls, M. J.; Puchades, R.; Maquieria, A., Site-Specific Immobilization of DNA on Silicon Surfaces by Using Thiol-Yne Reaction. *J. Mater. Chem. B* **2014**, *2*, 8510-8517.

11. Oberleitner, B.; Dellinger, A.; Deforet, M.; Galtayries, A.; Castanet, A. S.; Semetey, V., A Facile and Versatile Approach to Design Self-Assembled Monolayers on Glass Using Thiol–Ene Chemistry. *Chem. Commun.* **2013**, *49*, 1615-1617.

12. Zhang, L.; Vila, N.; Klein, T.; Kohring, G. W.; Mazurenko, I.; Walcarius, A.; Etienne, M., Immobilization of Cysteine-Tagged Proteins on Electrode Surfaces by Thiol-Ene Click Chemistry. *ACS Appl. Mater. Interfaces* **2016**, *8*, 17591-17598.

13. Luong, N. D.; Sinh, L. H.; Johansson, L. S.; Campbell, J.; Seppala, J., Functional Graphene by Thiol-Ene Click Chemistry. *Chem. - Eur. J.* **2015**, *21*, 3183-3186.

14. McKenas, C. G.; Fehr, J. M.; Donley, C. L.; Lockett, M. R., Thiol-Ene Modified Amorphous Carbon Substrates: Surface Patterning and Chemically Modified Electrode Preparation. *Langmuir* **2016**, *32*, 10529-10536.

15. Hoelz, K.; Lietard, J.; Somoza, M. M., High-Power 365 Nm Uv Led Mercury Arc Lamp Replacement for Photochemistry and Chemical Lithography. *ACS Sustainable Chem. Eng.* **2017**, *5*, 828-834.

16. Lockett, M. R.; Smith, L. M., Attaching Molecules to Chlorinated and Brominated Amorphous Carbon Substrates Via Grignard Reactions. *Langmuir* **2009**, *25*, 3340-3343.

17. Bansal, A.; Li, X. L.; Lauermann, I.; Lewis, N. S.; Yi, S. I.; Weinberg, W. H., Alkylation of Si Surfaces Using a Two-Step Halogenation Grignard Route. *J. Am. Chem. Soc.* **1996**, *118*, 7225-7226.

18. Wong, K. T.; Lewis, N. S., What a Difference a Bond Makes: The Structural, Chemical, and Physical Properties of Methyl-Terminated Si(111) Surfaces. *Acc. Chem. Res.* **2014**, *47*, 3037-3044.

19. Knapp, D.; Brunschwig, B. S.; Lewis, N. S., Chemical, Electronic, and Electrical Properties of Alkylated Ge(111) Surfaces. *J. Phys. Chem. C* **2010**, *114*, 12300-12307.

20. Collins, H.; Fleming, P.; Barth, S.; O'Dwyer, C.; Boland, J. J.; Morris, M. A.; Holmes, J. D., Alkane and Alkanethiol Passivation of Halogenated Ge Nanowires. *Chem. Mater.* **2010**, *22*, 6370-6377.

21. Lockett, M. R.; Smith, L. M., The Formation and Stability of Alkylthiol Monolayers on Carbon Substrates. *J. Phys. Chem. C* **2010**, *114*, 12635-12641.

22. Bansal, A.; Li, X.; Yi, S. I.; Weinberg, W. H.; Lewis, N. S., Spectroscopic Studies of the Modification of Crystalline Si (111) Surfaces with Covalently-Attached Alkyl Chains Using a Chlorination/Alkylation Method. *J. Phys. Chem. B* **2001**, *105*, 10266-10277.

23. Feng, W. Q.; Li, L. X.; Ueda, E.; Li, J. S.; Heissler, S.; Welle, A.; Trapp, O.; Levkin, P. A., Surface Patterning Via Thiol-Yne Click Chemistry: An Extremely Fast and Versatile Approach to Superhydrophilic-Superhydrophobic Micropatterns. *Adv. Mater. Interfaces* **2014**, *1*, 1400269.

24. Love, J. C.; Estroff, L. A.; Kriebel, J. K.; Nuzzo, R. G.; Whitesides, G. M., Self-Assembled Monolayers of Thiolates on Metals as a Form of Nanotechnology. *Chem. Rev.* **2005**, *105*, 1103-1170.

25. Frey, S.; Stadler, V.; Heister, K.; Eck, W.; Zharnikov, M.; Grunze, M.; Zeysing, B.; Terfort, A., Structure of Thioaromatic Self-Assembled Monolayers on Gold and Silver. *Langmuir* **2001**, *17*, 2408-2415.

26. Heister, K.; Zharnikov, M.; Grunze, M.; Johansson, L. S. O., Adsorption of Alkanethiols and Biphenylthiols on Au and Ag Substrates: A High-Resolution X-Ray Photoelectron Spectroscopy Study. *J. Phys. Chem. B* **2001**, *105*, 4058-4061.

27. Kariv-Miller, E.; Vajtner, Z., Electroreductive Dehalogenation of Fluorobenzenes. *J. Org. Chem.* **1985**, *50*, 1394-1399.

28. Denney, D. B.; Denney, D. Z.; Fenelli, S. P., Some Chemistry of Aromatic Fluorine Containing Radical Anions. *Tetrahedron* **1997**, *53*, 9835-9846.

29. Slocum, G. H.; Schuster, G. B., Photochemistry of Naphthylmethyl Halides. Direct and Sensitized Paths to Homolytic and Heterolytic Carbon-Halogen Bond Cleavage. *J. Org. Chem.* **1984**, *49*, 2177-2185.

30. Kosmrlj, B.; Sket, B., Photolysis of Bromo- and Chloro-Substituted Benzyl Derivatives. Competition between Ionic and Radical Pathways. *J. Org. Chem.* **2000**, *65*, 6890-6896.

31. Ago, H.; Kugler, T.; Cacialli, F.; Salaneck, W. R.; Shaffer, M. S. P.; Windle, A. H.; Friend, R. H., Work Functions and Surface Functional Groups of Multiwall Carbon Nanotubes. *J. Phys. Chem. B* **1999**, *103*, 8116-8121.

32. Colavita, P. E.; Sun, B.; Wang, X. D.; Hamers, R. J., Influence of Surface Termination and Electronic Structure on the Photochemical Grafting of Alkenes to Carbon Surfaces. *J. Phys. Chem. C* **2009**, *113*, 1526-1535.

33. Baker, S. E.; Tse, K. Y.; Hindin, E.; Nichols, B. M.; Clare, T. L.; Hamers, R. J., Covalent Functionalization for Biomolecular Recognition on Vertically Aligned Carbon Nanofibers. *Chem. Mater.* **2005**, *17*, 4971-4978.

34. Nichols, B. M.; Butler, J. E.; Russell, J. N.; Hamers, R. J., Photochemical Functionalization of Hydrogen-Terminated Diamond Surfaces: A Structural and Mechanistic Study. *J. Phys. Chem. B* **2005**, *108*, 20938-20947.

35. Crispin, X.; Geskin, V.; Crispin, A.; Cornil, J.; Lazzaroni, R.; Salaneck, W. R.; Bredas, J. L., Characterization of the Interface Dipole at Organic/Metal Interfaces. *J. Am. Chem. Soc.* **2002**, *124*, 8131-8141.

36. Alloway, D. M.; Hofmann, M.; Smith, D. L.; Gruhn, N. E.; Graham, A. L.; Colorado, R.; Wysocki, V. H.; Lee, T. R.; Lee, P. A.; Armstrong, N. R., Interface Dipoles Arising from Self-Assembled Monolayers on Gold: Uv-Photoemission Studies of Alkanethiols and Partially Fluorinated Alkanethiols. *J. Phys. Chem. B* **2003**, *107*, 11690-11699.

37. Robertson, J., Diamond-Like Amorphous Carbon. *Mater. Sci. Eng., R* **2002**, *37*, 129-281.

38. Sun, B.; Colavita, P. E.; Kim, H.; Lockett, M.; Marcus, M. S.; Smith, L. M.; Hamers, R. J., Covalent Photochemical Functionalization of Amorphous Carbon Thin Films for Integrated Real-Time Biosensing. *Langmuir* **2006**, *22*, 9590-9605.

CHAPTER 4- AZIDE-ALKYNE CLICK REACTIONS TO PREPARE CHEMICALLY MODIFIED AMORPHOUS CARBON ELECTRODES[3]

1. Introduction

In dye-sensitized solar and photoelectrosynthesis cells, molecular assemblies of both chromophores and catalysts are attached to the surface of a semiconductor. A prototypical example of such an architecture is the immobilization of ruthenium polypyridyl complexes onto the surface of an indium tin oxide film or nanoparticle.[1, 2] The long-term stability of these devices is dictated by the chromophores, the semiconductor surface, and the chemistry that links these two moieties. While metal oxide films have ideal optical and electronic properties to support light-driven reactions,[3] there are a limited number of chemistries to modify their surface stably. Alkylphosphonates, which form well-ordered monolayers on metal oxide surfaces,[4] are prone to hydrolysis in basic solutions and decompose under the high, positive potentials required for water oxidation. An alternative strategy, based on the work of Dichtel,[5, 6] used π-π interactions to physisorb pyrene-appended molecules to pyrene-modified indium tin oxide (ITO) films.[7] The long-term stability of these modified ITO surfaces is yet to be determined.

To best retain the surface-bound molecular assemblies that maintain the function of light-driven devices, alternative materials and linking chemistries are needed. Carbon-based materials are a promising alternative, offering tunable conductivities, wide electrochemical windows, and chemically stable surfaces that are not prone to oxidation in aqueous or organic solutions.[8-10] Magnetron sputtered amorphous carbon (aC) films offer additional advantages, making them

[3] This article previously appeared as an article in Applied Surface Science. The original citation is as follows: Fehr, J. M.; McKenas, C. G.; Liu, B.; Lockett, M. R. Azide-Alkyne Click Reactions to Prepare Chemically Modified Amorphous Carbon Electrodes. *Appl. Surf. Sci*. https://doi.org/10.1016/j.apsusc.2019.02.151

particularly well suited for these applications.[11-13] First, the films can be deposited at room temperature and have high adhesion, a combination that allows them to interface with a variety of materials, including electronic components. Second, the films are optically transparent across the visible and ultraviolet range for thicknesses of less than 100 nm. Finally, the films are graphitic in nature and thus serve as a model system to evaluate the stability and performance of chemically modified carbon nanomaterials.

Two well-established chemistries for modifying the surface of carbonaceous materials are the chemical reduction of aryldiazonium molecules and the photo-initiated attachment of alkene-containing molecules.[13-15] While both reactions result in a carbon-carbon bond with the surface, they are both limited by a propensity to form ill-defined multilayered structures.[15-17] We are developing a suite of chemistries in which nucleophilic species covalently attach to the aC film, displacing surface-bound chlorine atoms in an S_N2-like fashion. We recently used this approach to generate thiol-ene compatible surfaces, installing terminal thiol or vinyl groups.[18, 19] Despite our ability to rapidly pattern these surfaces with 365 nm photons, both surface chemistries were limited. The surface-bound thiol groups readily oxidized under atmospheric conditions, reducing the number of available groups that could participate in the thiol-ene reaction.[19] The attachment of thiol-containing molecules to vinyl-terminated aC films was successful but not selective, as the molecules also attached to control films containing terminal methyl groups.[18]

The copper-catalyzed azide-alkyne cycloaddition (CuAAC) reaction could append molecules onto the surface of aC films selectively.[20] The stability of the resulting surface linkage—a 1,2,3-triazole ring—is particularly attractive for dye-sensitized devices as it is not prone to hydrolysis, oxidation, or reduction.[21] The CuAAC reaction has been used to modify the surface of a number

of materials, including carbonaceous substrates, films, and nanomaterials.[10, 22-28] None of these examples have utilized the two-step approach we describe here to install a terminal azide group.

In this work, we characterize the chemical composition of aC films after each modification step shown in **Scheme 1**. We clearly show that azide molecules can replace surface-bound chlorine atoms, expanding the utility of the two-step modification approach we are developing for carbon materials. We also show that ethynyl ferrocene molecules selectively and covalently attach to the azide-terminated films, allowing us to generate chemically modified electrodes.

2. Materials and Methods

2.1 Reagents and Materials

All reagents were used as received unless otherwise specified. Anhydrous acetonitrile, anhydrous benzene, benzoyl peroxide, copper sulfate pentahydrate, 15-crown-5, anhydrous *N*,*N*-dimethyl formamide (DMF), ethynyl ferrocene, ferrocene, methanol, phosphorus pentachloride (PCl_5), sodium ascorbate, and sodium azide were purchased from Sigma-Aldrich. Ethanol, hydrogen peroxide (30%), conc. hydrochloric acid, and conc. sulfuric acid were purchased from Fisher Scientific. Tetrabutylammonium hexafluorophosphate (TBAPF, Oakwood Chemical, 98%) was recrystallized from ethanol and dried in vacuo before usage. Reverse osmosis purified water (RO water, 18 MΩ) was used in all experiments.

2.2 Amorphous carbon film deposition and functionalization

Amorphous carbon films (25 nm) were magnetron sputtered onto either silicon (100) or fluorine-doped tin oxide-coated glass substrates (FTO, 15 Ω/sq., Hartford Glass) from a graphite target, as previously detailed.[19] Prior to deposition, the FTO substrates were sonicated for 15-min

intervals in ethanol and 1M HCl in ethanol; the silicon and quartz substrates were immersed in piranha solution (3:1, 96.3% H_2SO_4: 30% H_2O_2) at 160 ^oC for 20 min and then thoroughly rinsed with RO water. ***Caution: piranha solution can react violently with organic materials.***

Azide-terminated aC films were prepared using the process outlined in Scheme 1. First, films were hydrogen terminated in a 13.56 MHz inductively coupled hydrogen plasma (Diener Electronic) for 10 min. Second, films were reacted at 80 ^oC for 15 min in a nitrogen-purged benzene solution containing 80 mM PCl_5 and 7 mM benzoyl peroxide. Finally, films were reacted at room temperature for 24 h in a nitrogen-purged DMF solution containing 50 mM sodium azide. After each step, the films were rinsed three times with ethanol, dried under a stream of nitrogen, and stored under vacuum until needed. CuAAC reactions were carried out at room temperature in a nitrogen-purged ethanol:water solution (1:2, v/v) containing 100 μM copper sulfate, 150 μM sodium ascorbate, and 2 mM ethynyl ferrocene for up to 96 hours. The ferrocene-terminated films were sonicated for 5-minute intervals in water and ethanol, dried under a stream of nitrogen, and stored under vacuum until needed.

2.3 Surface characterization

X-ray photoelectron (XP) spectroscopy was carried out in an ultrahigh-vacuum system (Kratos Axis Ultra DLD) with a base pressure of 5×10^{-9} Torr, a monochromatic Al Kα source, and a hemispherical analyzer. Survey (1.0 eV resolution) and high-resolution (0.1 eV resolution) spectra were collected at a 0° takeoff angle from surface normal. Each high-resolution spectrum was Shirley background corrected, referenced to the C 1s peak (284.6 eV), which was fit with Voigt functions (70% Gaussian, 30% Lorentzian). Nitrogen 1s peaks were also fit with Voigt functions for some analyses. Elemental ratios were determined with the following relative

sensitivity factors: 0.278 for C 1s, 0.780 for O 1s, 0.477 for N 1s, 0.891 for Cl 2p, and 2.957 for Fe 2p electrons.

All electrochemical measurements were performed in an N_2-filled glovebox equipped with a WaveDriver bipotentiostat (Pine) and a conventional three-electrode system. The working electrode (0.11 cm^2) was an aC film deposited on an FTO substrate. The auxiliary electrode was a polished 3-mm glassy carbon disk electrode. The pseudo-reference electrode was a silver wire submerged in 0.25 M TBAPF in acetonitrile. Residual ohmic drop in each CV measurement was compensated using an approach developed for the WaveDriver. All scans were referenced to a ferrocenium/ferrocene redox couple at 0 V.

3. Results

3.1 Characterization of the aC Films

We quantified the atomic composition of aC films after each chemical modification with XPS. **Table 1** summarizes these values as well as the oxygen-to-carbon ratios, which show that each reaction did not cause unwanted surface oxidation. Survey and high-resolution XP spectra confirmed the unmodified films were largely carbon (90.73 at. %) with small amounts of nitrogen (0.51 at. %) and oxygen (8.76 at. %). The representative high-resolution C 1s spectrum of an unmodified aC film on an FTO substrate shown in **Figure 1A** was fit with four components, which can be attributed to C=O (287.6 eV), C–O/C-N (286.2 eV), and C–C (285.1 and 284.6 eV) bonded species. Others have also noted the presence of oxygen in magnetron sputtered aC films.[29, 30] We attribute the oxygen to unwanted oxidation reactions caused by residual oxygen in the chamber at the time of deposition or from the oxidation of the graphite target prior to deposition.

We determined the surface of the unmodified films was largely sp^3 in nature using XPS. The ratio of the integrated areas of the sp^3– (284.6 eV) and sp^2–hybridized (285.1 eV) carbon components of the high-resolution C 1s XP spectrum was 2.65. The average optical bandgap of four independently prepared 25 nm aC films was 0.68 ± 0.1 eV, suggesting the bulk material was largely sp^2 in nature. This value was determined from the Tauc plot shown in **Figure S6**,[31] is similar to previously reported sputtered carbon films,[12] and much smaller than the bandgap of diamond (5.5 eV).

We also measured the heterogeneous electron-transfer rate constant of the unmodified films in a 1 mM solution of ferrocene in acetonitrile containing 0.25 M TBAPF. Figure 1B is a representative series of cyclic voltammograms with scan rates ranging from 0.025 to 50 V/sec. We determined a rate constant of 0.038 cm/s from these cyclic voltammograms with a Trumpet plot analysis (**Figure 1C**) initially described by Nicholson.[32]

3.2 Preparation, Characterization, and Reactivity of Azide-Terminated aC Films

To maximize the replacement of surface-bound chlorine atoms with azide groups, we investigated a number of reaction conditions, including sodium azide concentration, reaction time, reaction temperature, and the presence of a chelating agent. To evaluate the efficiency of each reaction, we relied on the high-resolution N 1s spectrum of each surface. **Table 2** summarizes the total atomic nitrogen incorporated onto the surface, the presence of the azide group, and the percentage of chlorine atoms that were lost and replaced by an azide group for a select number of reaction conditions; the SI contains a comprehensive list. The characteristic peak at 404.4 eV identified the presence of a surface-bound azide group.[33] A detailed explanation of the chlorine replacement percentage calculation is provided in Appendix E.

The highest azide incorporation onto the aC films was in a polar aprotic solvent, further supporting the S_N2-like mechanism proposed previously.[34] We also found that increases in reaction time and temperature increased the percentage of chlorine replacement, while the addition of a chelating agent had no significant effect. The reaction conditions that yielded the largest incorporation of azide groups on the surface, without surface oxidation, were 50 mM sodium azide in DMF at room temperature for 24 h. These reaction conditions were used for the remainder of this work.

We attached ethynyl ferrocene to azide-terminated aC films with the CuAAC reaction conditions developed by Das *et al*. to functionalize boron-doped diamond electrodes.[10] To assess the success of the reaction, we compared high-resolution N 1s spectra before and after the click reaction (**Figure 2A**). Before the reaction, the N 1s spectrum was fit with three components, which correspond to the middle nitrogen of the azide group (404.4 eV); the degradation product of the azide group (399.3), which occurs upon exposure to X-rays;[35] and the other nitrogen atoms in the azide group species (400.7 eV). After the reaction, the disappearance of the peak at 404.4 eV confirmed the formation of the triazole ring. The peak at 400.7 eV remained, indicating the ethynyl ferrocene was covalently attached to the surface. There also was a prominent doublet at 721.2 and 708.0 eV after the click reaction (**Figure 2B**). These peaks correspond to the $2p_{3/2}$ and $2p_{1/2}$ electrons of the iron (II) species in the ferrocene molecules.

To determine if the CuAAC reaction was selective, we also attempted to attach ethynyl ferrocene to two control films: hydrogen-terminated aC films that underwent no chemical manipulation and chlorine-terminated aC films to ensure chemical modification did not inadvertently make the surface more reactive to alkyne-containing molecules. Neither of these films contained a detectable iron signal in the survey or Fe 2p high-resolution XP spectra

(**Figure 2B**). Representative survey and high-resolution XP spectra for the azide-aC surfaces before and after the click reaction are included in the SI.

3.3 Electrochemical Characterization of Ferrocene-modified aC Films

To characterize the electrochemical performance of the ferrocene-modified aC films, we measured a series of cyclic voltammograms in acetonitrile containing 0.25 M TBAPF with scan rates ranging from 50 – 500 mV/sec (**Figure 3A**). The linear relationship between peak current and scan rate (**Figure 3B**) supported our XPS data and confirmed the ferrocene molecules were surface bound.[36] Surface coverage was calculated with Equation 1, where:

$$\Gamma = \frac{Q}{nFA} \qquad \text{Eqn. 1}$$

Γ is surface coverage, Q is charge, n is the number of electrons, F is Faraday's constant, and A is area of the electrode. The calculated coverage was 1.40×10^{13} molecules/cm^2 at 0.5 V/s. The E^o value for ferrocene (0.62 V) was cathodically shifted compared to previously reported values for modified carbon materials and the ΔE_p of each scan was larger than 0.17 V. **Table 3** summarizes our data as well as values collected by others where ferrocene was attached to carbon-based materials with the CuAAC reaction.

We note a second oxidative peak was present for a 10 mV/s scan rate (**Figure S7**). We hypothesize this peak is due to residual copper on the azide film, perhaps an intermediate of the CuAAC reaction. A high-resolution Cu 2p spectrum of the film confirmed a small amount of copper on the film.

4. Discussion

4.1 New Strategies for Generating CuAAC-compatible Surface Chemistries

Surface chemistries that can reproducibly install monolayers onto the surface of carbonaceous materials would provide an alternative and stable interface for fabricating light-driven devices. The installation of functional groups that are compatible with click chemistries is particularly compelling, as a single surface can be modified with a diverse set of molecules or functional groups. A number of chemical strategies for preparing CuAAC-compatible carbonaceous materials have been described, including: the attachment of aryldiazonium groups with terminal alkynes,[37, 38] the mesylate-assisted S_N2 replacement of primary alcohol with an azide,[27] the carbodiimide coupling of 4-azidobenzoic acid onto surface alcohols,[10] and gas-phase and wet-chemical Hassner-like reactions where IN_3 molecules install terminal azide groups directly onto the surface of glassy carbon and graphite.[22, 25]

Here, we attached azide groups onto the surface of aC films using a two-step reaction scheme. This approach, which replaces surface-bound chlorine atoms with nucleophilic species, has been used to covalently modify the surface of carbon, silicon, and germanium substrates.[18, 19, 39-41] For this particular reaction, we found the efficiency of this substitution reaction was greatly influenced by the solvent system, with the polar aprotic solvent DMF yielding the highest number of azide groups on the surface. Cao *et al*. also found that polar aprotic solvents were well suited for installing azides onto chlorine-terminated silicon surfaces.[42] In a separate study, Lange *et al.* showed aqueous solutions containing a chelating agent resulted in the greatest replacement of silicon nitride-bound amine groups with azides.[43] We were unable to detect azides on the aC films for reactions that used water as a solvent or included a chelator, 15-crown-5.

The successful attachment of ethynyl ferrocene to the azide-terminated films demonstrates the utility of this modification strategy and has superior stability and selectivity over our previous attempts at generating an aC surface that was compatible with thiol-ene reactions.

4.2 Amorphous Carbon Films as Modified Electrodes

There are a large number of studies that utilize carbon-based materials as electrodes, including aC films.[15, 44] The behavior of these electrodes is dictated by their surface properties as well as their bulk conductivity.[15] For aC films, these properties are tuned by altering the ratio of sp^2– and sp^3–hybridized carbons in the material.[11, 12] For magnetron sputtered films prepared in a non-reducing environment, aC films contain a large percentage of sp^2-hybridized carbons. Coskun *et al.* previously showed that the sp^3–to–sp^2 ratios obtained from fitting the C1s high-resolution XP spectrum correlated with sp^2–character estimates obtained from the optical bandgap.[11] Our XPS measurements suggest the films are largely sp^2 in nature as well as the optical bandgap measurements. Recently, Zemek *et al.* showed that the sp^3-to-sp^2 ratio of the surface (top 1 nm) of diamond-carbon was significantly different than bulk with angle-resolved XP measurements.[45] The heterogeneous electron transfer rate for ferrocene on the unmodified aC films (0.038 cm/s) further supports the graphitic composition of the surface as it more closely matches previously reported values of ferrocene in acetonitrile obtained with a glassy carbon electrode (2.3×10^{-4} cm/s) than with a boron-doped diamond electrode (5.8×10^{-2} cm/s).[46, 47]

To determine the utility of our method of preparing chemically modified electrodes, we compared the coverage and performance of our aC films with other carbon electrodes to which ferrocene was attached. **Table 3** summarizes these values. Despite differences in attachment chemistry, the calculated coverage for our aC films (1.40×10^{13} molecules/cm^2) is comparable to

modified graphene, carbon nanofibers, and glassy carbon substrates. Boron-doped diamond films had significantly higher densities of ferrocene, with 1.6×10^{14} and 3.46×10^{14} molecules/cm^2. Our results can be rationalized by the structure of the surface of aC films, which lack the crystalline structure of boron-doped diamond and more like graphitic carbon materials with regions of the highest reactivity toward chemical modification associated with edge planes.

The cyclic voltammograms of the ferrocene-modified films had significant peak-to-peak separation (ΔE_p = 0.19 V for a 100 mV/sec scan rate) compared to the ΔE_p = 0 mV, commonly accepted for idealized surface-bound species that are reversible.[48] Das *et al.* also reported a large ΔE_p value for boron-doped diamond electrodes, to which ethynyl ferrocene was attached to surface-bound 4-azidobenzoic acid molecules.[10] While this study attributed the large ΔE_p value to the semiconducting nature of their substrate, we attribute this large separation to two surface-centric possibilities: 1) the influence of neighboring ferrocene groups whose repulsive forces affect the ease of oxidation,[36] or 2) the proximity of the electroactive species and the electrode surface allowing for the possibility of the electric field of the double layer to affect electron transfer kinetics. Previous studies using “molecular rulers”—ferrocene-terminated alkylthiol self-assembled monolayers on gold substrates—showed that increasing the distance between the ferrocene and the initiation of the double layer influenced the electron transfer rate. This study was only able to probe 0.25 nm above a diluent monolayer making it difficult to discern the influence of the double layer’s electric field on electron transfer kinetics.[49] Further studies are needed to investigate the double layer’s potential field influence on the electron transfer of immobilized species near the electrode surface.

5. Conclusions

This work is the first of which we are aware that prepares, characterizes, and modifies azide-terminated aC films with a copper-catalyzed azide-alkyne cycloaddition reaction. Unlike the thiol-ene compatible aC films we reported previously, the azide-alkyne click reactions are selective with no unwanted attachment to control films that do not contain terminal azide groups. The number of ferrocene groups covalently attached to the surface is comparable to other graphitic carbon materials. The results presented here suggest that these films will support the attachment of chromophores, providing a stable interface that can, unlike alkylphosphonate-metal oxide linkages, withstand the reaction conditions used in dye-sensitized solar cells and dye-sensitized photoelectronsynthesis cells.

6. Figures and Tables

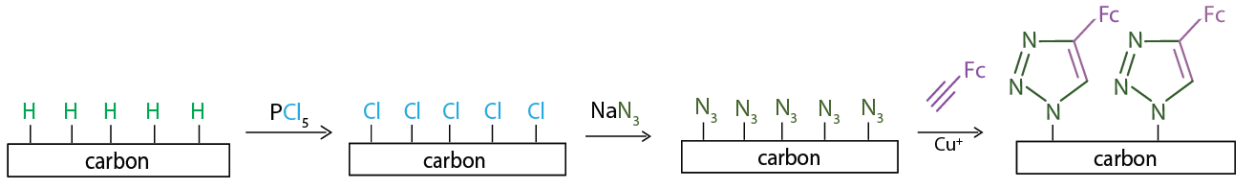

Scheme 4.1. Modification of aC films.

Table 4.1. Elemental composition of aC films after each chemical modification

aC film	Atomic Concentration (%)									O/C ratio
	C 1s	O 1s	N 1s components [a]				Cl 2p	Fe 2p	Cu 2p	
			Total	399 eV	400 eV	404 eV				
Unmodified	90.73	8.76	0.51	--	--	--	--	--	--	0.10
H-aC	89.50	10.50	0.00	--	--	--	--	--	--	0.12
Cl-aC	89.59	6.51	0.00	--	--	--	3.90	--	--	0.07
N_3-aC	89.28	7.32	1.00	0.4	0.48	0.12	2.40	--	--	0.08
Fc-aC	89.19	8.33	0.68	0.31	0.37	--	1.68	0.10	0.02	0.09

[a] Peak fitting was performed on the N 1s spectra for the N_3-aC and Fc-aC surfaces.

Table 4.2. Selected reaction conditions evaluated for azide attachment on aC films

					XPS Analysis		
NaN_3 (mM)	Solvent	Time (h)	Temp (^oC)	15-crown-5 (mM)	Chlorine lost and replaced by an azide group (%) [a]	Detectable azide signal at 404.4 eV	ΔO/C [b]
50	DMF:H_2O (1:1)	3	RT	—	—	X	
100	Methanol	3	RT	—	5.6	✓	–0.02
50	DMF	3	RT	—	—	X	+0.01
50	DMF	24	RT	—	41.7	✓	+0.01
50	DMF	24	RT	50	33.3	✓	+0.03
100	DMF	24	RT	—	33.7	✓	0.00
100	DMF	3	50	—	49.6	✓	+0.07

[a] Detailed calculation of percent chlorine replacement is in Appendix E.

[b] ΔO/C values are in relation to the O/C ratio of the chlorine-terminated aC films

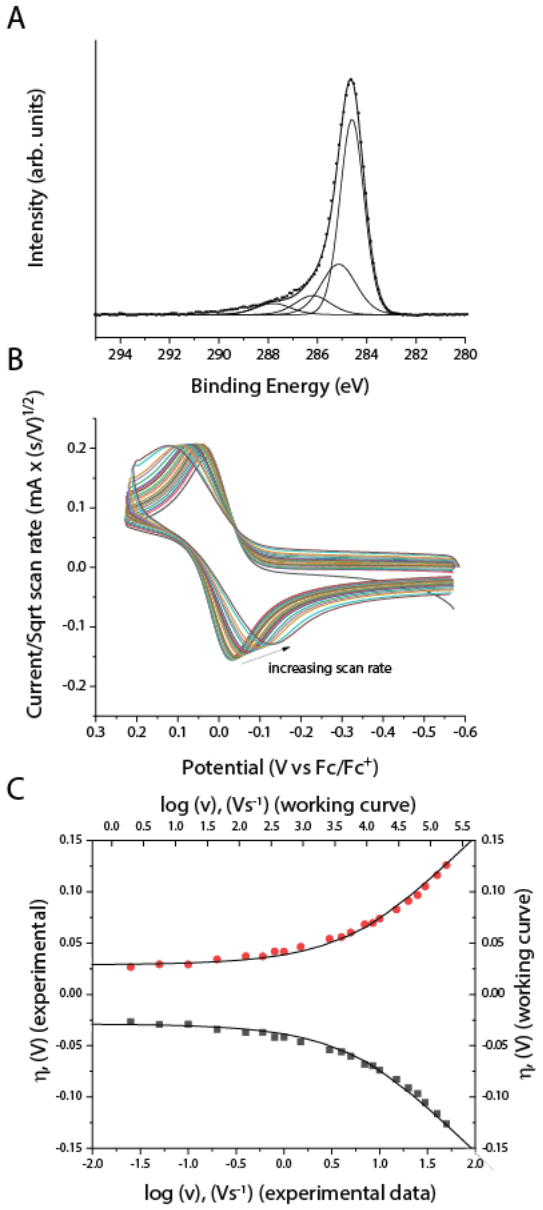

Figure 4.1. Summary of characterization of aC films as electrodes. (A) Representative C 1s high-resolution XP spectrum of an unmodified aC film on an FTO substrate with peak fits. (B) Cyclic voltammograms of an unmodified aC film on FTO at scan rates ranging from 0.025-50 V/sec in an acetonitrile solution containing ferrocene and 0.25 M TBAFP. Electrode area = 0.11 cm^2. (C) Experimental data (dots) and simulated working curves (lines) used to determine the heterogeneous electron-transfer rate constant with the CV data collected in B.

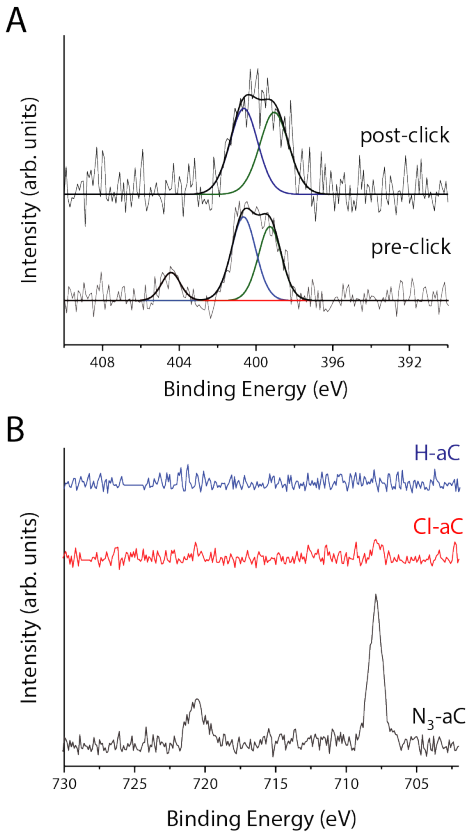

Figure 4.2. XPS summary for azide-alkyne click reaction. (A) Representative high-resolution N 1s XP spectra for an azide-terminated aC (N_3-aC) film before and after a CuAAC reaction with ethynyl ferrocene. (B) Representative high-resolution Fe 2p XP spectra for hydrogen-terminated (H-aC), chlorine-terminated (Cl-aC), and N_3-aC films after a CuAAC reaction with ethynyl ferrocene.

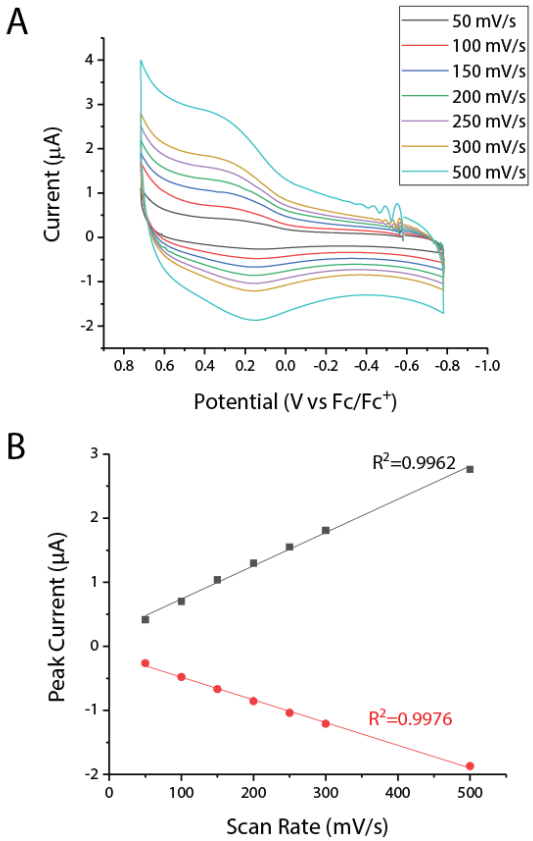

Figure 4.3. Summary of electrochemical data obtained for ferrocene-terminated aC film. (A) Cyclic voltammograms of a ferrocene-terminated aC film at different scan rates in an acetonitrile solution containing 0.25 M TBAFP. (B) Peak current as a function of scan rate with corresponding R^2 values.

Table 4.3. Electrochemical properties of ferrocene-modified carbon electrodes [a,b]

Electrode material	Terminal group	Linking chemistry	Chemical steps	Coverage ($\times 10^{13}$ molec/cm^2)	E^o_{red} vs. Ag/AgCl (V)	$E_{FWMH,\ reduction}$ (V)	ΔEp (V)	Scan Rate (V/sec)	Reference
aC	Azide	Replacement of surface-bound chlorine atoms	2	1.4	0.615	--	0.174	0.05	This work
GC	Azide	IN_3 gas	2	8 (1)	0.311	0.17 (0.01)	0.015	10	
	Azide	IN_3 hexane solution	2	6 (1)	NR	NR	NR	NR	[25]
	Azide	IN_3 acetonitrile solution	2	3 (1)	NR	NR	NR	NR	
PPF	Azide	IN_3 solution	1	2	NR	0.15	NR	5	[22]
VACNF	Azide	IN_3 solution	1	8.8 (0.7)	0.293	0.147 (0.015)	0.08	1	[24]
Diamond	Azide	Carbodiimide coupling of 4-azidobenzoic acid to surface hydroxyl groups	1	34.6 (0.5)	0.63	NR	0.296	0.1	[10]

Diamond	Azide	UV-initiated alkene attachment	2	16	0.39	0.12	0.04	0.1	[27]
PG	Azide	Reduction of aryldiazonium salt	1	86	0.372	0.17	0.045-0.055	0.1	[23]
	Alkyne		1	16.3	NR	NR	NR	NR	
GC	Azide	Reduction of aryldiazonium salt	1	20	NR	NR	NR	NR	[23]
	Alkyne		1	5.4	NR	NR	NR	NR	
PPF	Alkyne	Reduction of aryldiazonium salt (monolayer)	2	25.9	NR	NR	NR	NR	[38]
GC	Alkyne	Reduction of aryldiazonium salt (monolayer)	2	26.5	NR	NR	0.04	0.2	[37]
		Reduction of aryldiazonium salt (multilayer)	1	13.2	NR	NR	0.05	0.2	

[a] NR = not reported in publication.

[b] values in parentheses are standard deviations, as stated in cited works.

REFERENCES

1. D.L. Ashford, M.K. Gish, A.K. Vannucci, M.K. Brennaman, J.L. Templeton, J.M. Papanikolas, G.J. Meyer, Molecular chromophore-catalyst assemblies for solar fuel applications. *Chem. Rev.* **2015**, *115*, 13006-13049.

2. M.K. Brennaman, R.J. Dillon, L. Alibabaei, M.K. Gish, C.J. Dares, D.L. Ashford, R.L. House, G.J. Meyer, J.M. Papanikolas, T.J. Meyer, Finding the way to solar fuels with dye-sensitized photoelectrosynthesis cells. *J. Am. Chem. Soc.* **2016**, 1*38*, 13085-13102.

3. L. Alibabaei, H. Luo, R.L. House, P.G. Hoertz, R. Lopez, T.J. Meyer, Applications of metal oxide materials in dye sensitized photoelectrosynthesis cells for making solar fuels: Let the molecules do the work. *J. Mater. Chem. A* **2013**, *1*, 4133-4145.

4. J.T. Hyde, K. Hanson, A.K. Vannucci, A.M. Lapides, L. Alibabaei, M.R. Norris, T.J. Meyer, D.P. Harrison, Electrochemical instability of phosphonate-derivatized, ruthenium(III) polypyridyl complexes on metal oxide surfaces. *ACS Appl. Mater. Interfaces* **2015**, 7, 9554-9562.

5. J.A. Mann, W.R. Dichtel, Improving the binding characteristics of tripodal compounds on single layer graphene. *ACS Nano* **2013**, *7*, 7193-7199.

6. J.A. Mann, J. Rodriguez-Lopez, H.D. Abruna, W.R. Dichtel, Multivalent binding motifs for non-covalent functionalizationof graphene. *J. Am. Chem. Soc.* **2011**, *133*, 17614-17617.

7. C.M. Hanna, C.D. Sanborn, S. Ardo, J.Y. Yang, Interfacial electron transfer of ferrocene immobilized onto indium tin oxide through covalent and noncovalent interactions. *ACS Appl. Mater. Interfaces* **2018**, *10*, 13211-13217.

8. M.C. Granger, M. Witek, J.S. Xu, J. Wang, M. Hupert, A. Hanks, M.D. Koppang, J.E. Butler, G. Lucazeau, M. Mermoux, J.W. Strojek, G.M. Swain, Standard electrochemical behavior of high-quality, boron-doped polycrystalline diamond thin-film electrodes. *Anal. Chem.* **2000**, *72*, 3793-3804.

9. G.M. Swain, R. Ramesham, The electrochemical activity of boron-doped polycrystalline diamond thin-film electrodes. *Anal. Chem.* **1993**, *65*, 345-351.

10. M.R. Das, M. Wang, S. Szunerits, L. Gengembre, R. Boukherroub, Clicking ferrocene groups to boron-doped diamond electrodes. *Chem. Commun.* **2009**, *19*, 2753-2755.

11. O.D. Coskun, T. Zerrin, Optical, structural and bonding properties of diamond-like amorphous carbon films deposited by DC magnetron sputtering. *Diamond Relat. Mater.* **2015**, *56*, 29-35.

12. J. Robertson, Diamond-like amorphous carbon. *Mater. Sci. Eng., R*, **2002**, *32*, 129-281.

13. M.R. Lockett, L.M. Smith, Carbon substrates: A stable foundation for biomolecular arrays. *Annu. Rev. Anal. Chem.* **2015**, *8*, 263-285.

14. R.J. Hamers, Formation and characterization of organic monolayers on semiconductor surfaces. *Annu. Rev. Anal. Chem*. **2008**, *1*, 707-736.

15. R.L. McCreery, Advanced carbon electrode materials for molecular electrochemistry. *Chem. Rev.* **2008**, *108*, 2646-2687.

16. P.E. Colavita, J.A. Streifer, B. Sun, X. Wang, P. Warf, R.J. Hamers, Enhancement of photochemical grafting of terminal alkenes at surfaces via molecular mediators: The role of surface-bound electron acceptors. *J. Phys. Chem. C* **2008**, *112*, 5102-5112.

17. D.R. Jayasundara, R.J. Cullen, P.E. Colavita, Is situ and real time characterization of spontaneous grafting of aryldiazonium salts at carbon surfaces. *Chem. Mater.* **2013**, *25*, 1144-1152.

18. C.G. McKenas, J.M. Fehr, B. Liu, C.L. Donley, M.R. Lockett, Mechanistic insights into UV-initiated thiol-ene reactions on amorphous carbon films. *J. Phys. Chem. C* **2018**, *122*, 21854-21860.

19. C.G. McKenas, J.M. Fehr, C.L. Donley, M.R. Lockett, Thiol-Ene Modified Amorphous Carbon Substrates: Surface Patterning and Chemically Modified Electrode Preparation. *Langmuir* **2016**, *32*, 10529-10536.

20. H.C. Kolb, M.G. Finn, K.B. Sharpless, Click chemistry: Diverse chemical function from a few good reactions. *Angew. Chem. Int. Ed.* **2001**, *40*, 2005-2021.

21. H.C. Kolb, K.B. Sharpless, The growing impact of click chemistry on drug discovery. *Drug Discov. Today* **2003**, *8*, 1128-1137.

22. A. Devadoss, C.E.D. Chidsey, Azide-modified graphitic surfaces for covalent attachment of alkyne-terminated molecules by "click" chemistry. *J. Am. Chem. Soc.* **2007**, *129*, 5370-5371.

23. D. Evrard, F. Lambert, C. Policar, V. Balland, B. Limoges, Electrochemical functionalization of carbon surfaces by aromatic azide or alkyne molecules: A versatile platform for click chemistry. *Chem. - Eur. J.* **2008**, *14*, 9286-9291.

24. E.C. Landis, R.J. Hamers, Covalent grafting of redox-active molecules to vertically aligned carbon nanofiber arrays via “click” chemistry. *Chem. Mater.* **2009**, *21*, 724-730.

25. E.D. Stenehjem, V.R. Ziatdinov, T.D.P. Stack, C.E.D. Chidsey, Gas-phase azide functionalization of carbon. *J. Am. Chem. Soc.* **2013**, *135*, 110-1116.

26. Y. Zhang, H. He, C. Gao, J.Y. Wu, Covalent layer-by-layer functionalization of multiwalled carbon nanotubes by click chemistry. *Langmuir*, **2009**, *25*, 5814-5824.

27. R.E. Ruther, Q. Cui, R.J. Hamers, Conformational disorder enhances electron transfer through alkyl monolayers: Ferrocene on conductive diamond. *J. Am. Chem. Soc.* **2013**, *135*, 5751-5761.

28. H. Nandivada, X.W. Jiang, J. Lahann, Click chemistry: Versatility and control in the hands of materials scientists. *Adv. Mater.* **2007**, *19*, 2197-2208.

29. P.E. Colavita, B. Sun, K.Y. Tse, R.J. Hamers, Photochemical grafting of n-alkenes onto carbon surfaces: The role of photoelectron ejection. *J. Am. Chem. Soc.* **2007**, *129*, 1355-13565.

30. M.R. Lockett, L.M. Smith, Attaching molecules to chlorinated and brominated amorphous carbon substrates via Grignard reactions. *Langmuir* **2009**, *25*, 3340-3343.

31. J. Tauc, Optical properties and electronic structure of amorphous Ge and Si. *Mater. Res. Bull.* **1968**, *3*, 37-46.

32. R.S. Nicholson, Theory and application of cyclic voltammetry for measurement of electrode reaction kinetics. *Anal. Chem.* **1965**, *37*, 1351-1355.

33. E.W. Wollman, D. Kang, C.D. Frisbie, I.M. Lorkovic, M.S. Wrighton, Photosensitive self-assembled monolayers on gold: Photochemistry of surface-confined aryl azide and cyclopentadienyl manganse tricarbonyl. *J. Am. Chem. Soc.* **1994**, *116*, 4395-4404.

34. M.R. Lockett, L.M. Smith, The formation and stability of alkylthiol monolayers on carbon substrates. *J. Phys. Chem. C* **2010**, *114*, 12635-12641.

35. G. Zorn, H. Liu, L. Arnadottir, H. Wang, L.J. Gamble, D.G. Castner, M. Yan, X-ray photoelectron spectroscopy investigation of the nitrogen species in photoactive perfluorophenylazide-modified surfaces. *J. Phys. Chem. C* **2014**, *118*, 376-383.

36. A.J. Bard, L.R. Faulkner. *Electrochemical Methods: Fundamentals and Applications*, 2nd ed.; John Wiley & Sons, 2001.

37. Y.R. Leroux, H. Fei, J.M. Noel, C. Roux, P. Haipot, Efficient covalent modification of a carbon surface: Use of a silyl protecting group to form an active monolayer. J. *Am. Chem. Soc.* **2010**, *132*, 14039-14041.

38. S.Y. Sayed, A. Bayat, M. Kondratenko, Y. Leroux, P. Haipot, R.L. McCreery, Bilayer molecular electronics: All-carbon electronic junctions containing molecular bilayers made with "click" chemistry. *J. Am. Chem. Soc.* **2013**, *135*, 12972-12975.

39. D. Knapp, B.S. Brunschwig, N.S. Lewis, Chemical, electronic, and electrical properties of alkylated Ge(111) Surfaces. *J. Phys. Chem. C* **2010**, *114*, 12300-12307.

40. K.T. Wong, N.S. Lewis, What a difference a bond makes: The structural, chemical, and physical properties of methyl-terminated Si(111) surfaces. *Acc. Chem. Res* **2014**, *47*, 3037-3044.

41. P. Ardalan, C.B. Musgrave, S.F. Bent, Formation of alkanethiolate self-assembled monolayers at halide-terminated Ge surfaces. *Langmuir* **2009**, *25*, 2013-2025.

42. P.G. Cao, K. Xu, J.R. Heath, Azidation of silicon(111) surfaces. *J. Am. Chem. Soc.* **2008**, *130*, 14910-14911.

43. N. Lange, P.M. Dietrich, A. Lippitz, N. Kulak, W.E.S. Unger, New azidation methods for the functionalization of silicon nitride and application in copper-catalyzed azide-alkyne cycloaddition (CuAAC). *Surf. Interface Anal.* **2016**, *48*, 621-625.

44. R. Schlesinger, M. Bruns, H.J. Ache, Development of thin film electrodes based on sputtered amorphous carbon. *J. Electrochem. Soc.* **1997**, *144*, 6-15.

45. J. Zemek, J. Houdkova, P. Jiricek, M. Jelinek, Surface and in-depth distribution of sp2 and sp3 coordinate carbon atoms in diamond-like carbon films modified by argon ion beam bombardment during growth. *Carbon* **2018**, *134*, 71-79.

46. L. Xiao, E.J.F. Dickinson, G.G. Wildgoose, R.G. Compton, A comparison of electron transfer kinetics of three common carbon electrode surfaces in acetonitrile and in room temperature ionic liquid 1-butyl-3- methylimidazolium hexafluorophosphate: Correlation to surface structure and the limit of the diffusion domain approximation. *Electroanalysis* **2010**, *22*, 269-276.

47. D.Y. Kim, J.C. Yang, H.W. Kim, G.M. Swain, Heterogeneous electron-transfer rate constants for ferrocene and ferrocene carboxylic acid at boron-doped diamond electrodes in a room temperature ionic liquid. *Electrochim. Acta* **2013**, *94*, 49-56.

48. H.O. Finklea, D.D. Hanshew, Electron-transfer kinetics in organized thiol monolayers with attached pentaamine(pyridine)ruthenium redox centers. *J. Am. Chem. Soc.* **1992**, *114*, 3173-3181.

49. P.K. Eggers, N. Darwish, M.N. Paddon-Row, J.J. Gooding, Surface-bound molecular rulers for probing the electrical double layer. *J. Am. Chem. Soc.* **2012**, *134*, 7539-7544.

CHAPTER 5- MODIFICATION OF AMORPHOUS CARBON FILMS WITH IN SITU GRIGNARD REACTIONS

1. Introduction

Modification of materials to append molecules to generate a functional material has gained importance in many fields, including solar cells and photo-catalytic devices. For example, metal oxides have emerged as a popular material in both fields, therefore there is much investigation as to how to modify these materials, both non-covalently and covalently.[1–3] Non-covalent modification techniques often involve utilizing pi-pi stacking interactions; in order to utilize pi-pi stacking interactions on metal oxide materials, a carbon support must first be integrated onto the material.[2,3] Therefore, there have been a number of studies that have utilized carbon-based substrates as a proof of concept prior to the integration of carbon films onto metal oxides.[4–10] However, the strength of the pi-pi interactions is dependent on the solvent system used, as one study showed that the 1-pyrenylferrocene desorbed when a solvent it was soluble in was used.[2] Another type of non-covalent modification approach involves the use of carboxylic acid based monolayers; this approach is often characterized as a covalent modification approach, but the carboxylate group is only adsorbed to the metal oxide film.[1] Covalent modification includes the use of the following functional groups: silanes, phosphonates, catechols, amines, and alkenes/alkynes.[1] Silane monolayer formation is an attractive approach, as they form well-ordered monolayers and many silane molecules with varying terminal groups are available commercially. This versatility allows for other molecules to be installed on the surface with subsequent reactions;[11,12] for example, one study utilized an azide-terminated siloxane to attach

an alkyne-modified ruthenium dye complex via a copper-catalyzed azide-alkyne click reaction.[12] Phosphonate-based linkages have been shown to be prone to degradation under electrochemical cycling, making them unattractive as a long-term choice for linkage of dye molecules to metal oxide films.[13] Catechol-based modification is a relatively new field, and therefore the mechanism of attachment has not been fully characterized. The mechanism of amine-based monolayers is still being characterized, and it is possible that this approach is actually non-covalent in nature given the known mechanical instability and weak attachment to the metal oxide film. Molecules with terminal vinyl groups have been directly attached metal oxide films, either thermally or photochemically.[2,14] The mechanism of the photochemical attachment of alkenes to metal oxides is believed to be mediated via electron-hole pair formation at the metal oxide surface upon photon absorption; the hole is thought to be distributed over the hydroxyl group, allowing it to react with the vinyl group to form a carbon-oxygen bond.[15] However, this photochemical attachment mechanism forms multilayers lending to a less stable material and making it difficult for further modification of the material.[16] Thermal attachment of vinyl-terminated molecules to metal oxides offers an alternative approach that favors monolayer-formation and well-ordered materials.[14]

When developing modified materials for applications such as solar cells, it is important to understand the effect of the modification on the electron transfer process at the surface. Electron transfer of a species attached to an electrode surface was first studied on self-assembled monolayers (SAMs) on gold.[17–19] These monolayers form very well-ordered structures at the surface lending to outstanding electron transfer properties. For example, cyclic voltammetry of a ruthenium-modified gold electrode via thiol monolayers revealed: 1) a formal potential of the ruthenium similar to that found in solution, 2) equal integration of the anodic and cathodic peaks

that was not dependent on scan rate, 3) peak splitting of 0 mV, and 4) peak half-widths of 90-100 mV.[19] Furthermore, the peak current scales with scan rate for a surface-bound electron transfer process.[20] These characteristics have been held as the "gold standard" for surface-bound electron transfer even though SAMs on gold monolayers are not representative of the disordered monolayers commonly found on metal oxides or carbon-based materials. [1,21] The disordered monolayers that result from the direct attachment of alkene-containing molecules or silane molecules to metal oxide surfaces have non-ideal electrochemical behavior often resulting in significant peak splitting and larger peak half-widths.[2,11,12] This non-ideal surface-bound electron transfer behavior has also been observed for ferrocene molecules covalently attached to diamond,[22–24] glassy carbon,[25,26] amorphous carbon,[27,28] carbon nanofibers,[29] and silicon.[30–32] Explanations for this non-ideality include the nature of the semiconducting electrode, uncompensated resistance of the film, the insulating nature of the appended monolayer, and lateral interactions of the head groups. Laviron developed a theory and subsequently an equation that accounts for the effect of these repulsive or attractive lateral interactions on the relationship of peak current and scan rate.[33] However, none of the aforementioned studies utilize this relationship for their surface-bound electron transfer studies to understand the non-idealities in their electrochemical data.

Interestingly, disordered monolayers display trends opposite of SAMs on gold. For example, electron transfer rates for SAMs on gold have been shown to decrease with increasing spacer length between the electroactive molecule and electrode surface;[19] however, the opposite has been seen for boron-doped diamond, where the spacer length does not affect the kinetics but the conformational disorder allows for faster electron transfer.[22] While SAMs on gold offer an idealized surface-bound electron transfer model, it is clear that further understanding of the

electron transfer through disordered monolayers is needed as trends found for SAMs on gold may not hold true for monolayers formed via covalent attachment strategies.

Amorphous carbon films are easily deposited on a variety of substrates and can be readily covalently modified via click chemistries to form chemically modified electrodes.[27,28] Unfortunately, these studies had low coverages of ferrocene compared to other modification approaches used on carbon-based materials and non-idealities in the CV peak shape and peak-to-peak separation that was not fully understood. In this work, we utilize an *in situ* Grignard reaction to modify chlorine-terminated amorphous carbon films with ferrocene molecules. Through this modification approach, the electron transfer as a function of surface coverage for covalently-attached ferrocene molecules was more robustly characterized and studied in order to understand electron transfer in a disordered monolayer.

2. Materials and Methods

2.1 Chemicals and Materials

All materials were used as received unless otherwise noted. Anhydrous acetonitrile, anhydrous benzene, benzoyl peroxide, iodine, isopropanol, magnesium turnings, and phosphorus pentachloride were purchased from Sigma Aldrich. Ethanol (200 proof) was purchased from VWR. Hydrochloric acid (conc.) was purchased from Fisher Scientific. Tetrabutylammonium hexafluorophosphate (TBAPF, Oakwood Chemical, 98%) was recrystallized from ethanol and dried in vacuo before usage. Reverse osmosis purified water (RO water, 18 mΩ) was used in all experiments.

All reactions carried out in a nitrogen-purged glove box used dry solvents that were sparged with argon in a solvent system (Pure Process Technology): acetonitrile (Fisher Scientific, HPLC

grade, >99.9%) and diethyl ether (VWR, ACS reagents). The solvents were then stored in a N_2 filled glovebox over molecular sieves.

2.2 Amorphous carbon film preparation and functionalization

Amorphous carbon films (25 nm) were magnetron sputtered onto fluorine-doped tin oxide-coated glass substrates (FTO, 15 Ω/sq., Hartford Glass) from a graphite target, as reported previously.[27] Prior to deposition, the FTO substrates were sonicated for 15-min intervals in ethanol and 1M HCl in ethanol. Films were hydrogen terminated in a 13.56 MHz inductively coupled hydrogen plasma (Diener Electronic) for 10 min. The films were then reacted at 80 ^{o}C for 15 min in a nitrogen-purged benzene solution containing 80 mM PCl_5 and 7 mM benzoyl peroxide. Films were rinsed copiously with ethanol and dried under vacuum.

The following reactions were performed in a N_2-filled glovebox. 6-bromohexyl ferrocene, whose synthesis was previously described, [34] was attached to the aC films using a modified version of an *in situ* Grignard reaction described by Marrani, *et.al.*[35] The modified approach involved different amounts of iodine, 6-bromohexyl ferrocene was used rather than 2-bromoethyl ferrocene, and a different cleaning procedure was used following the reaction. For the high-coverage slide and H-aC control, magnesium turnings (1 mmol) and iodine (0.1 mmol) were added to diethyl ether (20 mL) and stirred for approximately ten minutes before 6-bromohexyl ferrocene (1 mmol, 5mL diethyl ether) was added. The reaction mixture was stirred for approximately 20 minutes before the aC films were added. After ~16 hours, the reaction was quenched with water. For the low-coverage slide, the same procedure was followed using reduced amounts of magnesium turnings (0.5 mmol) and 6-bromohexyl ferrocene (0.05 mmol). Films were stored in isopropanol when transferring out of the glovebox and sonicated for 5

minutes in water followed by 5 minutes in ethanol; films were then dried under nitrogen and stored under an inert atmosphere when not used immediately.

2.3 Surface characterization

X-ray photoelectron (XP) spectroscopy was performed as described previously.[27,28,36] Analysis was carried out in an ultrahigh-vacuum system (Kratos Axis Ultra DLD) with a base pressure of 5×10^{-9} Torr, a monochromatic Al Kα source, and a hemispherical analyzer. Survey (1.0 eV resolution) and high-resolution (0.1 eV resolution) spectra were collected at a 0° takeoff angle from surface normal. Each high-resolution spectrum was Shirley background corrected, referenced to the C 1s peak (284.6 eV), which was fit with Voigt functions (70% Gaussian, 30% Lorentzian).

Electrochemical measurements were performed as described previously.[28] All electrochemical measurements were performed in an N_2-filled glovebox equipped with a WaveDriver bipotentiostat (Pine) and a conventional three-electrode system. The working electrode (0.12 cm^2) was an aC film deposited on an FTO substrate. The auxiliary electrode was a polished 3-mm glassy carbon disk electrode. The pseudo-reference electrode was a silver wire submerged in 0.25 M TBAPF in acetonitrile. Residual ohmic drop in each CV measurement was compensated using an approach developed for the WaveDriver. All scans were referenced to a ferrocenium/ferrocene redox couple at 0 V. All data analysis was performed in Origin.

3. Results and Discussion

The surface of amorphous carbon films have been modified with photochemical grafting of alkenes,[37,38] Grignard reactions on chlorinated films,[39,40] aryl diazonium salt reductions,[41] and

click chemistries.[27,28,36] The efficiency of the photochemical attachment of alkenes requires terminal functional groups that can easily accept electrons into their lowest unoccupied molecular orbitals which limits the type of molecules that can be attached.[42] Grignard reagents are limited by only using molecules that will not react with the organometallic reagents used in this reaction.[42] The grafting behavior of aryl diazonium salt reductions are dependent on the substituents, leading to differences in coverage and reaction kinetics.[41] While click chemistries are notoriously efficient,[43] they are limited by the number of reactive molecules on the film. Previously, we attached thiols, alkene, and azide groups to the surface of chlorine-terminated aC films via an S_N^2-like mechanism.[27,28,36] Bansal et al. first described this mechanism as a way to passivate silicon surfaces with alkyl groups.[44] The thiol-termination approach resulted in low coverages and air-sensitive surfaces, making further wet chemical reactions less efficient.[27] Vinyl-termination via a vinyl magnesium bromide reagent was difficult to track as there was not a unique XPS signature with the replacement of chlorine with a vinyl group; therefore, only the loss of chlorine could be measured, making a precise measurement of surface coverage difficult. While the photo-initiated attachment of thiol-terminated molecules onto vinyl-terminated surfaces was more efficient than our previous study utilizing thiol-terminated films, the reaction was not selective to vinyl-terminated films.[36] The selectivity of azide-modified films was much improved over our previous modification studies, but the azide degraded upon x-ray exposure, making quantification difficult.[28] Finally, the cyclic voltammograms obtained from the vinyl-terminated films modified with ferrocene via thiol-ene click chemistry and the azide-terminated film modified with ferrocene via azide-alkyne click chemistry resulted in very large peak splitting, indicating that the electron transfer was kinetically slow at the modified aC film.[27,28]

Boukherroub et al. have shown that hydrogen-terminated silicon (111) reacts similarly eliminating the need for chlorination.[45] Utilizing hydrogen-terminated silicon (100) surfaces, Marrani et al. attached brominated reagents to the surfaces using a Grignard reaction.[35] In this study, we utilize 6-bromohexyl ferrocene to attach to chlorinated amorphous carbon films via a Grignard reaction.

In order to determine the selectivity of the Grignard reaction, hydrogen- and chlorinated-terminated aC films underwent the same reaction conditions and were then analyzed with XPS. Only the chlorinated film contained an iron signal; a double at 708 and 720 eV is indicative of iron in its +2 oxidation state, as expected for ferrocene (**Figure 1**). Therefore, any iron that is attach to the hydrogenated aC film was not detected via XPS. Given the bond dissociation energy of a C-H bond (339 $kJmol^{-1}$) compared to a Si-H bond (~293 $kJmol^{-1}$),[46] it is much easier for the radical-based reaction mechanism proposed by Fellah et al. to occur on a hydrogen-terminated silicon surface.[47] This control also indicated that this reaction had good selectivity towards our chlorinated films. Finally, this reaction did not cause unwanted contamination of bromine, iodine, or magnesium or surface oxidation as evidenced by the oxygen-to-carbon ratios (**Table 1**).

One important advantage of wet, chemical reactions is the ability to modify concentration, time, and temperature to fine-tune the reaction completion on the surface. In order to obtain a surface with a lower coverage of iron, the *in situ* Grignard reaction was repeated with a lower concentration of magnesium and 6-bromohexyl ferrocene and no initiator was used. These reaction conditions favored a lower amount of iron present on the surface (~40% less), but did cause a slight increase in surface oxidation (**Figure 1 and Table 1**).

Characterizing the electron transfer through a disordered monolayer on a surface as a function of surface coverage will allow for optimization of materials that favor fast electron transfer kinetics. One such study investigated the disordered monolayers of ferrocene formed on conductive diamond via a copper catalyzed azide-alkyne click reaction.[22] This reaction first involved the photochemical grafting of hydroxyl-terminated alkenes; these hydroxyl groups were converted to an azide group via a mesylate intermediate. To understand the effects of surface coverage, the illumination time of the photochemical alkene grafting step was modulated to obtain lower and higher coverages. Upon analysis of electrochemical data at different coverages, a model to understand the experimental data was proposed. This model proposed that at low coverages, ferrocene-terminated alkyl chains were able to "bend" towards the electrode surface favoring fast electron transfer kinetics. With higher coverages, the ferrocene head groups were thought to be forced away from the electrode surface due to lateral interactions of the head groups thus favoring slower electron transfer kinetics. However, there was no analysis of the extent of these lateral interactions as a function of surface coverage.

A linear dependence of peak current on scan rate indicates surface-bound species.[20] Laviron developed an approach to correct for deviations from this linearity, or more precisely accounted for the presence of diffusive characteristics on these surfaces (i.e., large peak splitting) by considering a Frumkin-type isotherm.[33,48] In this model, the peak current (i_p) is scaled with scan rate raised to a power (v^n). If $n = 1$, there are either no lateral interactions or, if they are present, they compensate each other; whereas, if $n < 1$, there are lateral interactions present.

CVs of ferrocene-terminated amorphous carbon films at low and high coverages confirmed differences in coverage of the two films (**Figure 2A and 2B**). The coverage on the high density ferrocene surface was 7.22 x 10^{14} molecules/cm^2, which is comparable and even surpasses other

coverages on carbon-based materials using a variety of attachment chemistries.[22,24,28,29,49–52] The coverage on the low density ferrocene surfaces was 7.22 x 10^{13} molecules/cm^2 (**Table 2**). The traditional linear fit for equations (**Figure 2C and 2D**) was excellent for the low density ferrocene surfaces, but it did not fit the high coverage data as well as evidenced by R^2 values (**Table 2**). When the fit that accounts for lateral head group interactions was applied, where scan rate was treated as a power dependent variable, the value of n was found to be 0.93 for the low coverage and 0.72 for the high coverage. This is indicative that there is a greater influence of lateral head group interactions at a higher coverage.

Ruther et al. also proposed that lower coverages led to faster electron transfer due to conformational disorder that is allowed to occur in the alkyl chain linker as well as a smaller contribution from lateral head group interactions. Laviron also developed an expression to determine the apparent electron transfer rate constant for strongly adsorbed or redox modified electrodes.[48] This analysis was performed on a plot of overpotential (n) versus log of scan rate to determine the rate constants for both coverages (**Figure 2E and 2F**). For the low coverage, the rate constant was found to be 24 s^{-1}; the high coverage was 14 s^{-1} (**Table 2**). These results seem to corroborate the findings of Ruther et al.; however, our results indicate that the faster electron transfer rate for a low coverage may simply be due to less lateral interactions rather than conformational disorder. Further studies need to be done to elucidate the contributions from both of these factors.

4. Conclusions

While SAMs on gold have been the “gold standard” to determine electron transfer processes at a surface, they are a poor model for disordered monolayers. As a test platform, a covalent

chemical modification of amorphous carbon films was performed. This study shows that the direct attachment of molecules to chlorine-terminated aC films affords the highest coverages reported thus far. Furthermore, the influence of surface coverage on the electron transfer rate was studied, and lateral head group interactions were found to be a contributive factor to the large peak splitting often seen in covalently modified materials. However, it is not yet understood how linker length influences the electron transfer rate. Further studies need to be conducted to understand this effect. Finally, the heterogeneity of the film, both unmodified and modified, needs to be studied in order to understand the effect of the localized electron environment at the electrode upon electron transfer rate. While Laviron mathematically treats non-homogenously modified surfaces similarly to modified surfaces experiencing lateral head group interactions, it is unclear if non-homogeneity leads to blocking of electroactive sites and, subsequently, kinetic heterogeneity. Therefore, further studies need to be performed to understand the influence of surface heterogeneity, as well.

5. Figures and Tables

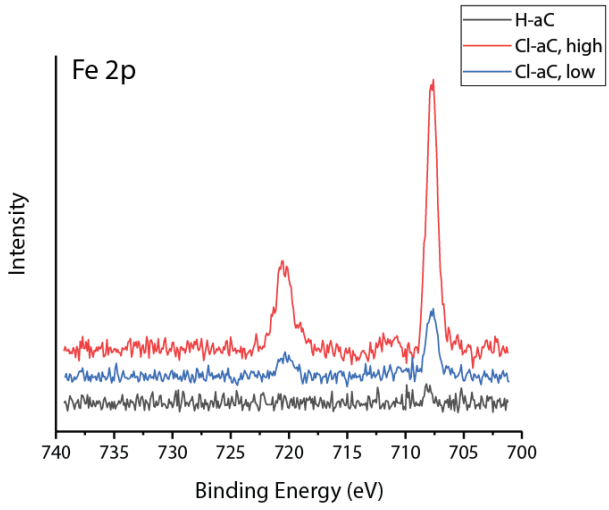

Figure 5.1. XPS data for Fe 2p region for an H-aC and Cl-aC films exposed to *in situ* Grignard reaction conditions. Cl-aC high and H-aC were exposed to reaction conditions that included the initiator; Cl-aC low was exposed to reaction conditions that did not include an initiator. Spectra are offset for clarity.

Table 5.1. XPS atomic concentration values for samples displayed in Figure 5.1: H-aC, Cl-aC high, and Cl-aC low film before (pre) and after (post) the *in situ* Grignard reaction.

			Atomic Concentration (%)								Ratios
Sample name	Pre/post click	Initiator?	C 1s	O 1s	N 1s	Cl 2p	Fe 2p	Br 3d	I 3d	Mg 1s	O/C
H-aC	Pre	Yes	90.77	9.23	0.00	0.00	--	--	--	--	0.10
	Post		91.16	8.84	0.00	0.00	0.00	0.00	0.00	0.00	0.10
Cl-aC, high	Pre	Yes	88.76	7.42	0.00	3.83	--	--	--	--	0.08
	Post		90.26	7.78	0.00	1.55	0.41	0.00	0.00	0.00	0.09
Cl-aC, low	Pre	No	89.15	7.30	0.00	3.55	--	--	--	--	0.08
	Post		89.60	8.64	0.00	1.50	0.26	--	--	--	0.10

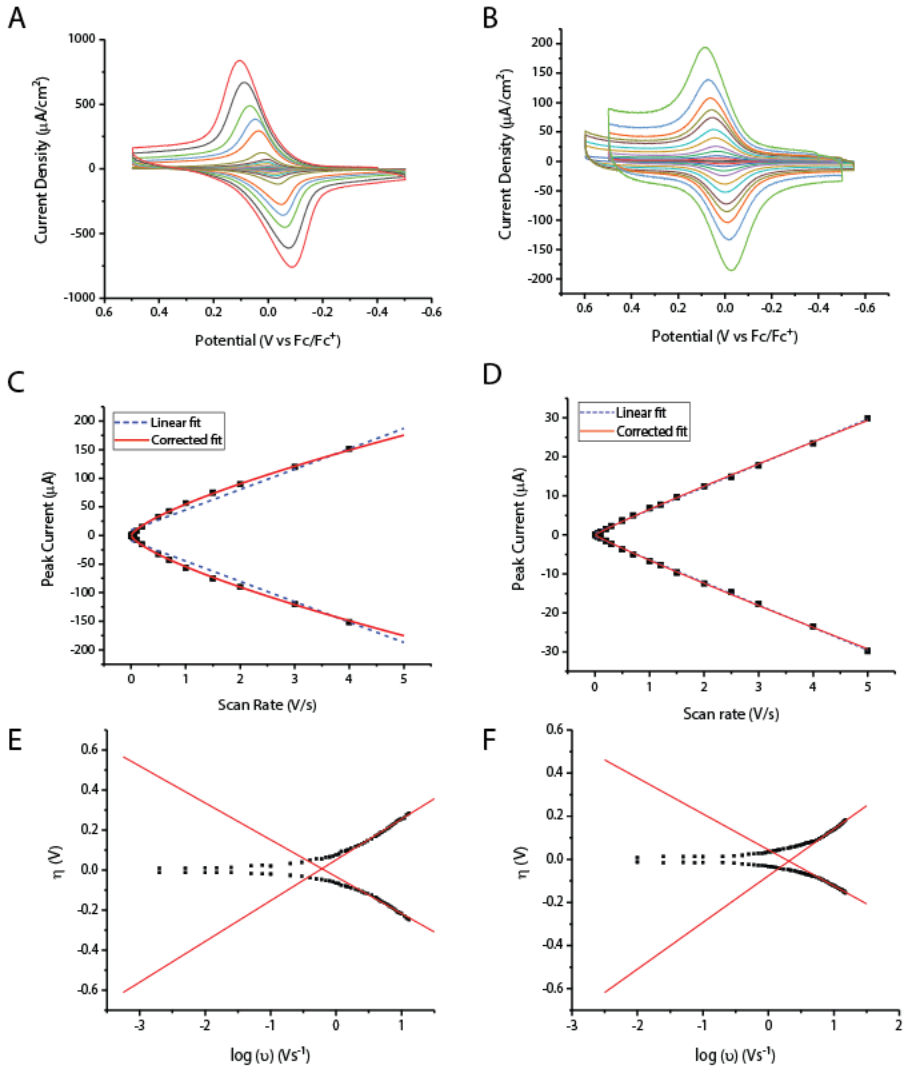

Figure 5.2. Summary of electrochemical data and analysis. Cyclic voltammograms obtained in 0.25 M TBAPF in ACN at various scan rates for a Cl-aC film modified with 6-bromohexyl ferrocene using an *in situ* Grignard reaction to obtain a (A) high coverage or (B) low coverage Fc-aC film. Peak current versus scan rate analysis with a linear fit and corrected fit accounting for lateral interactions for a (C) high coverage or (D) low coverage Fc-aC film. Trumpet plot analysis with Laviron fits for a (E) high coverage or (F) low coverage Fc-aC film.

Table 5.2. Summary of quantitative results. Coverage, rate constant, corrected n values, and R^2 values for a low or high coverage Fc-aC

	Coverage (molecules/cm^2)	Rate Constant (s^{-1})	Corrected "n" value	R^2 value (linear fit)	R^2 value, (corrected fit)
Fc-aC, low	7.22×10^{13}	24	0.93	0.9943	0.9988
Fc-aC, high	7.22×10^{14}	14	0.72	0.9733	0.9992

REFERENCES

1. Pujari, S. P.; Scheres, L.; Marcelis, A. T. M.; Zuilhof, H. Covalent Surface Modification of Oxide Surfaces Angewandte. *Angew. Chemie Int. Ed.* **2014**, *53*, 6322–6356.

2. Hanna, C. M.; Sanborn, C. D.; Ardo, S.; Yang, J. Y. Interfacial Electron Transfer of Ferrocene Immobilized onto Indium Tin Oxide through Covalent and Noncovalent Interactions. *ACS Appl. Mater. Interfaces* **2018**, *10* (15), 13211–13217.

3. Lydon, B. R.; Germann, A.; Yang, J. Y. Chemical Modification of Gold Electrodes: Via Non-Covalent Interactions. *Inorg. Chem. Front.* **2016**, *3* (6), 836–841.

4. Blakemore, J. D.; Gupta, A.; Warren, J. J.; Brunschwig, B. S.; Gray, H. B. Noncovalent Immobilization of Electrocatalysts on Carbon Electrodes for Fuel Production. *J. Am. Chem. Soc.* **2013**, *135* (49), 18288–18291.

5. Creus, J.; Matheu, R.; Peñafiel, I.; Moonshiram, D.; Blondeau, P.; Benet-Buchholz, J.; García-Antón, J.; Sala, X.; Godard, C.; Llobet, A. A Million Turnover Molecular Anode for Catalytic Water Oxidation. *Angew. Chemie - Int. Ed.* **2016**, *55* (49), 15382–15386.

6. Lei, H.; Liu, C.; Wang, Z.; Zhang, Z.; Zhang, M.; Chang, X.; Zhang, W.; Cao, R. Noncovalent Immobilization of a Pyrene-Modified Cobalt Corrole on Carbon Supports for Enhanced Electrocatalytic Oxygen Reduction and Oxygen Evolution in Aqueous Solutions. *ACS Catal.* **2016**, *6* (10), 6429–6437.

7. Li, F.; Zhang, B.; Li, X.; Jiang, Y.; Chen, L.; Li, Y.; Sun, L. Highly Efficient Oxidation of Water by a Molecular Catalyst Immobilized on Carbon Nanotubes. *Angew. Chemie Int. Ed.* **2011**, *50* (51), 12276–12279.

8. Maurin, A.; Robert, M. Noncovalent Immobilization of a Molecular Iron-Based Electrocatalyst on Carbon Electrodes for Selective, Efficient CO2-to-CO Conversion in Water. *J. Am. Chem. Soc.* **2016**, *138* (8), 2492–2495.

9. Oh, S.; Gallagher, J. R.; Miller, J. T.; Surendranath, Y. Graphite-Conjugated Rhenium Catalysts for Carbon Dioxide Reduction. *J. Am. Chem. Soc.* **2016**, *138* (6), 1820–1823.

10. Tran, P. D.; Le Goff, A.; Heidkamp, J.; Jousselme, B.; Guillet, N.; Palacin, S.; Dau, H.; Fontecave, M.; Artero, V. Noncovalent Modification of Carbon Nanotubes with Pyrene-Functionalized Nickel Complexes: Carbon Monoxide Tolerant Catalysts for Hydrogen Evolution and Uptake. *Angew. Chemie Int. Ed.* **2011**, *50* (6), 1371–1374.

11. Li, C.; Ren, B.; Zhang, Y.; Cheng, Z.; Liu, X.; Tong, Z. A Novel Ferroceneylazobenzene Self-Assembled Monolayer on an ITO Electrode : Photochemical and Electrochemical Behaviors. *Langmuir* **2008**, *24*, 12911–12918.

12. Wu, L.; Eberhart, M.; Shan, B.; Nayak, A.; Brennaman, M. K.; Miller, A. J. M.; Shao, J.; Meyer, T. J. Stable Molecular Surface Modification of Nanostructured, Mesoporous Metal Oxide Photoanodes by Silane and Click Chemistry. *ACS Appl. Mater. Interfaces*

2019, *11* (4), 4560–4567.

13. Hyde, J. T.; Hanson, K.; Vannucci, A. K.; Lapides, A. M.; Alibabaei, L.; Norris, M. R.; Meyer, T. J.; Harrison, D. P. Electrochemical Instability of Phosphonate-Derivatized, Ruthenium(III) Polypyridyl Complexes on Metal Oxide Surfaces. *ACS Appl. Mater. Interfaces* **2015**, *7* (18), 9554–9562.

14. Pujari, S. P.; Scheres, L.; Van Lagen, B.; Zuilhof, H. Organic Monolayers from 1-Alkynes Covalently Attached to Chromium Nitride: Alkyl and Fluoroalkyl Termination. *Langmuir* **2013**, *29* (33), 10393–10404.

15. Franking, R. A.; Landis, E. C.; Hamers, R. J. Highly Stable Molecular Layers on Nanocrystalline Anatase TiO2 through Photochemical Grafting. *Langmuir* **2009**, *25* (18), 10676–10684.

16. Franking, R.; Hamers, R. J. Ultraviolet-Induced Grafting of Alkenes to TiO2 Surfaces: Controlling Multilayer Formation. *J. Phys. Chem. C* **2011**, *115* (34), 17102–17110.

17. Lee, K. A. B. Electron Transfer into Self-Assembling Monolayers on Gold Electrodest. *Langmuir* **1990**, *6* (3), 709–712.

18. Chidsey, C. E. D.; Bertozzi, C. R.; Putvinski, T. M.; Mujsce, A. M. Coadsorption of Ferrocene-Terminated and Unsubstituted Alkanethiols on Gold: Electroactive Self-Assembled Monolayers. *J. Am. Chem. Soc.* **1990**, *112* (11), 4301–4306.

19. Finklea, H. O. Hanshew, D. D. Electron-Transfer Kinetics in Organized Thiol Monolayer with Attached Pentaamine(Pyridine)Ruthenium Redox Centers. *J. Am. Chem. Soc.* **1992**, *114* (4), 3173–3181.

20. Bard, A. J.; Faulkner, L. R. *Electrochemical Methods: Fundamentals and Applications*, 2nd ed.; John Wiley & Sons, 2001.

21. Maat, J. Ter; Regeling, R.; Yang, M.; Mullings, M. N.; Bent, S. F.; Zuilhof, H. Photochemical Covalent Attachment of Alkene-Derived Monolayers onto Hydroxyl-Terminated Silica. *Langmuir* **2009**, *25* (19), 11592–11597.

22. Ruther, R. E.; Cui, Q.; Hamers, R. J. Conformational Disorder Enhances Electron Transfer through Alkyl Monolayers: Ferrocene on Conductive Diamond. *J. Am. Chem. Soc.* **2013**, *135* (15), 5751–5761.

23. Meziane, D.; Barras, A.; Kromka, A.; Houdkova, J.; Boukherroub, R.; Szunerits, S. Thiol-Yne Reaction on Boron-Doped Diamond Electrodes: Application for the Electrochemical Detection of DNA-DNA Hybridization Events. *Anal. Chem.* **2012**, *84* (1), 194–200.

24. Das, M. R.; Wang, M.; Szunerits, S.; Gengembre, L.; Boukherroub, R. Clicking Ferrocene Groups to Boron-Doped Diamond Electrodes. *Chem. Commun. (Camb).* **2009**, No. 19, 2753–2755.

25. Yu, S. S. C.; Downard, A. J. Photochemical Grafting and Activation of Organic Layers on Glassy Carbon and Pyrolyzed Photoresist Films. *Langmuir* **2007**, *23*, 4662–4668.

26. Evrard, D.; Lambert, F.; Policar, C.; Balland, V.; Limoges, B. Electrochemical Functionalization of Carbon Surfaces by Aromatic Azide or Alkyne Molecules: A Versatile Platform for Click Chemistry. *Chem. - A Eur. J.* **2008**, *14* (30), 9286–9291.

27. McKenas, C. G.; Fehr, J. M.; Donley, C. L.; Lockett, M. R. Thiol-Ene Modified Amorphous Carbon Substrates: Surface Patterning and Chemically Modified Electrode Preparation. *Langmuir* **2016**, *32* (41), 10529–10536.

28. Fehr, J. M.; McKenas, C. G.; Liu, B.; Lockett, M. R. Azide-Alkyne Click Reactions to Prepare Chemically Modified Amorphous Carbon Electrodes. *Appl. Surf. Sci.* https://doi.org/10.1016/j.apsusc.2019.02.151.

29. Landis, E. C.; Harriers, R. J. Covalent Grafting of Redox-Active Molecules to Vertically Aligned Carbon Nanofiber Arrays via "Click" Chemistry. *Chem. Mater.* **2009**, *21* (4), 724–730.

30. Li, F.; Basile, V. M.; Pekarek, R. T.; Rose, M. J. Steric Spacing of Molecular Linkers on Passivated Si(111) Photoelectrodes. *ACS Appl. Mater. Interfaces* **2014**, *6* (22), 20557–20568.

31. Fabre, B.; Pujari, S. P.; Scheres, L.; Zuilhof, H. Micropatterned Ferrocenyl Monolayers Covalently Bound to Hydrogen-Terminated Silicon Surfaces: Effects of Pattern Size on the Cyclic Voltammetry and Capacitance Characteristics. *Langmuir* **2014**, *30* (24), 7235–7243.

32. Kang, O. S.; Bruce, J. P.; Herbert, D. E.; Freund, M. S. Covalent Attachment of Ferrocene to Silicon Microwire Arrays. *ACS Appl. Mater. Interfaces* **2015**, *7* (48), 26959–26967.

33. Laviron, E. Roullier, L. General Expression of the Linear Potential Sweep Voltammogram for a Surface Redox Reaction with Interactions between the Adsorbed Molecules Applications to Modified Electrodes. *J. Electroanl. Chem.* **1980**, *115*, 65–74.

34. Du, Z.; Ren, B.; Chang, X.; Dong, R.; Tong, Z. An End-Bifunctionalized Hydrophobically Modified Ethoxylated Urethane Model Polymer: Multiple Stimuli-Responsive Aggregation and Rheology in Aqueous Solution. *Macromolecules* **2017**, *50*, 1688–1699.

35. Marrani, A. G.; Cattaruzza, F.; Decker, F.; Galloni, P.; Zanoni, R. Chemical Routes to Fine Tuning the Redox Potential of Monolayers Covalently Attached on H – Si (1 0 0). *Electrochim. Acta* **2010**, *55* (20), 5733–5740.

36. McKenas, C. G.; Fehr, J. M.; Liu, B.; Donley, C. L.; Lockett, M. R. Mechanistic Insights into UV-Initiated Thiol-Ene Reactions on Amorphous Carbon Films. *J. Phys. Chem. C* **2018**, *122* (38), 21854–21860.

37. Wang, X.; Colavita, P. E.; Streifer, J. A.; Butler, J. E.; Hamers, R. J. Photochemical Grafting of Alkenes onto Carbon Surfaces: Identifying the Roles of Electrons and Holes. *J. Phys. Chem. C* **2010**, *114* (9), 4067–4074.

38. Colavita, P. E.; Sun, B.; Tse, K. Y.; Hamers, R. J. Photochemical Grafting of N-Alkenes onto Carbon Surfaces: The Role of Photoelectron Ejection. *J. Am. Chem. Soc.* **2007**, *129* (44), 13554–13565.

39. Lockett, M. R.; Smith, L. M. Attaching Molecules to Chlorinated and Brominated Amorphous Carbon Substrates via Grignard Reactions. *Langmuir* **2009**, *25* (6), 3340–3343.

40. Lockett, M. R.; Smith, L. M. Formation and Stability of Alkylthiol Monolayers on Carbon Substrates. *J. Phys. Chem. C* **2010**, *114* (29), 12635–12641.

41. Murphy, D. M.; Cullen, R. J.; Jayasundara, D. R.; Scanlan, E. M.; Colavita, P. E. Study of the Spontaneous Attachment of Polycyclic Aryldiazonium Salts onto Amorphous Carbon Substrates. *RSC Adv.* **2012**, *2* (16), 6527.

42. Lockett, M. R.; Smith, L. M. Carbon Substrates: A Stable Foundation for Biomolecular Arrays. *Annu. Rev. Anal. Chem.* **2015**, *8* (1), 263–285.

43. Kolb, H. C.; Finn, M. G.; Sharpless, K. B. Click Chemistry : Diverse Chemical Function from a Few Good Reactions. *Agnew. Chem. Int. Ed.* **2001**, *40*, 2004–2021.

44. Bansal, A.; Li, X.; Lauermann, I.; Lewis, N. S. Alkylation of Si Surfaces Using a Two-Step Halogenation / Grignard Route. *J. Am. Chem. Soc.* **1996**, *118* (11), 7225–7226.

45. Boukherroub, R.; Morin, S.; Bensebaa, F.; Wayner, D. D. M. New Synthetic Routes to Alkyl Monolayers on the Si(111) Surface. *Langmuir* **1999**, *15* (11), 3831–3835.

46. Rumble, J. R. Bond Dissociation Energies in Diatomic Molecules. In *CRC Handbook of Chemistry and Physics*; CRC Press/Taylor & Francis: Boca Raton, FL, 2018.

47. Fellah, S.; Boukherroub, R.; Ozanam, F.; Chazalviel, J. N. Hidden Electrochemistry in the Thermal Grafting of Silicon Surfaces from Grignard Reagents. *Langmuir* **2004**, *20* (15), 6359–6364.

48. Laviron, E. The Use of Linear Potential Sweep Voltammetry and of A.C Voltammetry for the Study of the Surface Electrochemical Reaction of Strongly Adsorbed Systems and of Redox Modified Electrodes. *J. Electroanal. Chem.* **1979**, *100*, 263–270.

49. Stenehjem, E. D.; Ziatdinov, V. R.; Stack, T. D. P.; Chidsey, C. E. D. Gas-Phase Azide Functionalization of Carbon. *J. Am. Chem. Soc.* **2013**, *135* (3), 1110–1116.

50. Devadoss, A.; Chidsey, C. E. D. Azide-Modified Graphitic Surfaces for Covalent Attachment of Alkyne-Terminated Molecules by “Click” Chemistry. *J. Am. Chem. Soc.* **2007**, *129* (17), 5370–5371.

51. Hapiot, P.; McCreery, R. L.; Sayed, S. Y.; Bayat, A.; Leroux, Y.; Kondratenko, M. Bilayer Molecular Electronics: All-Carbon Electronic Junctions Containing Molecular Bilayers Made with “Click” Chemistry. *J. Am. Chem. Soc.* **2013**, *135* (35), 12972–12975.

52. Hapiot, P.; Noël, J.-M.; Fei, H.; Leroux, Y. R.; Roux, C. Efficient Covalent Modification of a Carbon Surface: Use of a Silyl Protecting Group To Form an Active Monolayer. *J. Am. Chem. Soc.* **2010**, *132* (40), 14039–14041.

APPENDIX A: SUPPLEMENTAL INFORMATION FOR CHAPTER 2

Table S2.1. Attempted thiolation reaction conditions [a]

Reagent(s), concentration	**Reaction Temperature (°C)**	**Monolayer coverage** [b]
NaSH, 100 mM	25	0.15
NaSH, 100 mM	50	0.26
NaSH, 100 mM	85	0.23
NaSH, 500 mM	25	0.27
NaSH, 500 mM	50	0.23
NaSH, 100 mM; TBAI, 10mM	25	0.19
NaSH, 500 mM; TBAI, 10mM	25	0.26
NaSH, 500 mM; TBAI, 10mM	50	0.24 ± 0.01[e]
NaSH, 500 mM; TBAI, 10 mM [c]	*50*	*0.20 ± 0.06* [f]
CH_3COSK, 100 mM	25	0.14
CH_3COSK, 100 mM	50	0.26
$C(NH_2)_2S$, 150 mM [d]	110	0.17

[a] Each reaction was performed in anhydrous DMF for 24 hours with a Cl-aC substrate, unless otherwise noted. The amount of chlorine on each surface was similar, as determined by XP survey spectrum, for all surfaces prior to thiolation. Values represent n = 1 aC film, unless otherwise noted. Italicized conditions were the conditions used in this work.

[b] Determined from XP high-resolution spectrum, using a overlayer model (ref. 35, manuscript).

[c] Reactions performed for 8 hours.

[d] Reaction performed in 2:1 (v/v) acetic acid: hydrogen bromide for 24 hours (ref. 31, manuscript).

[e] n=6 aC films.

[f] n=7 aC films.

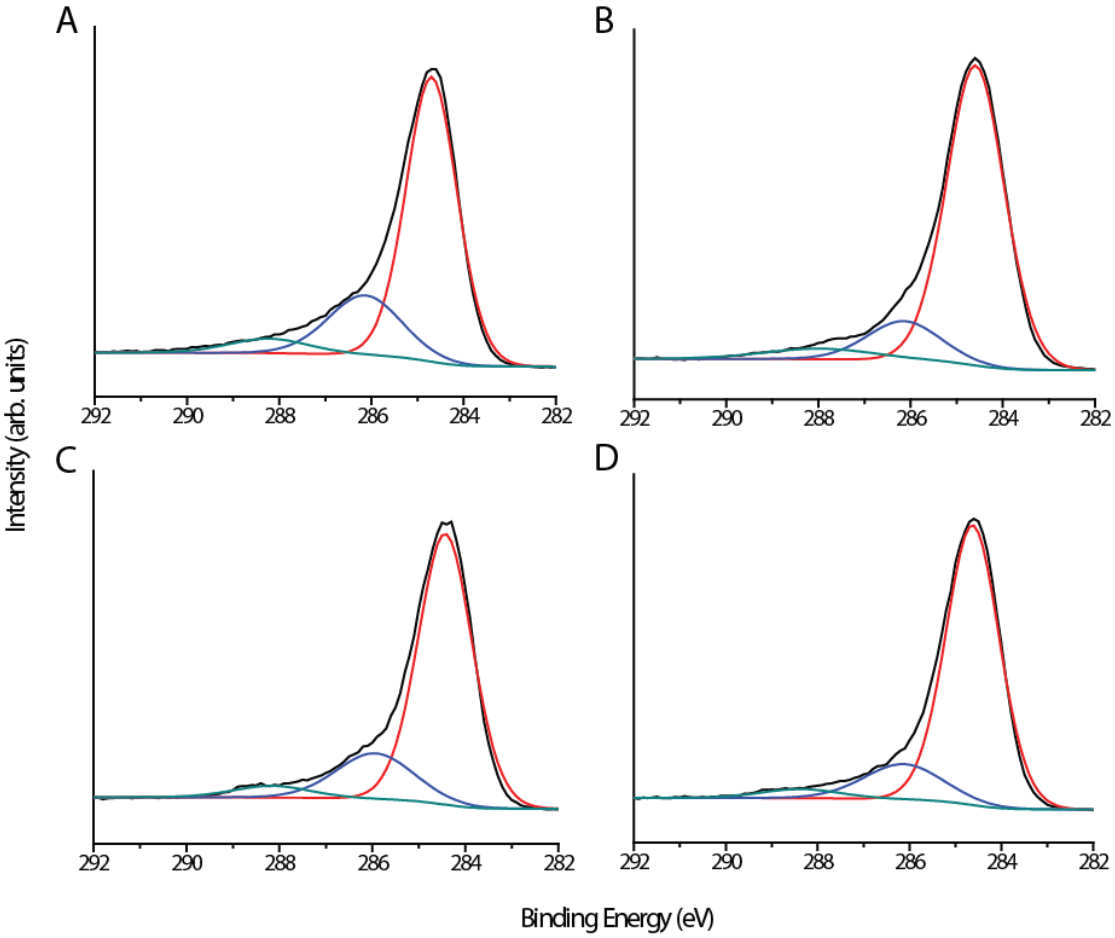

Figure S2.1. Representative high-resolution XP spectra of the C1s electrons of an (A) aC, (B) H-aC, (C) Cl-aC, and (D) HS-aC film. The black line is the raw data; colored lines denote individual Voigt-fit components.

Table S2.2. Binding energies and relative composition values of representative high-resolution C1s XP spectra in Figure S2.

	Position, eV (Percentage of peak, %) [a]		
	C – C	**C – X** [b]	**C = O**
aC	284.6 (72.6)	286.1 (21.8)	288.1 (5.7)
H-aC	284.6 (81.2)	286.1 (13.4)	288.0 (5.4)
Cl-aC	284.6 (76.8)	286.2 (18.5)	288.3 (4.7)
HS-aC	284.6 (81.2)	286.1 (15.0)	288.4 (3.8)

[a] Binding position information was obtained from the Handbook of X-Ray Photoelectron Spectroscopy (ref. 51, manuscript).

[b] X represents the heteroatom O, Cl, or S.

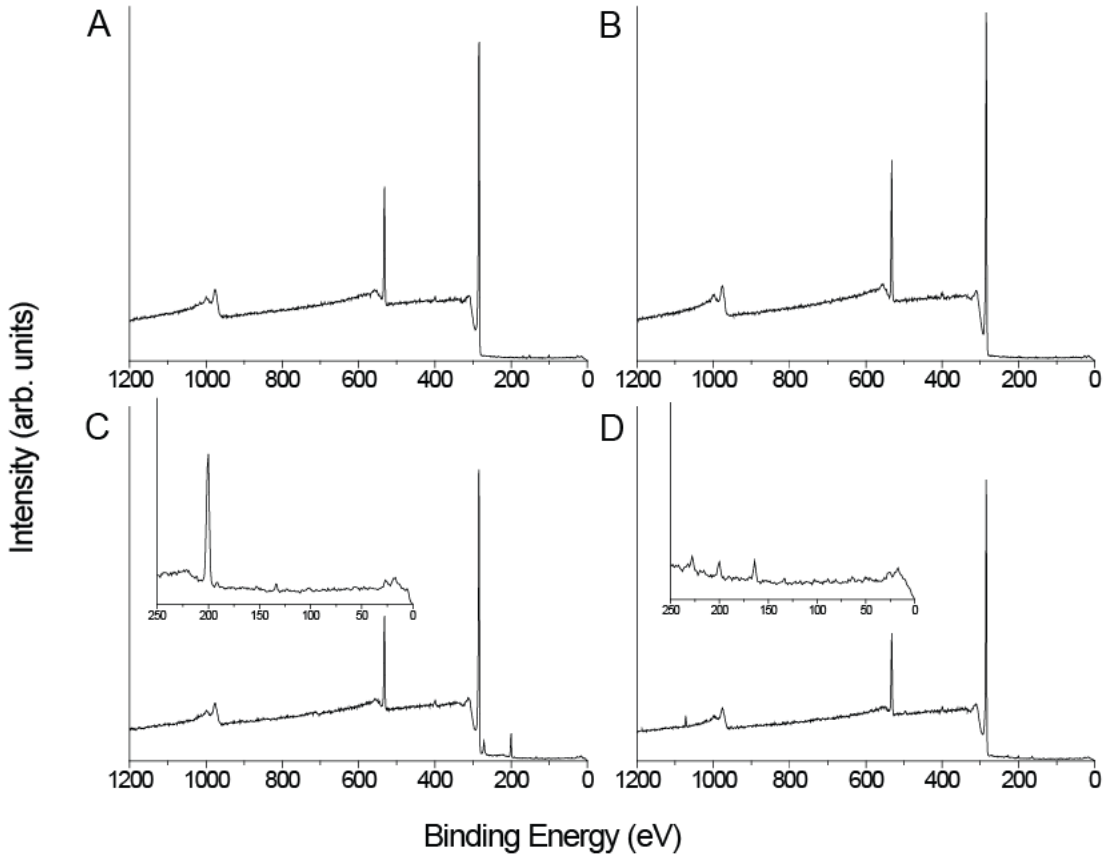

Figure S2.2. Representative XP survey spectra of an (A) aC, (B) H-aC, (C) Cl-aC, and (D) HS-aC film. Binding energy assignments are as follows: Na1s, 1072 eV; O KLL, 990 eV; O1s, 532 eV; N1s, 400 eV; C1s, 285 eV; Cl2s, 271 eV; S 2s, 228 eV; Cl2p, 200 eV; S2p, 164 eV. All spectra were calibrated to the C1s peak at 284.6 eV. Insets highlight the S2s, Cl2p, and S2p binding energy regions.

Table S2.3. Elemental composition of aC films, determined from high resolution XP spectra in Figure S3. [a]

	Atomic concentration (%)					Ratios	
	C 1s	**O 1s**	**N 1s**	**Cl 2p**	**S 2p**	**O:C**	**N:C**
aC	87.01 ± 1.81	11.94 ± 1.92	1.05 ± 0.21	--	--	0.14 ± 0.02	0.012 ± 0.002
H-aC	89.01 ± 0.73	10.06 ± 0.87	0.94 ± 0.22	--	--	0.11 ± 0.01	0.010 ± 0.002
Cl-aC	85.76 ± 0.82	9.62 ± 0.94	0.96 ± 0.37	3.66 ± 0.73	--	0.11 ± 0.01	0.011 ± 0.004
HS-aC	85.96 ± 1.85	11.81 ± 1.80	0.99 ± 0.32	0.45 ± 0.20	0.79 ± 0.23	0.14 ± 0.02*	0.012 ± 0.004

[a] Each value is the average and standard deviation of: n = 3 aC films; n = 4 H-aC films; n = 5 Cl-aC surfaces; n = 7 replicates for HS-aC surfaces. Each replicate was prepared and analyzed on separate days.

* indicates a statistically significant ($p<0.05$) ratio from the H-aC films.

Table S2.4. Percentage of reduced and oxidized sulfur atoms on aC film as a function of storage.

		Percent (%) [a]			
Storage location		**Day 1**	**Day 3**	**Day 9**	**Day 28**
In a desiccator	Reduced thiol	85.80	73.30	60.00	56.70
	Oxidized thiol	14.20	26.70	39.90	43.20
Ambient	Reduced thiol	90.90	77.30	69.90	63.50
	Oxidized thiol	9.10	22.60	30.10	36.50
Under vacuum	Reduced thiol	92.90	86.30	82.50	78.60
	Oxidized thiol	7.10	13.70	17.40	21.40

[a] The doublet at 164 eV was used to calculate the percentage of reduced thiol, and the doublet at 168 eV was used to calculate the percentage of oxidized thiol.

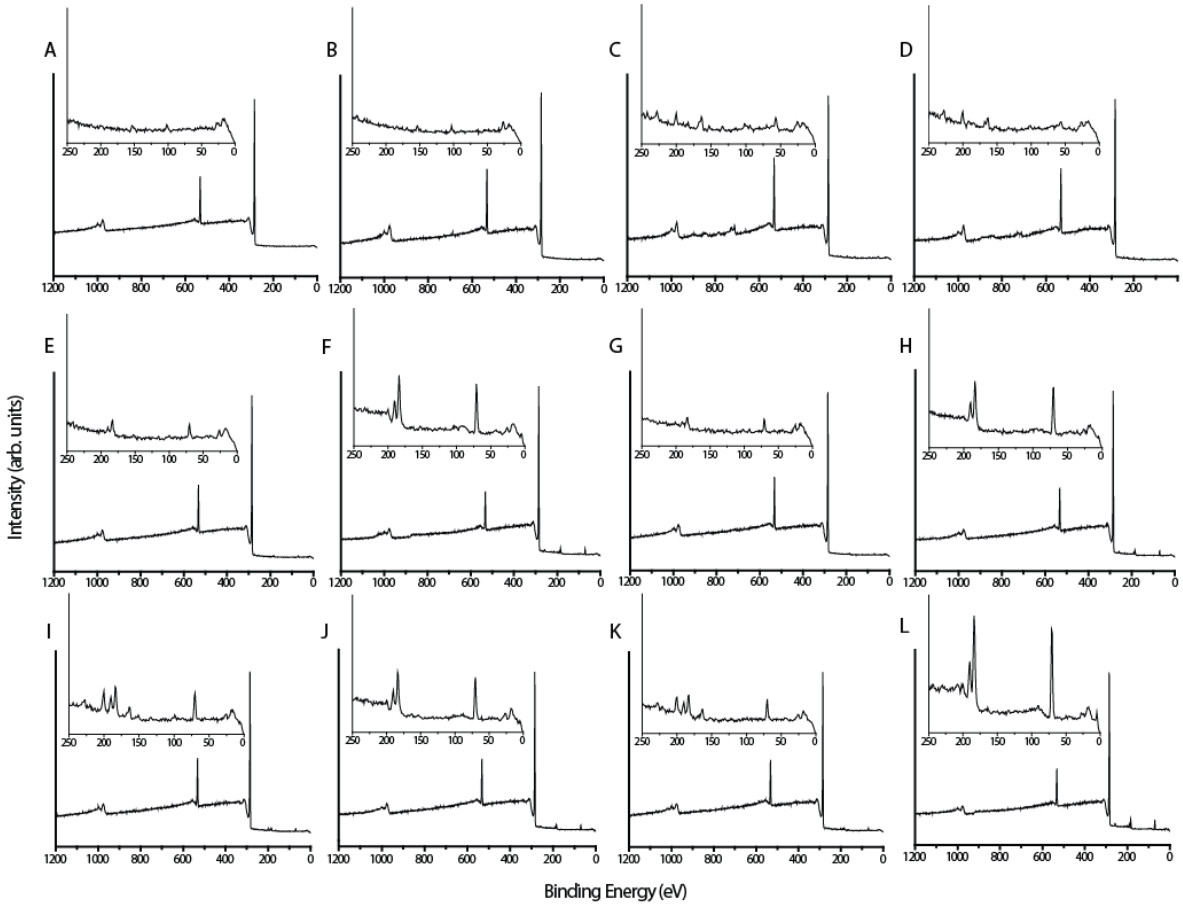

Figure S2.4. Representative XP survey spectra of H-aC films exposed to neat BUD molecules for 1 hour in the dark, in the (A) absence or (B) presence of 1% (w/w) DMPA; HS-aC exposed to neat BUD molecules for 1 hour in the dark, in the (C) absence or (D) presence of 1% (w/w) DMPA; H-aC surfaces exposed to neat BUD molecules, illuminated with 300 ± 100 nm light for (E) 10 or (F) 60 minutes; H-aC surfaces exposed to neat BUD molecules, 1% (w/w) DMPA, and illuminated with 300 ± 100 nm light for (G) 10 or (H) 60 minutes; HS-aC surfaces exposed to neat BUD molecules and illuminated with 300 ± 100 nm light for (I) 10 or (J) 60 minutes; HS-aC surfaces exposed to near BUD molecules, 1% (w/w) DMPA, and illuminated with 300 ± 100 nm light for (K) 10 or (L) 60 minutes. Insets highlight the Cl2p (200 eV), S2p (164 eV) and Br3d (70 eV) binding energies; each spectrum have the same intensity scale.

Table S2.5. XPS elemental composition of aC films in Figure S4, expressed as atomic concentration percentages.

	Atomic Concentration (%) [a]					
	C 1s	**O 1s**	**N 1s**	**Br 3d**	**S 2p**	**Cl 2p**
H-aC, 60 mins						
Alkene	88.07 ± 0.34	10.92 ± 0.23	1.01 ± 0.2	0.00 ± 0.00	--	--
Alkene, DMPA	86.96 ± 1.60	12.62 ± 1.40	12.62 ± 1.40	0.01 ± 0.01	--	--
HS-aC, 60 mins						
Alkene	86.00 ± 1.6	12.15 ± 1.72	1.10 ± 0.13	0.00 ± 0.00	0.49 ± 0.02	0.26 ± 0.02
Alkene, DMPA	86.68 ± 0.45	12.25 ± 0.47	0.34 ± 0.29	0.04 ± 0.04	0.49 ± 0.20	0.20 ± 0.10
H-aC, 10 mins						
Alkene + light	89.06 ± 0.95	10.41 ± 0.78	0.39 ± 0.40	0.13 ± 0.08	--	--
Alkene + light + DMPA	88.90 ± 0.44	10.46 ± 0.30	0.55 ± 0.48	0.10 ± 0.09	--	--
H-aC, 60 mins						
Alkene + light	89.89 ± 0.77	9.20 ± 0.98	0.26 ± 0.39	0.65 ± 0.12	--	--
Alkene + light + DMPA [b]	88.75 ± 1.06	9.71 ± 1.60	0.53 ± 0.33	1.01 ± 0.65	--	--
HS-aC, 10 mins						
Alkene + light	87.50 ± 1.22	10.88 ± 0.90	0.56 ± 0.49	0.36 ± 0.03	0.35 ± 0.04	0.35 ± 0.08

Alkene + light + DMPA	87.60 ± 1.16	10.74 ± 0.84	0.69 ± 0.26	0.32 ± 0.05	0.35 ± 0.10	0.30 ± 0.03
HS-aC, 60 mins						
Alkene + light	87.91 ± 1.09	10.40 ± 1.37	0.35 ± 0.46	0.99 ± 0.24	0.17 ± 0.08	0.19 ± 0.08
Alkene + light + DMPA	88.45 ± 0.40	9.72 ± 0.86	0.34 ± 0.40	1.11 ± 0.36	0.20 ± 0.05	0.19 ± 0.05

[a] Each value is the average and standard deviation of n = 3 replicate films, unless otherwise stated. Individual surfaces were prepared and analyzed on separate days; 300 ± 100 nm light used for all trials.

[b] n=5.

Table S2.6. Bromine-to-carbon ratios of aC films covered with BUD molecules and irradiated with 360 ± 15 nm light for 6 hours.

Surface	**Br/C ratio**
H-aC	0.002
HS-aC	0.007

APPENDIX B: SUPPLEMENTAL INFORMATION FOR CHAPTER 3

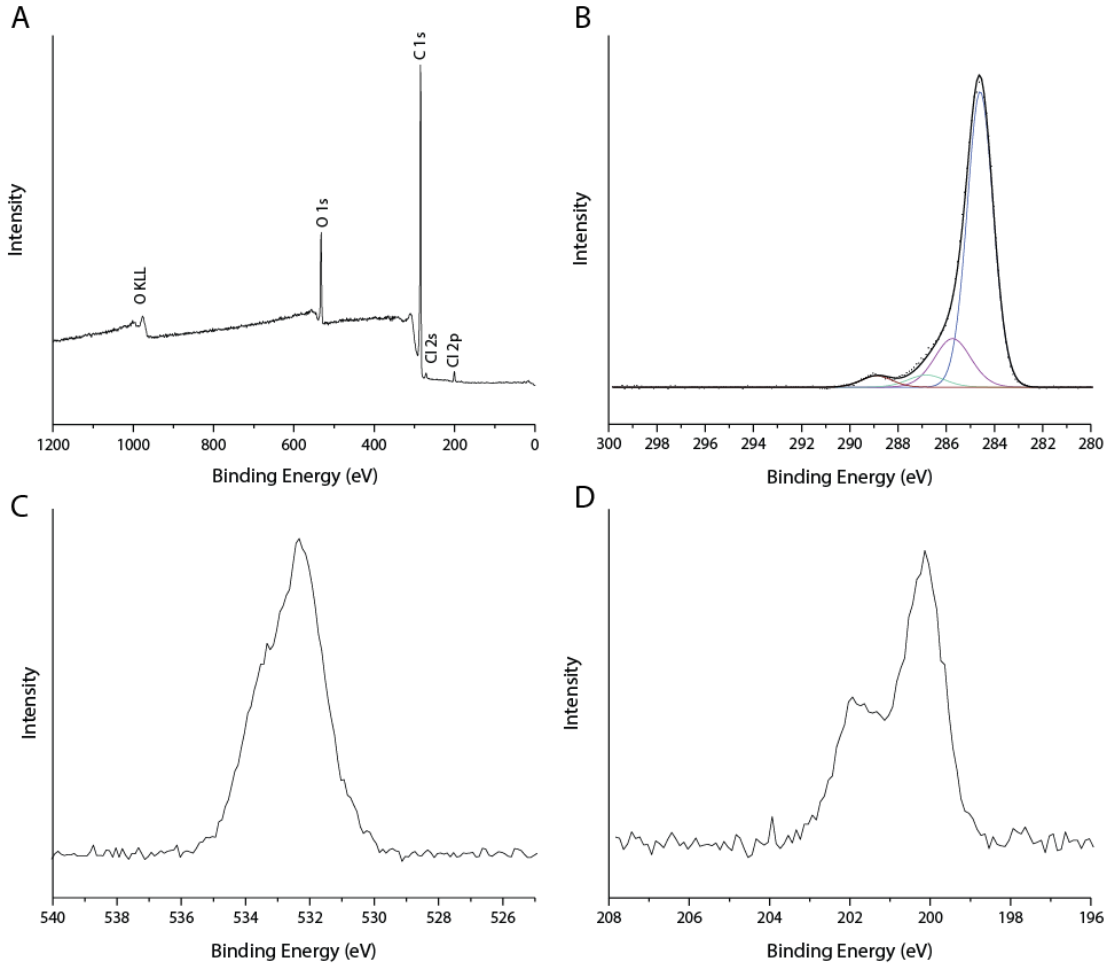

Figure S3.1. Representative XPS datasets for methyl-aC films: (A) a survey spectrum; (B) a C1s high-resolution spectrum fit with Voigt functions, (C) an O1s high-resolution spectrum, and (D) a Cl2p high-resolution spectrum.

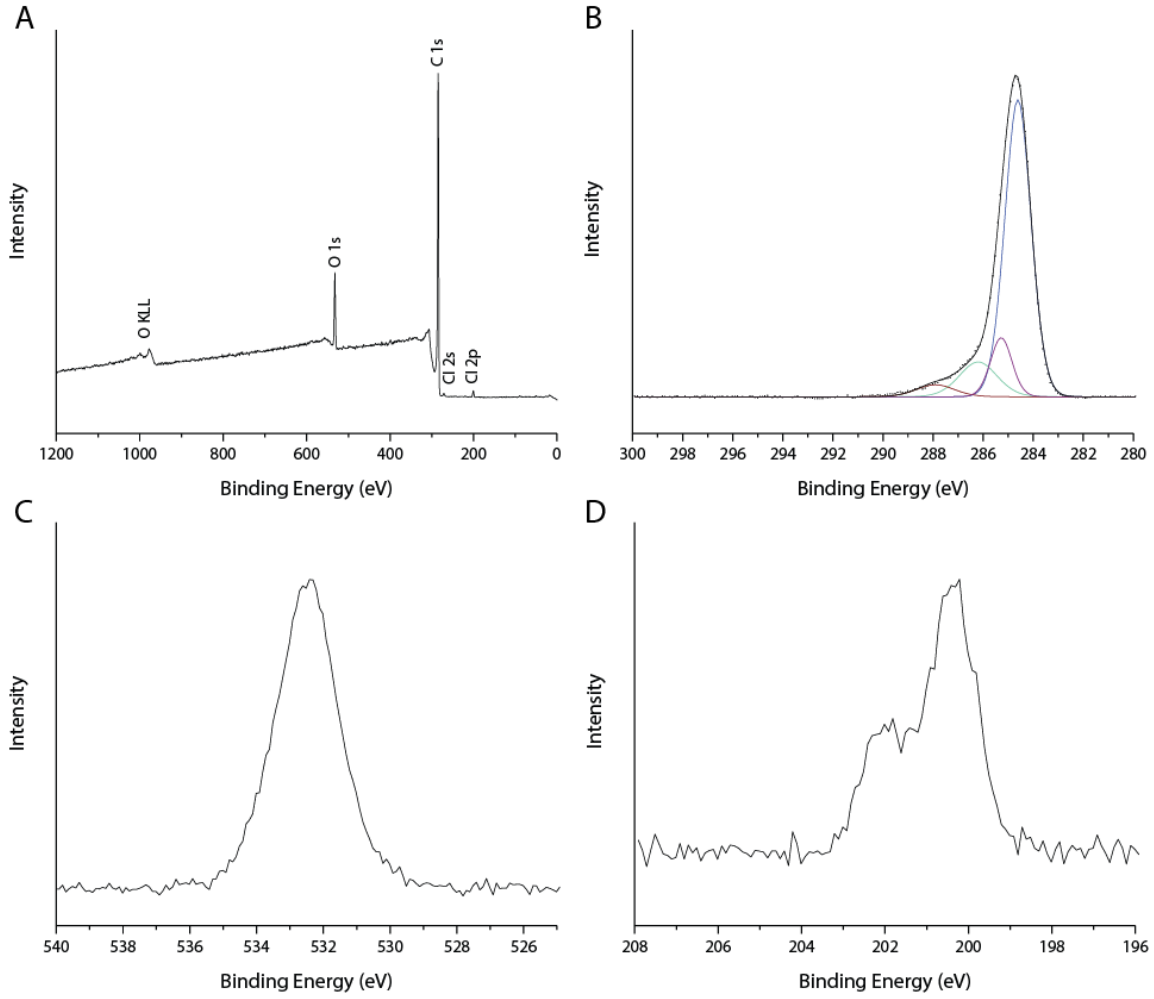

Figure S3.2. Representative XPS datasets for vinyl-aC films: (A) a survey spectrum; (B) a C1s high-resolution spectrum fit with Voigt functions, (C) an O1s high-resolution spectrum, and (D) a Cl2p high-resolution spectrum.

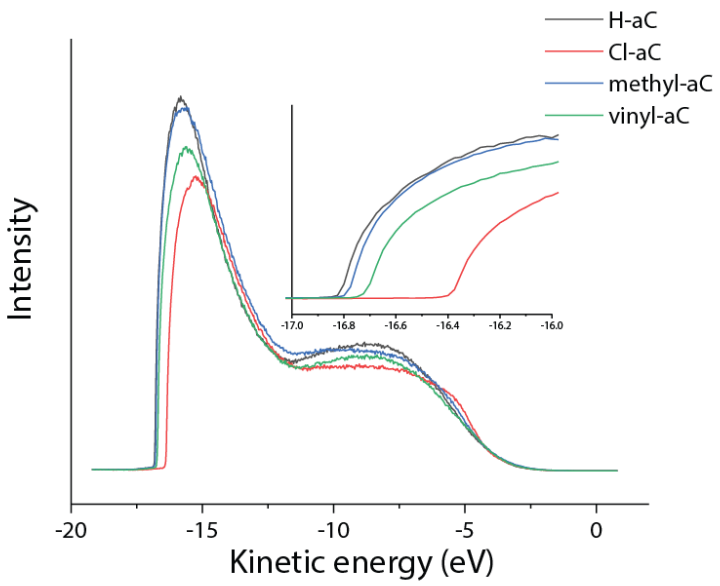

Figure S3.3. Representative UPS datasets for H-aC, Cl-aC, methyl-aC, and vinyl-aC films. Kinetic energy is with respect to the Fermi energy.

Table S3.1. ΔO/C ratios for vinyl-aC films as a function of storage condition.

Surface type	Aqueous solution (24 hours)	Organic solution (24 hours)	Vacuum (3 days)	UV light (2 hours)
vinyl-aC	-0.01	0	0.01	0.01

Table S3.2. Sulfur-to-carbon (S/C) and fluorine-to-carbon (F/C) ratios for different surface chemistries exposed to 1 M of 4-fluorobenzyl mercaptan in benzene and irradiated with either 20 or 200 mW of UV light.[a,b]

H-aC	S/C	F/C	F/S
20	0.0015 ± 0.0002	0.0009 ± 0.001	0.5 ± 0.3
200[c]	0.0044 ± 0.002	0.0027 ± 0.002	0.5 ± 0.3
vinyl-aC			
20[d]	0.0032 ± 0.001	0.0023 ± 0.001	0.7 ± 0.2
200	0.0065 ± 0.001	0.0047 ± 0.001	0.07 ± 0.1
methyl-aC			
20	0.0010 ± 0.0004	0.0010 ± 0.0003	1.2 ± 0.8
200	0.0054 ± 0.0002	0.0045 ± 0.0004	0.8 ± 0.1
4-FBM on Au[e]			1.4

[a] The S/C values for vinyl-aC and methyl-ac correspond to the values reported in Figure 1 of the manuscript. [b] Values are for n=3 surfaces unless otherwise noted. [c] Values are n=4 surfaces. [d] Values are n=6 surfaces. [e] Self-assembled monolayer of 4-flurobenzyl mercaptan obtained by submerging a gold surface in 100 mM ethanolic solution for 23 hours.

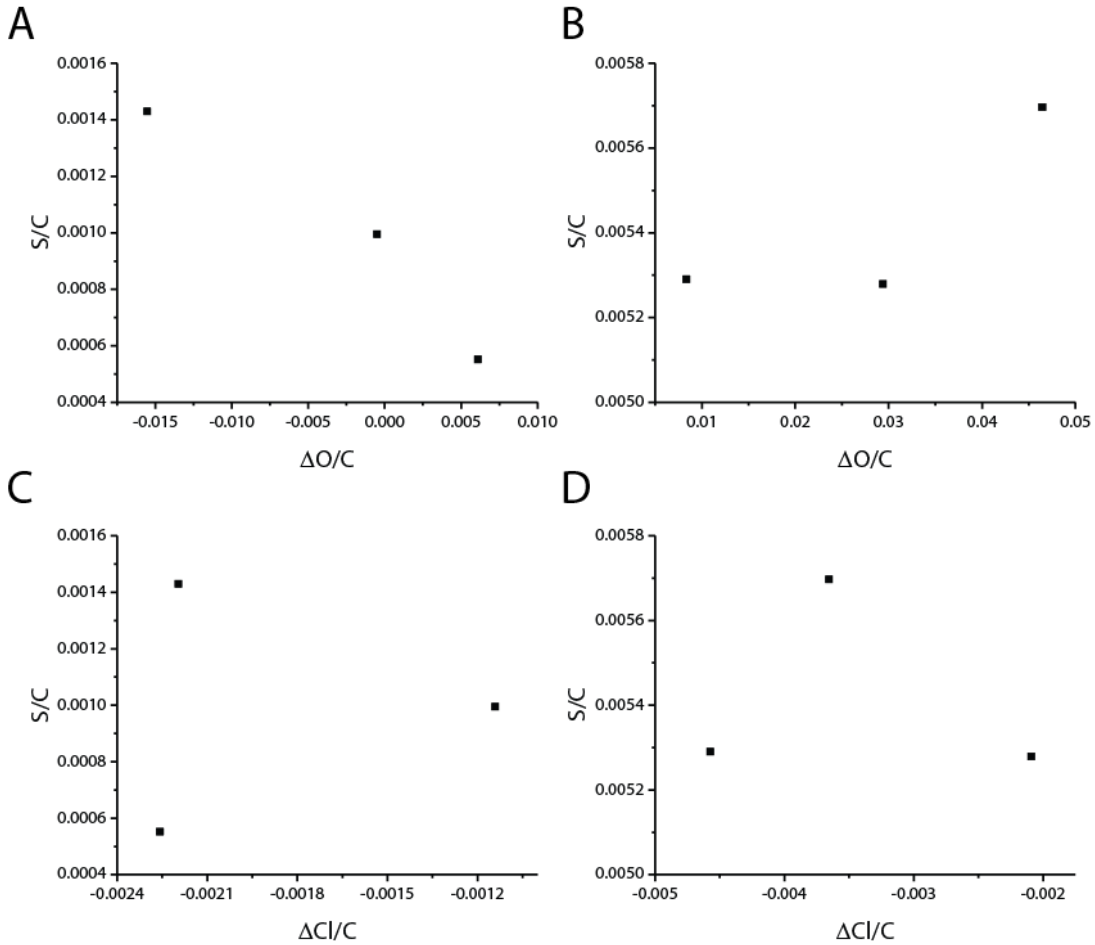

Figure S3.4. S/C ratios as a function of ΔO/C for methyl-aC films illuminated with 365 nm photons in the presence of 1 M 4-FBM at either (A) 20 mW or (B) 200 mW; S/C ratios as a function of ΔCl/C for methyl-aC films illuminated with 365 nm photons in the presence of 1 M 4-FBM at either (C) 20 mW or (D) 200 mW.

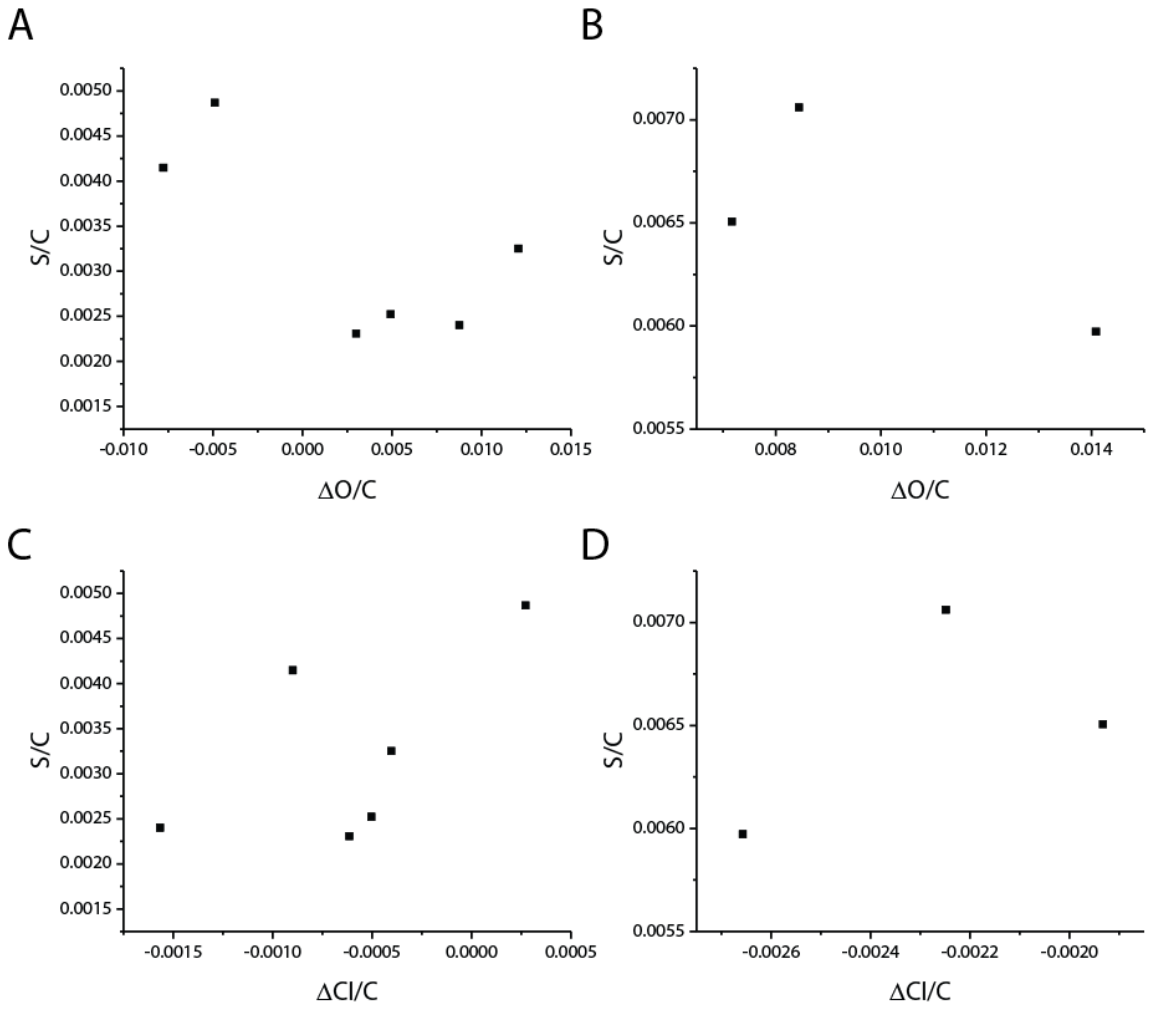

Figure S3.5. S/C ratios as a function of ΔO/C for vinyl-aC films illuminated with 365 nm photons in the presence of 1 M 4-FBM at either (A) 20 mW or (B) 200 mW; S/C ratios as a function of ΔCl/C for vinyl-aC films illuminated with 365 nm photons in the presence of 1 M 4-FBM at either (C) 20 mW or (D) 200 mW for 4-FBM reactions on vinyl-aC films.

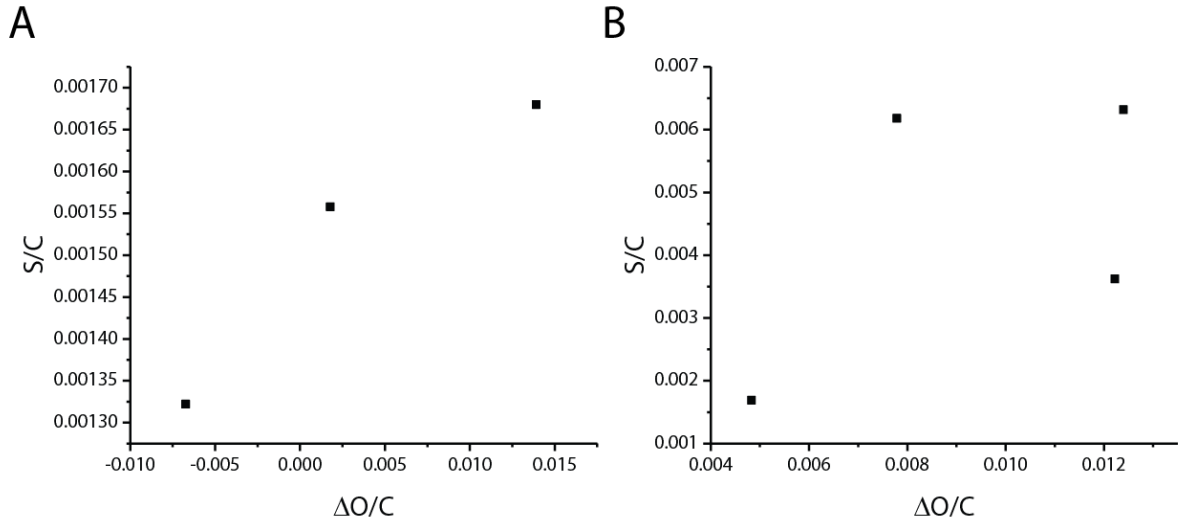

Figure S3.6. S/C ratios as a function of ΔO/C for H-aC films illuminated with 365 nm photons in the presence of 1 M 4-FBM at either (A) 20 mW or (B) 200 mW for 4-FBM reactions on H-aC films.

Table S3.3. Summary of XPS data for vinyl-aC films modified with 4-fluorobenzyl mercaptan molecules, analyzed immediately after preparation and again after a 48-hour exposure to air.

	Before	After
Reduced sulfur (%)	100	45
Oxidized sulfur (%)	0	55
O/C	0.11	0.13
F/C	0.0047	0.0039
S/C	0.0033	0.0033

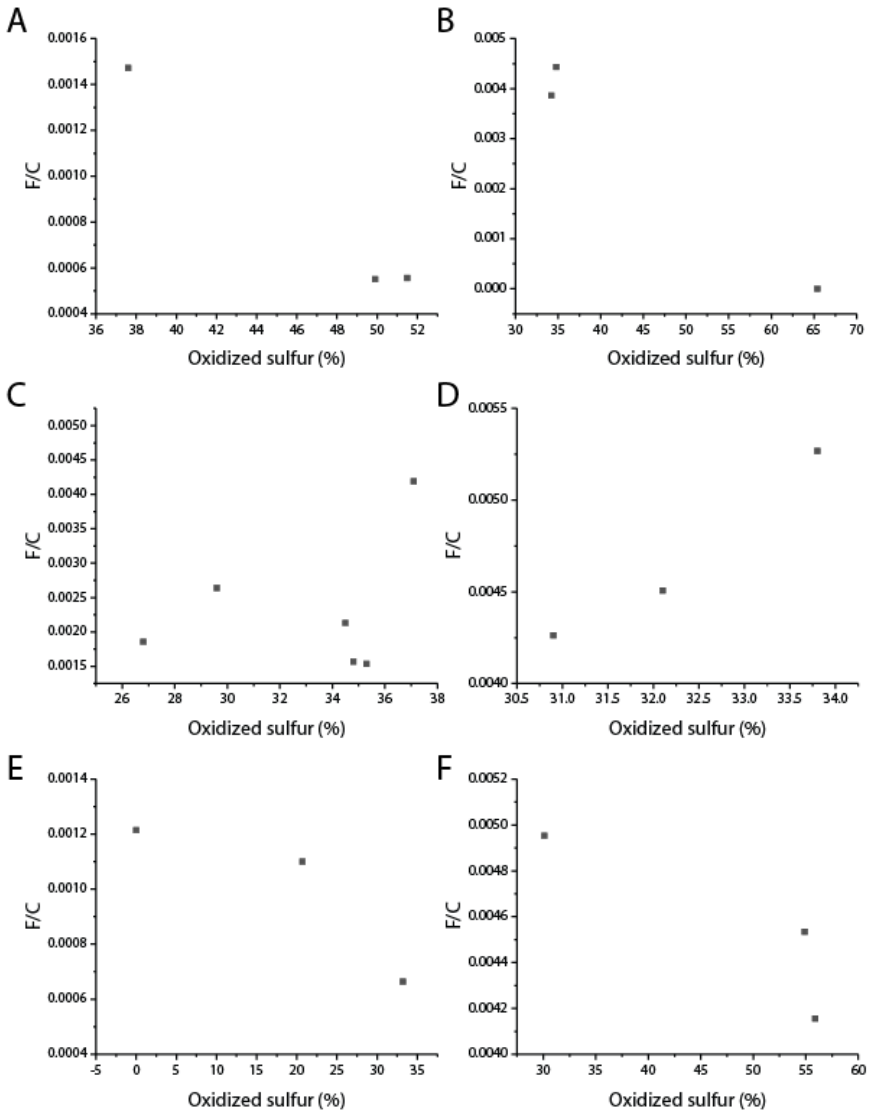

Figure S3.7. F/C ratios as a function of percentage of oxidized sulfur for: H-aC films after illumination at (A) 20 and (B) 200 mW; vinyl-aC films after illumination at (C) 20 and (D) 200 mW, and; methyl-aC films after illumination at (E) 20 and (F) 200 mW.

Table S3.4. F/C and S/C ratios for H-aC and vinyl-aC films exposed to benzene containing 1 M 4-FBM and 0.01 μM butylated hydroxytoluene (BHT), illuminated for 60 minutes with 365 nm photons at either 20 or 200 mW.

	F/C	S/C
H-aC, 20 mW	0.000	0.001
vinyl-aC, 20 mW	0.003	0.004
H-aC, 200 mW	0.003	0.005
Vinyl-aC, 200 mW	0.006	0.007

Table S3.5. Work function and elemental composition data obtained from UPS and XPS measurements on the same aC films.

	Work-function (eV)	Cl/C	O/C
H-aC	4.4	--	0.09
Cl-aC	4.8	0.03	0.12
Vinyl-aC	4.5	0.004	0.11
Methyl-aC	4.4	0.006	0.10

Table S3.6. F/C and S/C ratios for vinyl-aC reacted with 4-FBM or thiol-aC films reacted with 4-FS molecules as a function of illumination time.

	vinyl-aC, 20 mW		thiol-aC, 20 mW		thiol-aC, 90 mW	
Time (min)	F/C	S/C	F/C	S/C	F/C	S/C
15	0.0000	0.0000	0.0000	0.0089	0.0006	0.0064
30	0.0000	0.0000	0.0000	0.0087	0.0022	0.0096
60	0.0042	0.0049	0.0000	0.0062	0.0035	0.0077
120	0.0041	0.0038	0.0000	0.0063	0.0014	0.0061

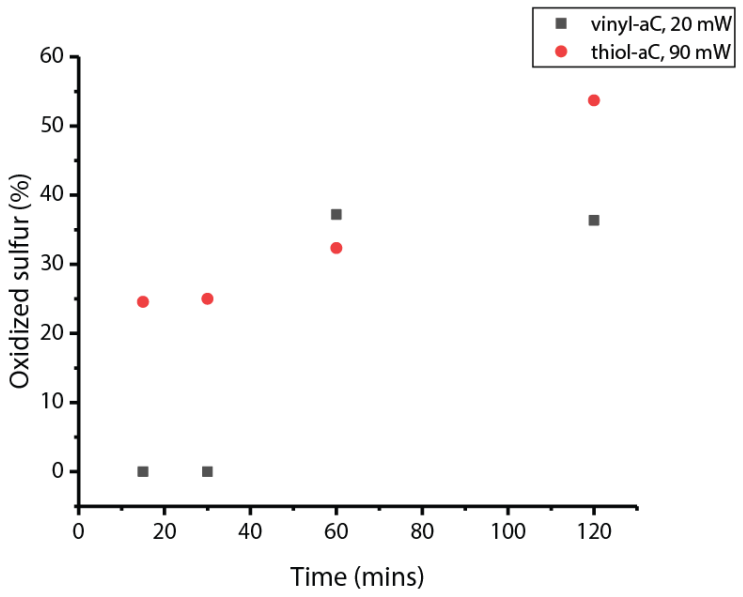

Figure S3.8. Oxidized sulfur percentages for vinyl-aC and thiol-aC films exposed to benzene containing either 1M 4-FBM or 1M 4-FS, at different powers of UV light.

APPENDIX C: EXAMPLE CALCULATION FOR CHAPTER 3

Reaction Completion Percentage Calculation:

The amount of chlorine loss due to vinyl groups replacing the surface-bound chlorines ($\frac{Cl}{C}_{vinyl}$) was determined with Equation 1. The initial chlorine-to-carbon ratio ($\frac{Cl}{C}_{initial}$) was determined before vinyl-termination and the final chlorine-to-carbon ratio ($\frac{Cl}{C}_{final}$) was determined after vinyl-termination. The non-specific loss of chlorine due to the reaction conditions ($\frac{Cl}{C}_{control}$) was determined for a control surface that was exposed to THF at 80°C. This value is the amount of non-specific chlorine loss due to reaction conditions, and not to displacement by the vinyl Grignard reagent.

$$\frac{Cl}{C}_{vinyl} = \frac{Cl}{C}_{initial} - \left(\frac{Cl}{C}_{final} + \frac{Cl}{C}_{control}\right) \qquad \text{Equation 1}$$

Equation 2 was used to determine the reaction completion percentage for the vinyl-aC films. This value is percentage of surface-bound vinyl groups that reacted with 4-fluorobenzyl mercaptan molecules to form a thioether bond. The reaction completion is a ratio of the sulfur-to-carbon ratio of the clicked surface ($\frac{S}{C}_{click}$) and the chlorine-to-carbon ratio of the vinyl surface.

$$\text{Reaction completion percentage} = \left(\frac{\frac{S}{C}_{click}}{\frac{Cl}{C}_{vinyl}}\right) * 100\ \% \qquad \text{Equation 2}$$

Equation 3 was used to determine the reaction completion percentage for the thiol-aC films. This value is the percentage of surface-bound thiols that reacted with 4-fluorosytrene molecules to form a thioether bond. The sulfur-to-carbon ratio was determined for the films after thiol-termination ($\frac{S}{C}_{thiol}$). The fluorine-to-carbon ratio was determined after the click reaction ($\frac{F}{C}_{click}$).

$$\text{Reaction completion percentage} = \left(\frac{\frac{F}{C}_{click}}{\frac{S}{C}_{thiol}}\right) * 100\ \% \qquad \text{Equation 3}$$

APPENDIX D: SUPPLEMENTAL INFORMATION FOR CHAPTER 4

Table S4.1. Reaction conditions tested to prepare N_3-aC films.[a]

[NaN_3]	[15-crown-5]	Solvent	Time	Temperature	ΔO/C	O/C of Cl-aC	% chlorine replacement [b]	Azide signal?
100 mM	—	MeOH	3 h	RT	-0.02	0.11	5.6	✓
100 mM	—	MeOH	6 h	RT	-0.02	0.11	10.6	✓
100 mM	—	MeOH	33 h	RT	-0.01	0.11	9.1	✓
100 mM	—	DMF	24 h	RT	0.00	0.08	33.7	✓
50 mM	—	DMF	3 h	RT	0.01	0.08	—	X
50 mM	—	DMF	24 h	RT	0.01	0.07	41.7	✓
50 mM	—	1:1 DMF:H_2O	3 h	RT	0.00	0.07	—	X
50 mM	50 mM	1:1 DMF:H_2O	3 h	RT	0.01	0.08	—	X
50 mM	100 mM	1:1 DMF:H_2O	3 h	RT	0.01	0.08	—	X
50 mM	50 mM	DMF	24 h	RT	0.03	0.07	33.3	✓
100 mM	—	DMF	3 h	50°C	0.07	0.10	49.6	✓
100 mM	—	DMF	6 h	50°C	0.08	0.10	21.3	✓

[a] The red-boxed conditions were used to modify the aC films with ferrocene in this work.

[b] An example of this calculation is detailed below.

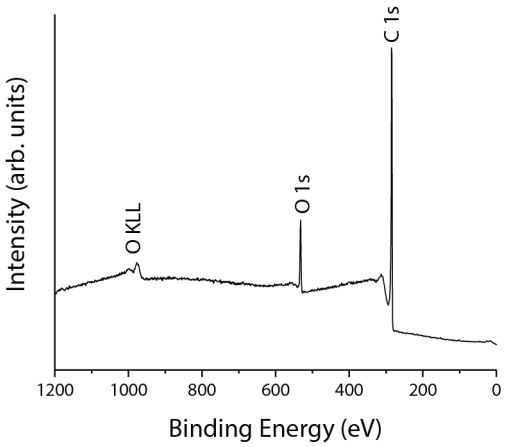

Figure S4.1. Representative XP survey spectrum of an unmodified aC film on an FTO substrate.

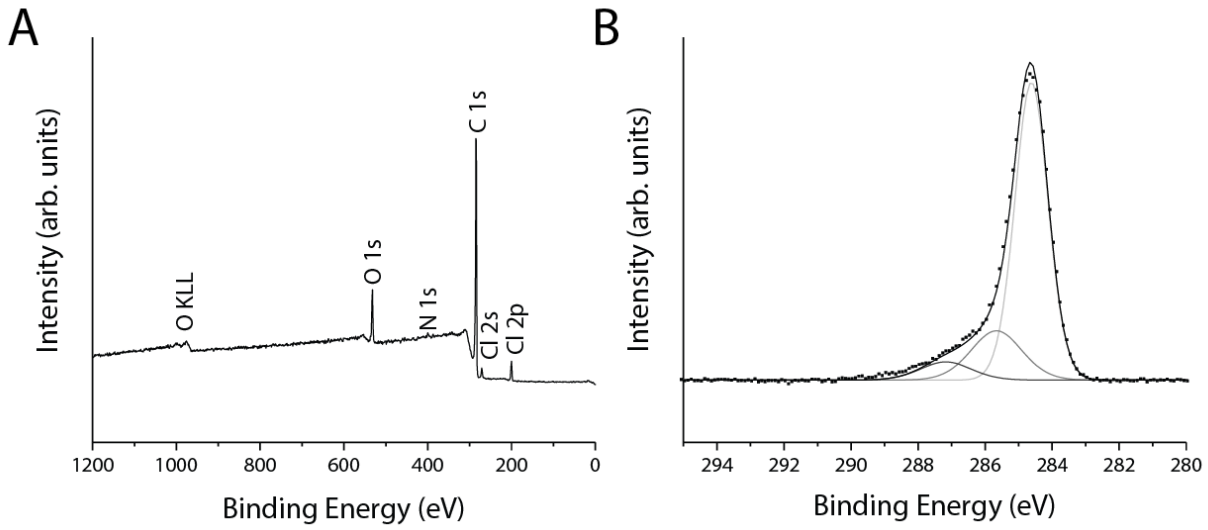

Figure S4.2. Representative XPS data. (A) survey spectrum and (B) high-resolution C 1s spectrum of an azide-terminated aC film on an FTO substrate. Peak fitting of the C 1s spectrum is detailed in the Materials and Methods section of the manuscript.

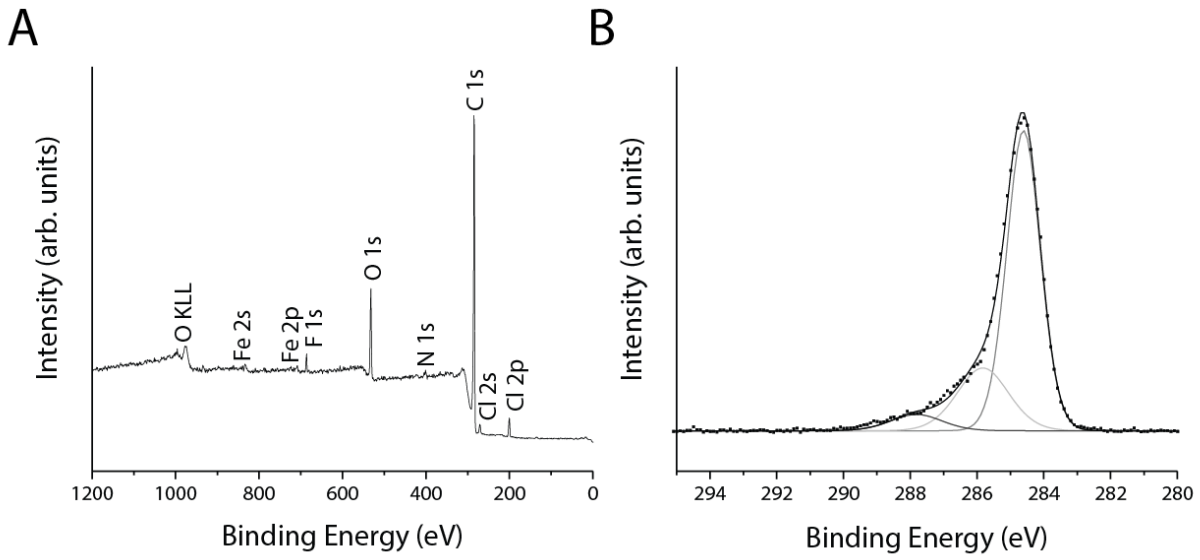

Figure S4.3. Representative XPS data. (A) survey spectrum and (B) high-resolution C 1s spectrum of an azide-terminated aC film on an FTO substrate, after a CuAAC reaction with ethynyl ferrocene. Peak fitting of the C 1s spectrum is detailed in the Materials and Methods section of the manuscript. The F 1s peak present in the survey spectrum is due to surface contamination.

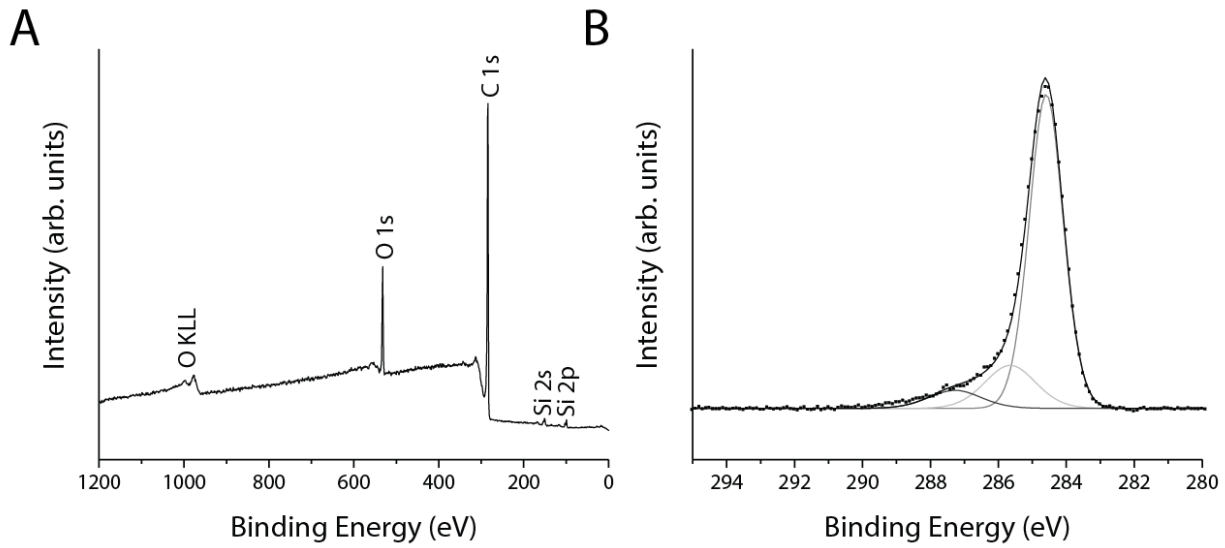

Figure S4.4. Representative XPS data. (A) survey spectrum and (B) high-resolution C 1s spectrum of a hydrogen-terminated aC film on a silicon substrate, after exposure to a CuAAC reaction with ethynyl ferrocene. The reaction conditions used here are the same as those used in Figure S3. Peak fitting of the C 1s spectrum is detailed in the Materials and Methods section of the manuscript.

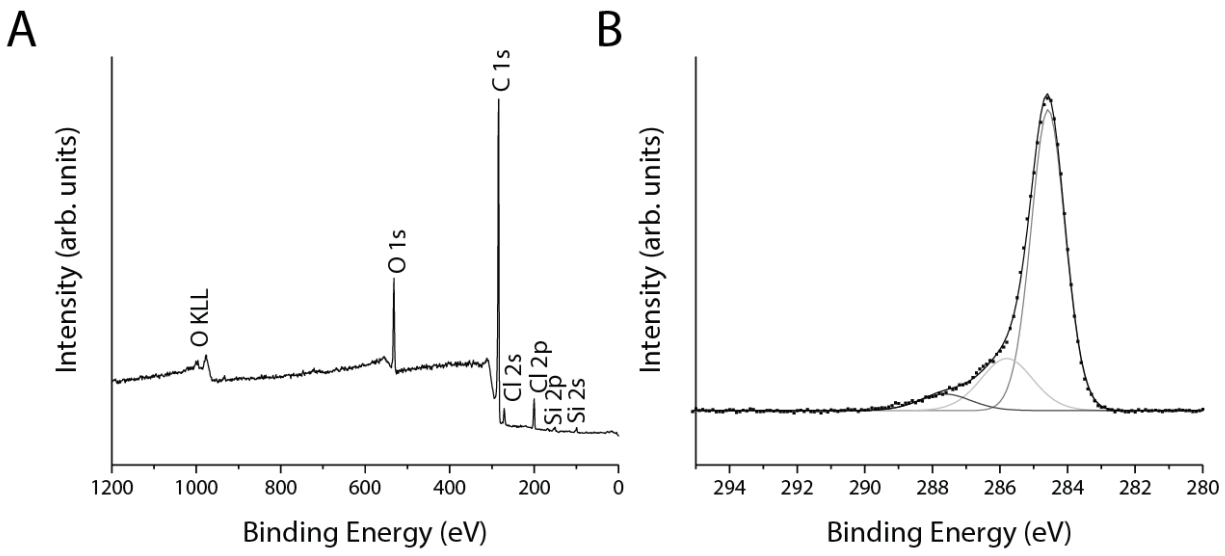

Figure S4.5. Representative XPS data. (A) survey spectrum and (B) high-resolution C 1s spectrum of a chlorine-terminated aC film on a silicon substrate, after exposure to a CuAAC reaction with ethynyl ferrocene. The reaction conditions used here are the same as that used in Figure S3. Peak fitting of the C 1s spectrum is detailed in the Materials and Methods section of the manuscript.

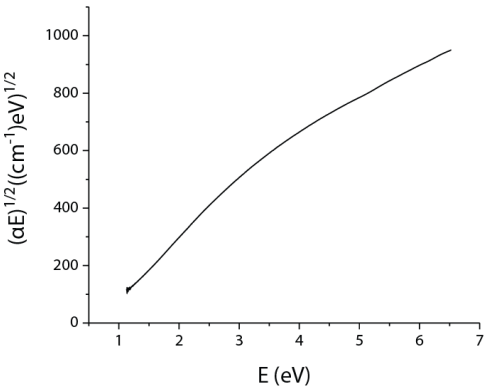

Figure S4.6. Tauc plot of aC film on a quartz substrate. Each data point is the average of absorption values for four aC on films on quartz substrates. The thickness of each aC film was 25 nm.

Table S4.2. Cyclic voltammetry data for ferrocene-terminated aC films.

Scan Rate (mV/s)	ΔE (mV)	E^o (mV)
50	173.58	204.96
100	193.82	239.93
150	198.43	252.40
200	195.86	253.61
250	177.88	252.51
300	193.83	254.94
500	183.28	239.97

Table S4.3. Scan rate values used to obtain the CVs displayed in **Figure 1** of the text.

Scan rate (V/s)
0.025
0.05
0.1
0.2
0.4
0.6
0.8
1
1.5
3
4
5
7
8.5
10
15
20
25
40
50

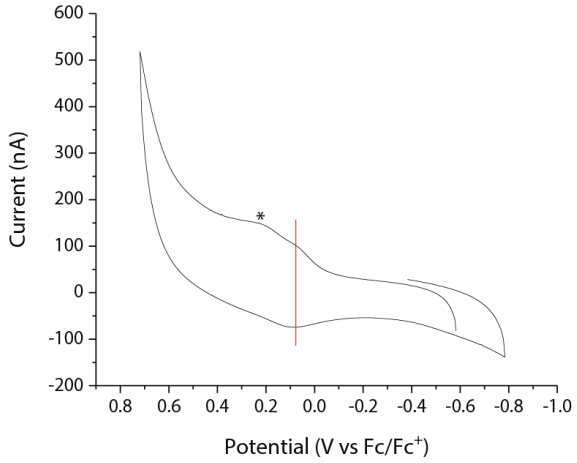

Figure S4.7. Cyclic voltammogram of ferrocene-modified aC film on FTO at 10 mV/s. The starred peak indicates an unexpected peak, which we attribute to copper contamination. The vertical red line indicates the peaks associated with the ferrocene-ferrocenium couple.

APPENDIX E: EXAMPLE CALCULATION FOR CHAPTER 4

Percentage of surface-bound chlorines removed that was replaced with an azide group:

Prior to the azide reaction, the chlorine-to-carbon ($\frac{Cl}{C}_{initial}$) and nitrogen-to-carbon ($\frac{N}{C}_{initial}$) ratios were determined for each film. After the azide reaction, the chlorine-to-carbon ($\frac{Cl}{C}_{final}$) and nitrogen-to-carbon ($\frac{N}{C}_{final}$) ratios were determined for each film. A corrected nitrogen-to-carbon ratio was calculated (Eq. 1) to account for any nitrogen present on the surface before the azide reaction, and then divided by three to account for the number of nitrogen atoms in each azide molecule (Eq. 2).

$$\frac{N}{C}_{corrected} = \frac{N}{C}_{final} - \frac{N}{C}_{initial} \qquad \text{Eq. 1}$$

$$\frac{N}{C}_{azide} = \frac{\frac{N}{C}_{corrected}}{3} \qquad \text{Eq. 2}$$

To determine the chlorine removed from the surface during the azide reaction ($\frac{Cl}{C}_{lost}$), the final chlorine-to-carbon ratio was subtracted from to initial chlorine-to-carbon ratio (Eq. 3).

$$\frac{Cl}{C}_{lost} = \frac{Cl}{C}_{initial} - \frac{Cl}{C}_{final} \qquad \text{Eq. 3}$$

To determine the reaction completion percentage, we calculated the ratio of azide groups on the surface ($\frac{N}{C}_{azide}$) and the chlorine atoms lost during the reaction ($\frac{Cl}{C}_{lost}$) (Eq. 4).

$$Reaction\ completion\ percentage = \left(\frac{\frac{N}{C}_{azide}}{\frac{Cl}{C}_{lost}}\right) * 100 \qquad \text{Eq. 4}$$

APPENDIX F: EXAMPLE CALCULATION FOR CHAPTER 4

***Heterogeneous electron transfer rate constant determination**:*

This calculation was based on methods previously described Dempsey and colleagues[1] and are based on work originally described by Nicholson.[2] Briefly, a plot of η versus log (v) was plotted, and a simulated working curve was used to fit the experimental data (experimental data referred to with subscript Fc). The following parameters were used to simulate the data: D_{sim}= 1 x 10^{-5} cm^2/s and $k_{s,\ sim}$= 1 cm/s. The following equation was used to solve for the rate constant:

$$\Lambda_s = k_s \sqrt{\frac{RT}{FvD}}$$

where k_s is the rate constant, R is the gas constant, T is temperature, F is Faraday's constant, and D is the diffusion constant. To solve this equation, the x-axes of the two plots were made to overlap with each other so that $\Lambda_{s,sim} = \Lambda_{s,Fc}$. Through simple algebra, the rate constant was determined for our experimental data.

REFERENCES

1. E.S. Rountree, D.J. Martin, B.D. McCarthy, J.L. Dempsey, Linear free energy relationships in the hydrogen evolution reaction: Kinetic analysis of a cobaloxime catalyst, ACS Catalysis, 6 (2016) 3326-3335.

2. R.S. Nicholson, Theory and application of cyclic voltammetry for measurement of electrode reaction kinetics, Anal. Chem., 37 (1965) 1351-1355.